Characterization and Performance Assessment of a Novel NiO-Fe_3O_4-Polythiophene Nanocomposite for Asphaltene Precipitation Inhibition

By

Mardan Serikbay

Thesis submitted to the School of Mining and Geosciences of Nazarbayev University in Partial Fulfillment of the Requirements for the Degree of

Master of Science in Petroleum Engineering

Nazarbayev University

April 2024

ORIGINALITY STATEMENT

I, Mardan Serikbay, hereby declare that this submission is my own work and to the best of my knowledge it contains no materials previously published or written by another person, or substantial proportions of material which have been accepted for the award of any other degree or diploma at Nazarbayev University or any other educational institution, except where due acknowledgement is made in the thesis.

Any contribution made to the research by others, with whom I have worked at NU or elsewhere is explicitly acknowledged in the thesis.

I also declare that the intellectual content of this thesis is the product of my own work, except to the extent that assistance from others in the project's design and conception or in style, presentation and linguistic expression is acknowledged.

Signed on **15.04.24**

_____

NOMENCLATURE

Acronyms and Abbreviations

AOP	Asphaltene onset point
BET	Brunauer-Emmett-Teller
DLS	Dynamic light scattering
EOR	Enhanced oil recovery
FTIR	Fourier transform infrared spectroscopy
HPHT	High Pressure High Temperature
IFT	Interfacial tension
NC	Nanocomposite
n-heptane	Normal heptane
NP	Nanoparticle
PAH	Polycyclic aromatic hydrocarbon
RFF	Relevancy factor function
SEM	Scanning electron microscope
SLE	Solid-liquid equilibrium
SPA	Surface Plasmon resonance
TEM	Transmission electron microscopy
TGA	Thermogravimetric analysis
XRD	X-ray diffraction

Symbols

A	Surface area of NC, m^2/g
A_d	Asphaltene absorbance after dilution
A_i	Initial absorbance of asphaltene
C_d	Concentration of asphaltene after dilution
C_e	Equilibrium asphaltene concentration, mg/L

C_0	Initial asphaltene concentration, mg/L
C_{NP}	Nanoparticle concentration, g/L
K_F	Freundlich constant, $(mg/g)/(mg/L)^n$, and $0 < n < 1$
K_L	Langmuir constant
M	Mass of asphaltene, mg
m	Mass of NC, g
mi	Initial mass, mg
mt	Final mass, mg
MW	Molecular Weight, mol/g
1/n	intensity factor (dimensionless)
Q_e	equilibrium adsorbed mass of asphaltene, (mg/g)
Q_{max}	Maximum amount of adsorbed asphaltene per surface area, (mg/m^2)
V_1	Volume of synthetic oil, ml
V_2	Volume of toluene, ml
wt%	Weight percent, %

Greek Letters

θ	Diffraction angle
λ	Spectrophotometry wavelength, nm

Metric Conversion Factors

1 nm	10^{-9} m

ABSTRACT

Precipitation and deposition of asphaltene represents a significant challenge in the oil industry. Nanomaterials are considered as proper candidates for asphaltene adsorption and precipitation owing to their exceptional physical and chemical features. In this dissertation, first, a novel NiO-Fe_3O_4-Polythiophene nanocomposite (NC) was characterized using various advanced analytical methods to ensure its authenticity. X-ray diffraction (XRD) was used to determine the crystallite size and explore structures of the NC. Scanning electron microscopy (SEM) was used to investigate surface morphology and assess the particle size of the NC qualitatively. Fourier transform infrared spectroscopy (FTIR) methods was used to identify functional groups and elemental bonding of the NC. Brunauer-Emmett-Teller (BET) method was used to determine surface area of the NC. Thermogravimetric analyzer (TGA) was used to explore thermal stability of the NC. Using the XRD data the crystallite size was determined 33.2 nm. The particle size of the NC ranges from 60 to 400 nm based on SEM images, and surface area of the NC was determined 55.83 m^2/g using the BET test data. TGA analysis revealed that the NC is thermally stable with a negligible mass loss under reservoir conditions (80°C). To assess efficacy of the novel NC for adsorption and inhibition of asphaltene, UV-spectroscopy technique was used to determine Asphaltene Onset Point (AOP) in presence and absence of the NC and then supernatant obtained from TGA analysis was used for adsorption kinetics isotherm modeling. Adsorption kinetics isotherm modeling was done using the Langmuir (R^2 = 0.98) and Freundlich (R^2 = 0.95) isotherm models. The experimental data matched well both models which suggests monolayer and multilayer adsorption behavior for adsorption of asphaltene onto the surface of the NC. A maximum adsorption capacity of 1.116 mg/m^2 was obtained for the NC. TGA analysis confirmed that oxidation of virgin asphaltene started at around 400-450°C; while oxidation of 5,000 ppm sample with NC started at around 350°C. The NC has catalyzed oxidation of the asphaltene. An optimum NC concentration of 0.3 wt% was obtained and an AOP shifting from 40% to 48% volume of *n*-heptane was observed for the optimum concentration. The outcomes prove that, the novel NC is an effective nano-inhibitor for asphaltene under laboratory conditions.

***Keywords*:** Asphaltene precipitation inhibition, nano-inhibitors, NiO-Fe_3O_4-Polythiophene nanocomposite, AOP, adsorption, TGA

ACKNOWLEDGMENTS

I would like to sincerely appreciate my supervisor, Dr. Ali Shafiei, for his counselling, agency, and promotion throughout my thesis project. His extensive expertise and enthusiasm for the project have been instrumental in shaping my dedication and grasp in my program.

I express my gratitude to Dr. Timur Atabaev, for his invaluable collaboration as well as using his scientific testing facility that allowed successful completion of some of my laboratory experiments. Furthermore, I would like to thank Dr. Baharak Sajjadi (University of Oklahoma) and Dr. Azza Hashim Abbas for reviewing my dissertation and providing useful and constructive comments.

This work was conducted as part of the Collaborative Research Proposal Faculty grant project (OPCRP2020015), titled: “A comprehensive study on asphaltene characterization and screening asphaltene deposition inhibitors for Kazakhstan crude oils.” I am grateful to Nazarbayev University for the financial support extended through this grant.

In addition, I want to express my gratitude to the school faculty for offering us the resources and materials we needed to complete our research. Their unwavering faith in our expertise and assistance have been crucial to the success of our endeavor. I also want to thank my family and colleagues Kemelkhan Kaliolla and Kamilya Arstanova, for their unwavering support and tolerance amid my difficult but worthwhile path.

LIST OF FIGURES

LIST OF TABLES

1 INTRODUCTION

In this chapter, first a brief background is provided on definition of asphaltene, problems caused because of asphaltene precipitation and deposition in the oil industry, and possible solutions including use of nanotechnology. Then, the statement of research problem, research objectives, and research methodology were described. In the end, the thesis structure and organization is explained, briefly.

1.1 Background

Asphaltene is a complex mixture of hydrocarbons found in some crude oils. It is well-known for its heavy, thick, and highly aromatic nature that dissolves in aromatic solvents such as toluene but it is insoluble in *n*-alkanes (Zhang et al., 2020). Characterization and understanding asphaltene behavior including its adsorption kinetics, structure, and chemistry is essential to comprehend how crude oils behave during production, transportation, and processing (Ghamartale et al., 2021).

Asphaltene deposition represents a widespread and major challenge in the oil industry causing significant economic loss and operational difficulties. Precipitation of asphaltene in oil production facilities can result in equipment failure, reduced oil production rates, and pipe blockages (Figure 1-1). It is crucial to understand the behavior of asphaltene and create effective techniques to either inhibit its precipitation and deposition to use mitigation measures to eliminate depositions (Sheu, 2001).

Figure 1-1. Asphaltene deposits after pigging operations (Hussein, 2023).

To explain basic structure of asphaltene molecules, the modified "Yen-Mullins" model is currently considered the most acceptable considering molecular structure of asphaltene and mechanism of cluster formation in crude oil medium. With peripheral alkanes, the main part of molecular structure of asphaltene is composed of a single, rather large polycyclic aromatic hydrocarbon (PAH). These single disordered PAH stacks are formed by asphaltene molecules in nanoaggregates with aggregation counts of about six. Clusters consisting of asphaltene nanoaggregates can have an aggregation number of around eight. (Mullins, 2011).

Several factors and conditions leads to asphaltene precipitation and flocculation. For instance, reservoir pressure and temperature changes, crude oil density, and viscosity (Alimohammadi et al., 2019). This is further elaborated in chapter 2. In fact, asphaltene precipitation is not governed only by a single process. The point at which asphaltene starts to aggregate is known as AOP. Investigating the asphaltene onset point (AOP) is a vital task which can be done using different laboratory methods (Sullivan et al., 2020).

Several methods are proposed in the literature as solutions or mitigation measures to tackle adverse effects of asphaltene deposition in the oil industry. They include mainly mechanical and chemical treatments. Mechanical treatments include pigging, vibration, and manual removal. The earliest known technique for removing asphaltene or other accumulated heavy hydrocarbons is hand stripping. The tube is scraped mechanically to complete the process. Although pigging technique is successful it works best for removing wax deposits and emulsions. This approach is ineffective in eliminating thick organic particles in formations, even if it can be somewhat successful in clearing pipes and tubing. Furthermore, the process of mechanically removing the depositions may require stopping operations which can cause financial loss (Akbar & Saleh, 1989). Solvent-based chemical elimination is used to eliminate asphaltene accumulation when mechanical approaches prove ineffective (Voloshin et al., 2005). Aromatic solutions make up the majority of asphaltene solvents. King and Cotney (1996) investigated dissolution of asphaltene in various petroleum solutions including inexpensive deasphaltened hydrocarbons with a rich aromatic component as a substitute for expensive chemical agents. Considering its minimal flash temperatures of 28°C, xylene is certainly the oldest widely used aromatic solution (Trbovich & King, 1991). Although toluene is less effective, it is nevertheless used despite being significantly more flammable with flash point 5° (Galoppini, 1994). However, there are a number of concerns why the application of such petroleum solvents is restricted, including the possibility of corrosion

and hazard issues due to their minimal flash point and the consequent safety concerns (Shirdel, 2012).

Nanotechnology is considered as a promising technology and a hot research area in various sectors of the Exploration & Production (E&P) industry in the past 3 decades with limited filed implementations owing exceptional characteristics of the nanomaterials because of their small particle size (Franco et al., 2021). Exploration, completion, EOR, and formation damage are a few of these pertinent field (Franco et al., 2017). Zabala et al. (2012) investigated asphaltene formation damage inhibition by Al_2O_3 NPs. Results showed that application of NPs increased cumulative oil production up to 0.27Mbbl (Zabala et al., 2014). According to Zabala et al. (2016), using nanofluids containing Al_2O_3 NPs improved mobility of heavy oils in real field. This led to enhancing production per day up to 310 bbl and decreasing basic sediment and water (BSW) (Zabala et al., 2016). Metal oxide NPs possibly able to stabilize asphaltene particulates. Mohammadi et al. (2011) described about asphaltene stabilizing process applying NPs like TiO_2, ZrO_2 and SiO_2. Mechanism for this process explained by hydrogen binding among NPs surface and asphaltene in acidic state (Mohammadi et al., 2011). It can be suggested combine NPs to get enhancing results for asphaltene precipitation inhibition. In addition, Alomair et al. observed increasing volume of recoverable hydrocarbon due to application of combined silica and alumina NPs (Alomair et al., 2015).

1.2 Statement of Problem

Being arguably the most challenging parts of the oil, asphaltene is a polar complex organic material with a large molecular size, complex composition and architecture (Fakher et al., 2019). Both upstream and downstream oil industry can suffer from flow assurance issues caused by asphaltene deposition. Precipitation and deposition of asphaltene during crude oil production, transportation, and other related processes causes serious problems. These undesirable effects of asphaltene precipitation and deposition includes clogging of the pore channels, modification of the wettability of the reservoir towards a more unfavorable state (i.e., oil wet), and reduction in permeability the formation (Leontaritis et al., 1994). Deposition of asphaltene in downstream petroleum industry causes particles to accumulate and deposit in surface facilities including storage tanks, soiling of safety controls, and blocking of flow lines (Seifried et al., 2013). Moreover, asphaltene can intoxicate catalysts used in refinery plants and impair their functioning and efficiency (Powers et

al., 2016). Several mitigation measures are proposed and some are in use in the oilfield such as mechanical and chemical methods and every method has their own advantages and disadvantages including cost and effectiveness. This is why development and testing new agent for asphaltene precipitation inhibition is vital. Nano-inhibitors also considered as chemical mitigation measures take the advantage of extraordinary features of nanomaterials to inhibit precipitation and deposition of asphaltene particles. NPs possess a large surface area which enables them to inhibit precipitation of asphaltene via adsorption of its particles onto their surface, effectively. By adjusting the chemical properties on the surface of the NPs also known as functionalization, some properties of the NPs can be improved (Shojaati et al., 2017). Functionalization includes synthesis of a nanocomposite (NC) made of two or more NPs and coating the surface of the NP with polymer or adding surfactants or nano-clays. The novelty of this research work is introduction of a novel NC which consists of two different NPs coated with a polymer. Then novel NC is characterized by laboratory methods to determine its surface area, crystalline structure, and particle size to enable a better understanding of its asphaltene inhibitory efficacy. The primary and main objective of this research work was to investigate efficacy of the novel NiO-Fe_3O_4-Polythiophene NC for adsorption and oxidation of asphaltene particles in a synthetic crude oil medium under laboratory conditions and exploring the mechanisms involved.

1.3 Relevance to the oil industry

Asphaltene accumulation is a widespread problem in Kazakhstan and around the world. Some of undesirable effects of asphaltene deposition in reservoirs is change in wettability (Buckley & Liu, 1998) that can cause reduction in crude oil recovery and financial loss. Precipitation and deposition of asphaltene occurs in oil reservoirs clogging the pores, near wellbore vicinity, alongside wells, pipes, tubing, and surface facilities, depending on thermodynamic conditions and composition of the crude oil (P-T-X). It is preferable to avoid asphaltene precipitation and deposition rather than deadline with its consequences since the former reduces the productivity. Nanotechnology has revolutionized a number of fields including computing and medicine (Paul & Robeson, 2008). It is anticipated that the energy sector would experience similar advancements compared to the other industries (Fleming, 2013). In this instance, invention and use of nanomaterials in the petroleum sector have received a lot of interest. Nanomaterials are anticipated to have a major impact on advancement of petroleum-based fuel innovations and production of hydrocarbons

(Krishnamoorti, 2006). Application of nanotechnology and novel materials in drilling, production, and other related sectors is being investigated by several researchers around the world (Li et al., 2013). The key factors in design of asphaltene inhibitors are the type and dosage of the chemicals used including nanomaterials. If a nano-inhibitor is not designed properly, asphaltene precipitation issue might even become worse. Furthermore, the effects on safety, health, and the environment should be considered while developing new nano-inhibitors (Ghamartale et al., 2021).

1.4 Research Objectives

The major aims of the present research work were to first characterize and evaluate the novel NiO-Fe_3O_4-Polythiophene NC. Then, to assess its efficacy as an asphaltene inhibition agent in crude oil system. These require intensive experimental research consisting of several steps and each step has its own objective which collectively enabled characterization and performance assessment of the novel nanocomposite for asphaltene precipitation inhibition. The goals of each step:

- To characterize composition and crystallite structure of the nanocomposite using x-ray diffraction, measuring surface area using Brunauer-Emmett-Teller approach, using scanning electron microscopy to describe morphology and size of nanocomposite.

- Determine asphaltene onset point (AOP) in presence and absence of the NC to determine optimum concentration of the NC. Wavelength for UV-visible chosen 700 nm for measuring absorption values.

- Evaluate efficacy of the NC by TGA analysis. It contains thermal stability of NC, oxidation and kinetics of asphaltene and asphaltene adsorption isotherms.

1.5 Research Methodology

Methodology of research thesis work contains several procedures:

- Extraction of asphaltene according to the IP 143 standard,
- Synthetic oil preparation,
- Characterization of the novel NC by using laboratory techniques such as FTIR, XRD, SEM, DLS, TGA, and BET,

- Determining AOP using UV-spectroscopy and TGA analysis in absence and presence of NC and using various concentrations of the novel NC,
- Using thermogravimetric analysis to evaluate thermal stability of the novel NC and oxidation of asphaltene in absence and presence of the novel NC.

1.6 Thesis structure

This dissertation consists of five chapters in. A brief background on definition and properties of asphaltene and the associated problems with precipitation and deposition of asphaltene in petroleum industry plus the problem statement, aims of the proposed research, and the proposed research methodology to meet the research objectives. A comprehensive literature review of the relevant researches with focus on asphaltene characterization, mechanisms of asphaltene precipitation and deposition, and application of NPs as asphaltene inhibitors is presented in chapter two. The proposed research methodology and the step by step laboratory procedures and methods designed to conduct the research work and to achieve the research objectives is presented in chapter 3. The results obtained from this experimental research work are presented and discussed in chapter four. A brief summary of the main findings of this research work plus some recommendations for further research are presented in chapter five.

2 LITERATURE REVIEW

In chapter 2, a brief review of asphaltene and asphaltene deposition, problem caused by asphaltene deposition and mitigation measures are described. Asphaltene adsorption kinetics and isotherms, phase behavior, factors affecting asphaltene deposition are also discussed following this. Some recent research works reported on nano-inhibition and application of NPs and NCs in asphaltene adsorption and inhibition are presented.

Precipitation and deposition of asphaltene represents a significant challenge in the oil industry. This can cause significant economic losses and operational difficulties. Asphaltene precipitation can unfavorably impact the work of production systems, in all sectors. For example, blocking the pore space, changing of reservoir rock's wettability, and an impairing permeability of the reservoir rock are some of negative consequences of the asphaltene deposition. Moreover, asphaltene deposition in wellbore can plug flow lines and surface facilities and deposition of solid particle in storage tanks (Alimohammadi et al., 2019).

2.1 Asphaltene definition and precipitation

The word "asphaltene" was first used by Boussingault to characterize bitumen which is not soluble in alcohol (Murgich et al., 1996). Nowadays the main factor used to characterize asphaltene is its solubility. Asphaltene particles are insoluble in *n*-alkanes but are soluble in aromatic solvents like toluene. Asphaltene is a heavy and complicated component of crude oil and it contains aromatic compounds and has high molecular weight (Bauget et al., 2001). To describe behavior of asphaltene it is important to firstly study formation of asphaltene.

Asphaltene precipitation and deposition can cause blockage of flow in facilities (Jamialahmadi et al., 2009). Asphaltene can precipitate and deposit at various times and points during crude oil production, transportation, and storage (i.e., reservoir, tubing, pipes, storage tanks, and surface facilities). Hence, a thorough understanding of asphaltene precipitation mechanics is essential in design of effective asphaltene precipitation prevention agents (Eskin et al., 2011).

Self-aggregation, interfacial and intrinsic properties of asphaltene have traditionally been obstacles in asphaltene research. The fluid stage mobility alters the exterior hydrophobicity, its original wetting capacity, and decreases oil permeability, thereby decreasing or, to some extent,

increasing the mass transmission friction and restricts the motion of crude oil. The alteration in feature leads to precipitation of asphaltene (Alshareef, 2019). Asphaltenes typically contain C, H_2, O_2, N_2, S and minimum amounts of heavy metals (Speight, 2014).

2.1.1 Asphaltene Characterization

The modified "Yen-Mullins" concept is currently considered the most widely accepted model (Figure 2-1). With peripheral alkanes, the main molecular structure of asphaltene is composed of a single, rather large polycyclic aromatic hydrocarbon (PAH). Single disordered PAH stacks are formed by asphaltene molecules in nanoaggregates with aggregation counts of about six. Clusters consisting of asphaltene nanoaggregates can have an aggregation number of around eight. (Mullins, 2011).

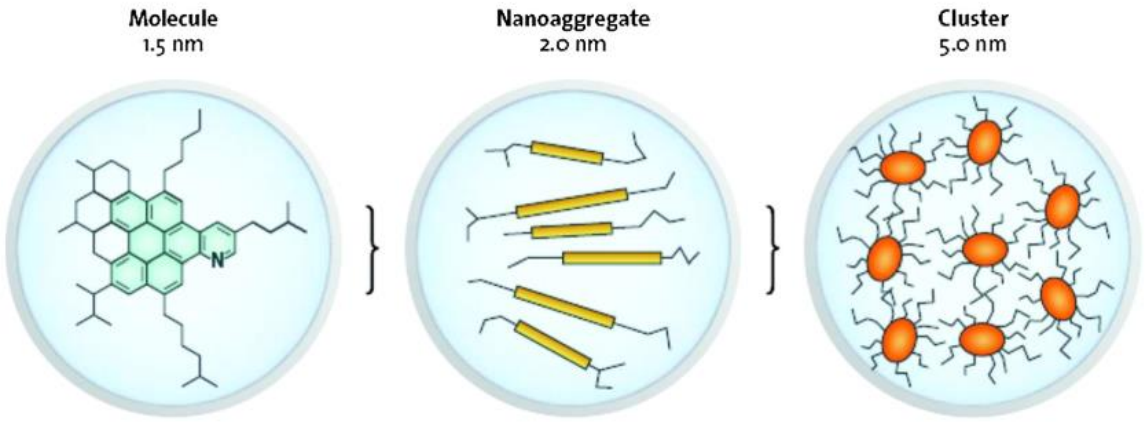

Figure 2-1. The asphaltene molecular structure model (Mullins, 2011).

That self-aggregation feature of asphaltene is related by these structural characteristics. Asphaltene from unstable crude oils that has a poor hydrogen content and a high aromaticity, in particular, aggregate at a smaller amount in the examined solutions than asphaltene from stable crude oils that has a higher hydrogen content and a poor aromaticity (Leon et al., 2000).

Various analytical methods have been used to characterize asphaltene molecules (Hassanzadeh & Abdouss, 2022). Some of the techniques commonly used include: Fluorescence spectroscopy (FS) to analyze size of aromatic rings and self-aggregation characteristics of asphaltene particles. The capture and release spectrum of luminescence are similar even when the asphaltene particulates are different and their pigments are only marginally affected by variations in concentration (Abdallah & Yang, 2012). Results of experiments by FS showed that, applying

Gaussian method, the molecular architecture and size of the aromatic sheet ranges from 1.52−1.88 nm for all the samples included in this investigation. Experimental Raman spectra of a pure asphaltene provided by Wu and Kessler (2015) is presented in Figure 2-2. The results displayed two separate bands, the G and D1 bands, approximately 1580 cm^{-1} and 1350 cm^{-1}, correspondingly. Presence of a short range order in asphaltene's aromatic sheet was identified by the smaller G peak compared with the larger D1 peak. Furthermore, the computed value of aromatic core size was 1.74 nm, indicating that about 6-7 aromatic rings were joined altogether throughout the formation of the asphaltene molecule's polyaromatic nucleus (Wu & Kessler, 2015).

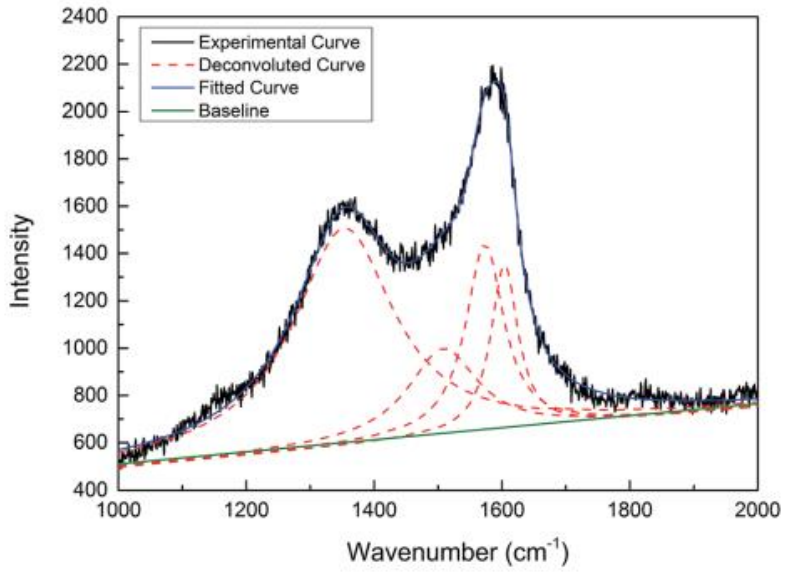

Figure 2-2. Raman spectra of a pure asphaltene sample (Wu & Kessler, 2015).

Mass spectrometry is used to assess the mass ratio of particulates and their structural appearance. It considers mass of the molecules and its range in addition to alkyl chains carbon quantity (Bojkovic et al., 2021). Research results proves Mullins model that, aromatics has less molecules. In addition, nitrogen atom consisted in higher asphaltene molecules. Island architecture of asphaltene prevails in pure asphaltene (Koolen et al., 2018). The island model for asphaltene structure proposed by Mullin is presented in Figure 2-3. The PAH in asphaltene gets attracted with dipoles and London dispersion forces. Steric repulsion is produced by the alkane substituents on asphaltene surface (Mullins, 2011). According to the continental model, asphaltene has several aliphatic splits connected to a large collection of aromatic rings (a single dominant aromatic ring

complex) at the particle's core. This model is also called the condensed aromatic (island) model since it is often associated with lower molecular weight asphaltene molecules.

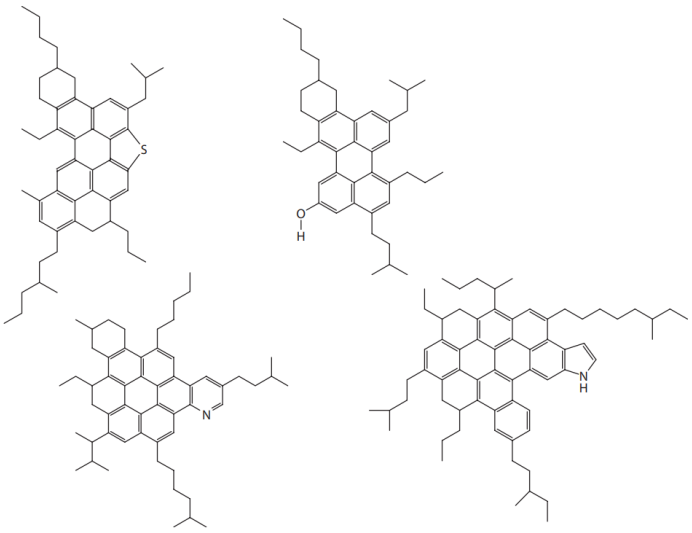

Figure 2-3. Island model of asphaltene molecular structure (Mullins, 2011).

Average molecular weight of asphaltene molecules was determined 1000 g/mol by field ionization mass spectroscopy that works by passing asphaltene through an electric field (Boduszynski, 1982). Petroleum asphaltenes are reported to have mean molecular weights of around 750 g/mol with a variance of 500-1000 g/mol, determined by time resolved fluorescence depolarization (Groenzin & Mullins, 2000). Merdrignac et al. have reported atmospheric pressure photoionization MS experiments. The range of their average MW for pure asphaltene was 500–800 g/mol (Merdrignac et al., 2004).

A FTIR spectrum for pure asphaltene is presented in Figure 2-4. The highlighted peaks can be classified into three groups according to its complex chemical structure: polar functioning, aliphatic, and aromaticity (Fossen et al., 2011). The identified absorption spectrums at 750, 808, and 866 cm^{-1} for the aromatic molecules. For instance, matched the out-of-plane C–H bending in 1,2-disubstituted aromatic, 1,4-substituted aromatic, and 1,3-disubstituted aromatic, accordingly. The aromatic structure's C=C stretching resonance got attributed at 1602 cm^{-1}. The aliphatic signature involved the assignment of C–H stretching oscillations to CH_2 and CH_3 at 2922 and 2852 cm^{-1}, and C–H bending oscillations to CH_2 and CH_3 at 1458 and 1375 cm^{-1}. Stretching oscillations

of -OH and -NH for polar features were observed at about 3458 cm^{-1}. Next, at 1031 cm^{-1}, stretching oscillations of S=O in sulfoxides were detected (Wu & Kessler, 2015).

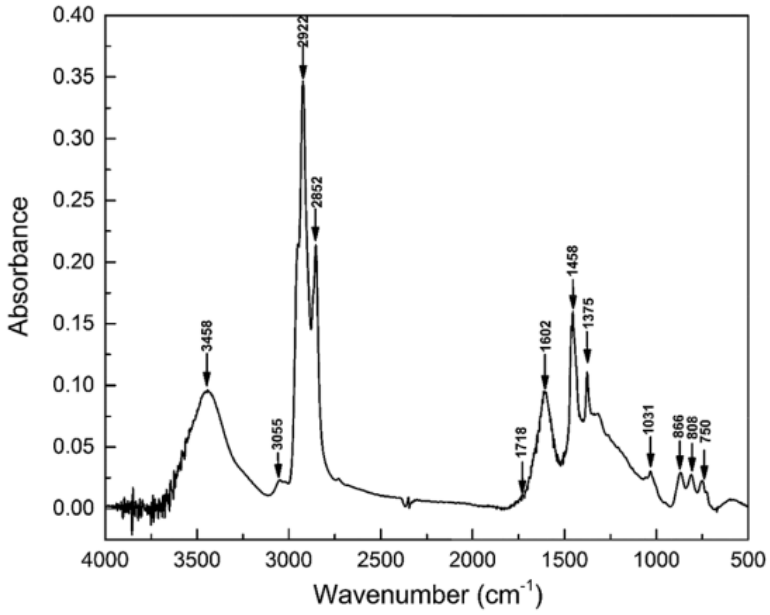

Figure 2-4. FTIR analysis of a pure asphaltene (Wu & Kessler, 2015)

Nuclear magnetic resonance spectroscopy (NMR) is used to clearly define the atomic-level chemistry of asphaltene molecules. ^{1}H NMR spectra of a pure asphaltene is presented in Figure 2-5, where solution spectrometer typically has a range of 0.00 to 15.00 ppm (Ok & Mal, 2019). A common NMR spectrum of asphaltenes are frequently divided into multiple subdivisions for analysis. For instance, organometallic substances with vanadium (V) and nickel (Ni) at the center of their architecture, including porphyrins, are identified by resonances at negative intensities in their NMR spectra. The following priority range is from 0.00 to 1.00 ppm. Approximately 0.90 ppm is the proton indication produced in this area by $-CH_3$ chains of either linear or branched alkanes (Majumdar et al., 2013). Additional indications in this band are from $>CH-$ and CH_2- sites of cyclic aliphatic hydrocarbons (Vuković et al., 2015). Protons that are diaromatic, tri-, and tetra-aromatic make up the majority of the vibrations around 7.20 and 8.30 ppm (Ok & Mal, 2019). Lower concentrations of aldehyde or carboxyl hydrogen molecules are seen around 9.00 and 12.00 ppm (Xu et al., 2014). It should be point out here that carboxylic protons additionally exist in the porphyrins found in asphaltene (Bondon et al., 1994).

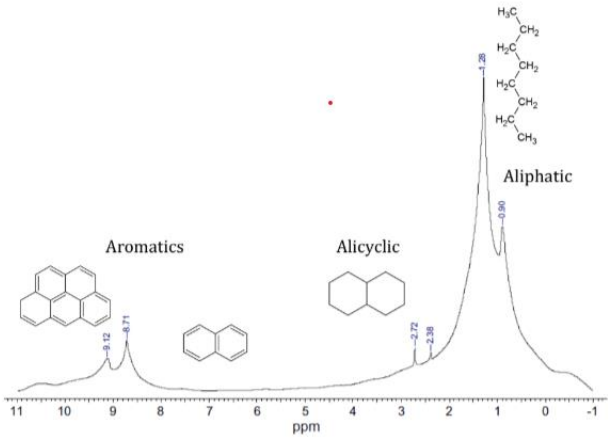

Figure 2-5. NMR spectrum of asphaltene (Ok & Mal, 2019).

Scanning electron microscopy or SEM is sued to visually characterize asphaltene crystalline particles. A SEM image of asphaltene generated by backscattered electrons together with the corresponding energy-dispersive spectroscopy or EDS is presented in Figure 2-6. Massive, irregularly shaped particulates with diameters between 0.2 and 1.2 μm were seen. There can be no discernible intensity variations since the contrast is consistent according to the specified range. The elemental chemical structure is homogeneous because SEM gathers backscattered electrons to the scale displayed, dark contrasting evaluation is necessary for assessing elemental variations (Luo et al., 2010). According to the EDS scan, the predominant components C, O, V, and S are present in the following concentrations: 72.23, 7.79, 0.62, and 19.36 wt%, correspondingly (Arenas-Alatorre et al., 2016).

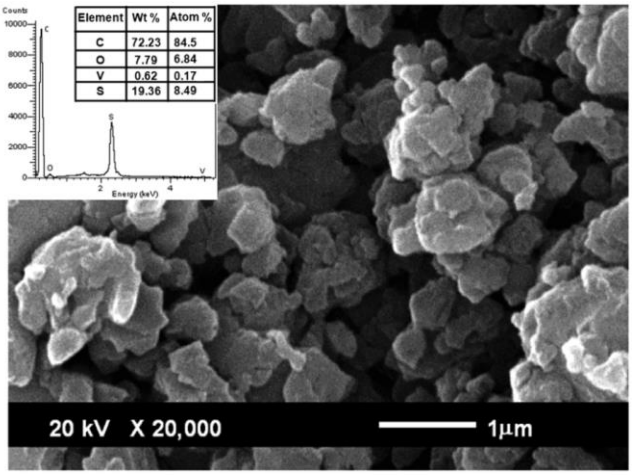

Figure 2-6. SEM image of a pure asphaltene with EDS analysis (Arenas-Alatorre et al., 2016).

2.1.2 Asphaltene phase envelope

Asphaltene begins to deposit in the wellbore and the associated production equipment when the wellhead pressure of particular wells fell below the onset pressure Po. Asphaltene deposition ceases when the pressure exceeds the Po (Leontaritis and Mansoori, 1989). Hence, initiation of asphaltene flocculation is influenced by pressure, primarily. Wellbores operating at greater production rates, which resulted in higher temperatures, have a lower onset pressure (Po) compared with wellbores running at lower temperatures. This suggests that the onset pressure is also temperature dependent. Hence, creation of the asphaltene phase relies on combination of pressure and temperature condition (Leontaritis, 1996).

Asphaltene Deposition Envelope or ADE is the P-T diagram of asphaltenic fluids. A crude oil's ADE and V-L envelope are shown in Figure 2-7. The VLE and ADE overlap greatly. The is no critical point in this P-T diagram because to have a critical point a fluid requires to have the both bubble point and dew point lines. The difference between black oil and asphaltenic fluid is important. Dew point lines are absent in asphalt. Asphaltenes breakdown at high temperatures nd does not vaporize. The P-T diagram of an asphaltenic fluid should show a bubble point line, upper and lower asphaltene deposition envelope (ADE) boundaries, and asphaltene phase quality lines.

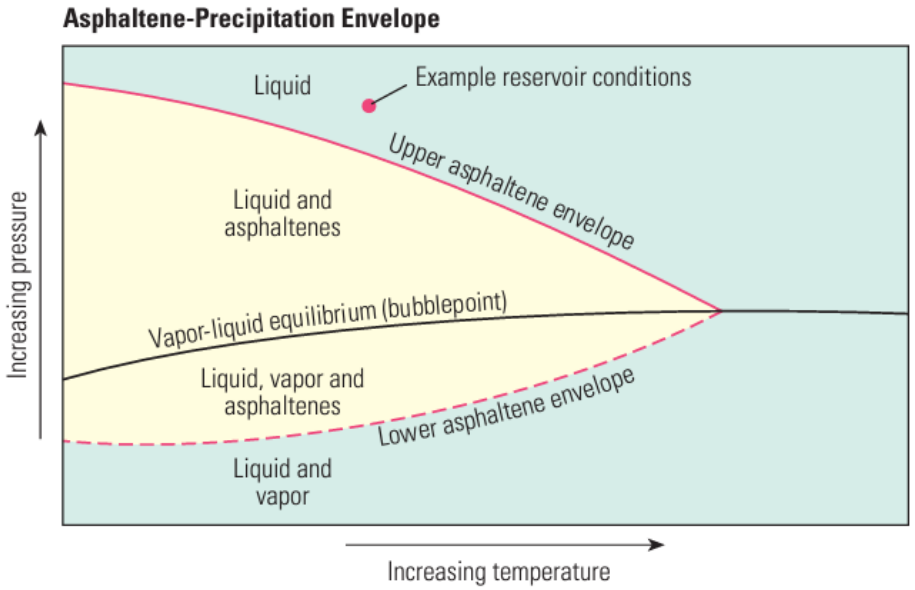

Figure 2-7. Asphaltene precipitation envelope (Akbarzadeh et al. 2007).

Certain reservoir fluids with asphaltenes flocculate irreversibly. After reaching the top ADE threshold some asphaltenes will not disperse, either during sampling or production stage and return back to a stable suspension by reversal of the thermodynamic condition. Since one must exceed the ADE to achieve a lower ADE limit for reservoir fluids, it is sometimes hard to determine the reversibility. Due to irreversible clumping, the asphaltenes and lower (and higher) ADE boundary would change permanently. Reaching the bottom of the Asphaltene Deposition Envelope (ADE) without asphaltene flocculation may be possible (Leontaritis, 1996).

2.1.3 Asphaltene adsorption mechanism

Asphaltenes' carboxylic and phenolic acid classes cause them to adsorb on solid objects either as single particles or in the form of colloidal clusters of varying dimensions. The interactions exerted by the functional chains of the NPs used and the primary active groups of the asphaltenes, such as carbonyl, sulphite, and thiophenic, contribute the asphaltenes to adsorb more favorably onto NPs. Mechanism of how asphaltene particles adsorbs onto NPs are illustrated in Figure 2-8 (Medina et al., 2019).

Figure 2-8. Asphaltene adsorption mechanism onto NPs (Medina et al., 2019).

Solid-liquid equilibrium theory (SLE) has been used to examine the interactions between asphaltenes and NPs. The model provides identifying the adsorption isotherms of *n*-C_7 asphaltenes through various solid surfaces based on three parameters: Henry's law constant (H), constant of *i*-mer reactions (K), and maximum amount adsorbed. H express the adsorption affinity between the adsorbent-adsorbate pair, where the higher the H value, the lower the affinity. K is an index of

quick aggregation of asphaltenes once the primary sites over the NPs are engaged (Montoya et al., 2014).

2.1.4 Asphaltene deposition mechanism

Asphaltenes typically consist of aliphatic and aromatic chains in their molecular structure. The aromatic half contains a polynuclear aromatic group; whilst, the aliphatic side that is the first region surrounded by the following includes alkyl chains of various scale. The π–π and H-bond affinities within the aromatic compounds are linked to the binding of the asphaltene particles. On the other hand, steric reluctance among aromatic layers is induced by aliphatic chains. It implies that the coexistence of polar and nonpolar groupings enhances their propensity for self-association (Medina et al., 2019).

Asphaltene particles naturally form aggregates through a series of processes including precipitation, flocculation, and deposition (see Figure 2-9). Asphaltenes particles experience flocculation after precipitation resulting in formation of larger molecules that remain suspended in the solution (Nghiem et al., 1993). Due to their large size, the flocculated asphaltenes have the ability to either remain suspended in crude oil flow or settle on formation rock surfaces causing damage (Sanchez, 2007). Conversely, the term "deposition" specifically describes the process of asphaltene flocculated particles settling on rock surfaces (Bin-Shan et al., 2001). Occasionally, the process of precipitation is confused or interchangeable sued with deposition. It is important to understand that the process of deposition during production is very complex compared with precipitation. Asphaltene deposition occurs through mechanisms of adsorption, plugging, and entrainment as illustrated in Figure 2-9. If the local oil velocity is high, then the flocculated asphaltenes can either be adsorbed onto the rock surface, trapped in porous media, or washed away by oil through entrainment. The deposition process begins when the flocculated asphaltene particulates adsorb onto the rock surface. Adsorption follows the principles of irreversible thermodynamics. Research suggests that asphaltene deposition occurs when the particles are adsorbed and retained hydrodynamically at pore throats. Deposition occurs not only due to adsorption, but also as a result of mechanical trapping. This trapping has similarities to the deposition of particles on a porous material. Deposition through mechanical entrapment, sometimes referred to as plugging deposit, is a very complex process that plugs the pore throat. Asphaltene deposition and adsorption are influenced by various factors including presence,

thickness, and durability of water layer on the rock surface, mineralogy of the reservoir rock, and resin content of crude oil (Khanifar et al., 2011).

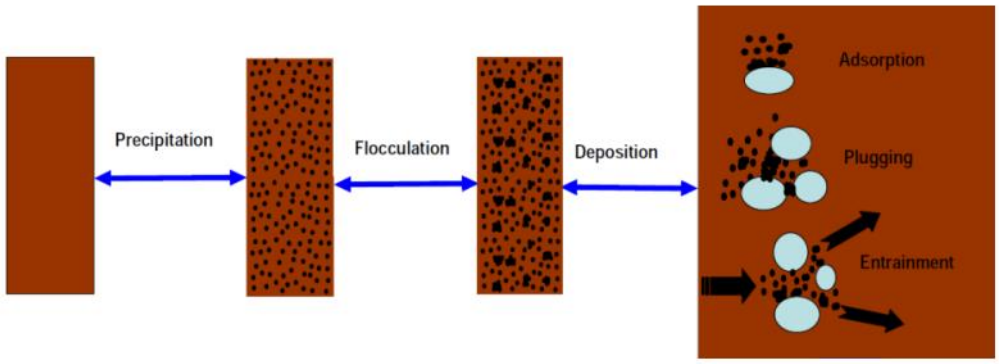

Figure 2-9. Asphaltene deposition process (Yi et al., 2009).

2.1.5 Asphaltene related issues

Asphaltenes can solidify and create deposits in porous materials, pipelines, production lines, and refining plants and equipment because of composition (X), pressure (P), and temperature (T) of the crude oil. These deposits can lead to operational problems (Demirbas, 2016). Occurrence of asphaltene precipitation and deposition problems in oil fields is illustrated in Figure 2-10. Asphaltenes in their solid state can obstruct the pores in the formations, decrease the effective porosity, impair the permeability, and alter the rock's wettability, and crude oil viscosity, resulting in significant damages to the reservoir causing economic loss (Soulgani et al., 2011). Nevertheless, asphaltenes might give rise to several complications during the refining process. Buildup of coke on equipment decreases its operational lifespan and increases the maintenance costs. When asphaltenes undergo thermal decomposition, coke is deposited on refining equipment. Coke hinders the movement of fluids and heat, leading to decreased efficiency and operational problems (Hassanzadeh & Abdouss, 2023).

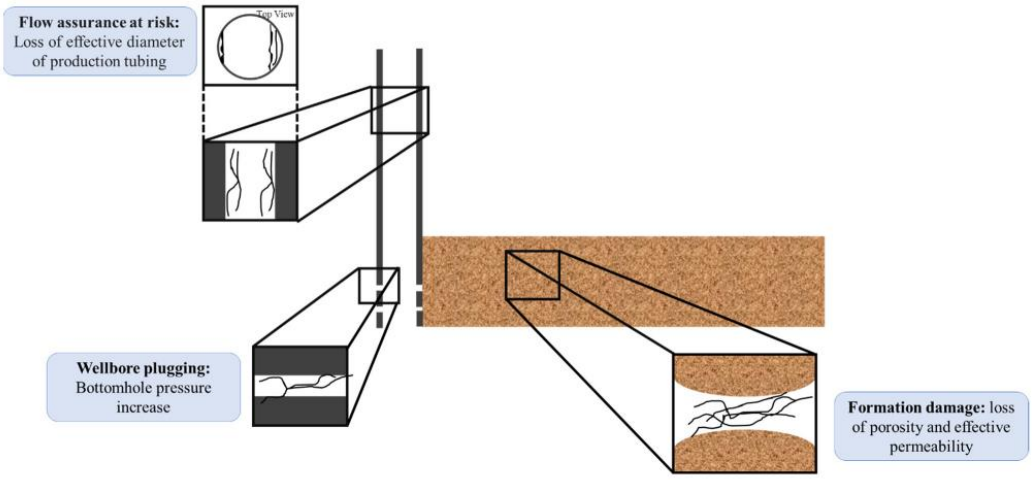

Figure 2-10. Asphaltene deposition consequences (Guerrero-Martin et al., 2023).

The postulated mechanism of "pore throat plugging" results in permeability reduction. A schematic representation of these four mechanisms is presented in Figure 2-11. When the openings in the pores are blocked, the speed of the fluid flow increases at the center of the pore and around the narrow parts of the pore because the available space for the fluid to flow through is limited. This happens as long as the pressure at the entrance remains the same. The flow of crude oil containing particles increases the velocity of the fluid in the pores and causes mixing at a small scale, which results in entrainment of certain asphaltene particles on the inner surfaces. In addition, the higher pore velocity causes expulsion of asphaltene particles from narrow passages in the pores, which enables the fluids carrying the particles to flow more easily through partially reopened constrictions in the pores. The "pore throat opening" mechanism may account for the partial re-opening of the clogged pore throats, which could explain why a porous medium never becomes entirely blocked during natural depletion (Kord et al., 2014).

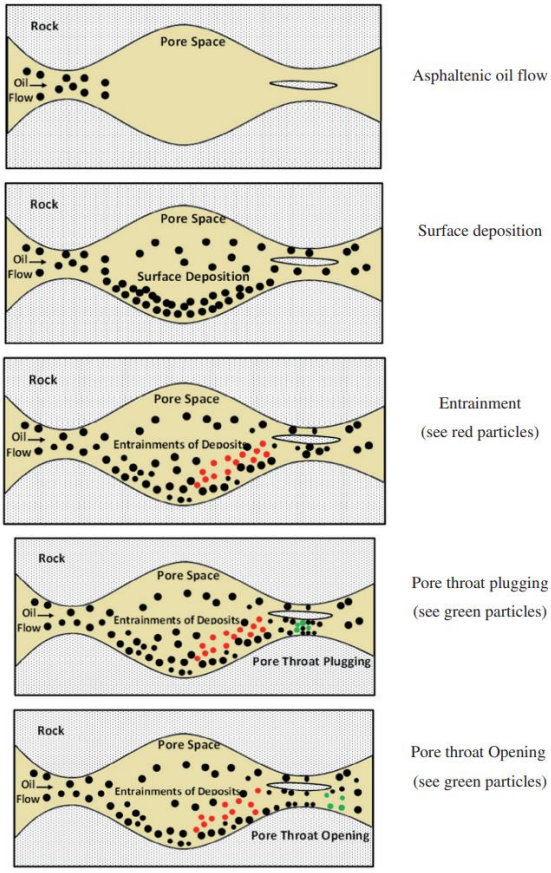

Figure 2-11. Asphaltene surface deposition (Kord et al., 2014).

2.2 Factors affecting asphaltene precipitation

2.2.1 Change in pressure

The solubility of asphaltene in crude oil is affected mostly by pressure changes. Above the bubble point pressure (P_b), reducing pressure leads to decrease in crude oil density and solubility until it reaches to its minimum value at P_b (Figure 2-12). Reduced pressure, however, causes gas to come out of solution from the crude oil below the P_b, increasing the solubility. Increasing pressure leads to an increase in both asphaltene deposition rate and amount (Burke et al., 1990). Asphaltene deposition usually occurs due to pressure depletion, and several researchers have reported an increase in pressure drop when asphaltene is deposited on tubing's walls (Broseta et al., 2000). Soorghali et al. also reported increase in asphaltene deposition on slide glasses in a HPHT cell with increase in pressure (Soorghali et al., 2014).

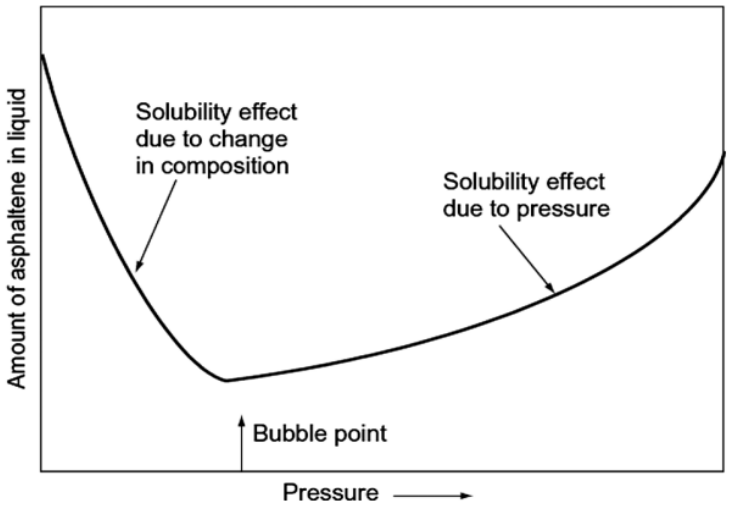

Figure 2-12. Effect of pressure on asphaltene solubility (Burke et al., 1990).

2.2.2 Temperature change

The impact of temperature on asphaltene deposition is a contentious issue because of many contradictory trends. In general, is it believed that when temperature rises, asphaltene deposition increases (Mohammadi et al., 2016). The influence of surface temperature on asphaltene deposition is presented in Figure 2-13. Deposition of asphaltenes is primarily influenced by diffusivity of asphaltene particles and the rate at which they bind to surfaces, both of which are affected by surface temperature. There is a linear correlation between mass transfer coefficients and temperature; while, the attachment rate constants exponentially increase with increase in surface temperature based on the Arrhenius relationship. The presence of a non-linear trend in Figure 2-13 indicates that both approaches make a significant contribution to the overall deposition rate (Jamialahmadi et al., 2009).

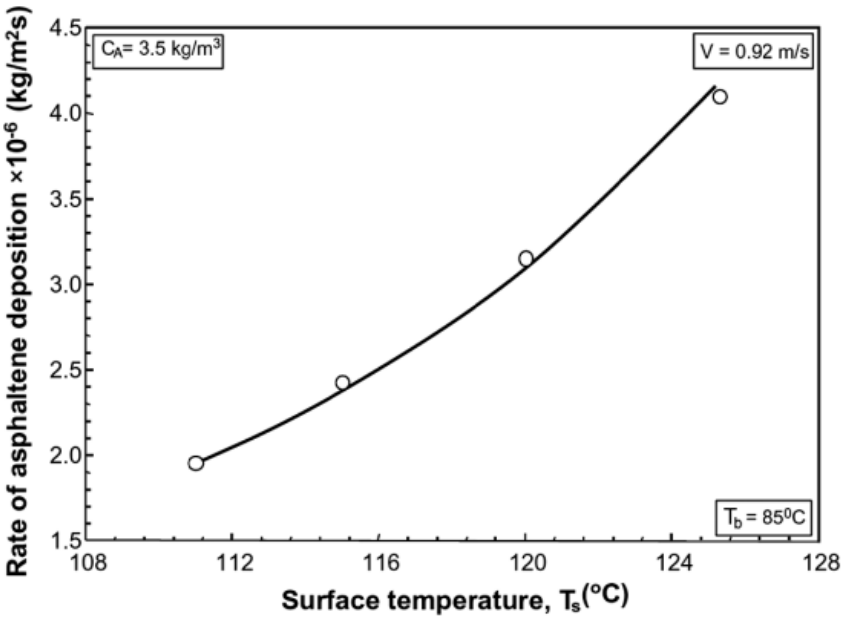

Figure 2-13. The effect of temperature on degree of asphaltene deposition (Jamialahmadi et al., 2009).

2.2.3 Amount of precipitant

According to Wang et al. (2004), concentration of *n*-alkane in crude oil has an impact on asphaltene deposition. The solubility characteristics of the fluid was examined to ensure asphaltene deposition. For higher *n*-alkanes, a greater asphaltene deposition amount was achieved (Wang et al., 2004). Lawal et al. (2012) examined how various *n*-alkanes affected the deposition of asphaltene in a capillary tube and reported that using precipitates with higher carbon ratios increased the intensity of deposition (Figure 2-14). However, the authors were unable to correlate the amount of precipitant and rate of the deposition (Lawal et al., 2012). In general, the findings point on to the possibility that the type and proportion of the precipitant used may have an impact on concentration and thickness of the asphaltene deposition.

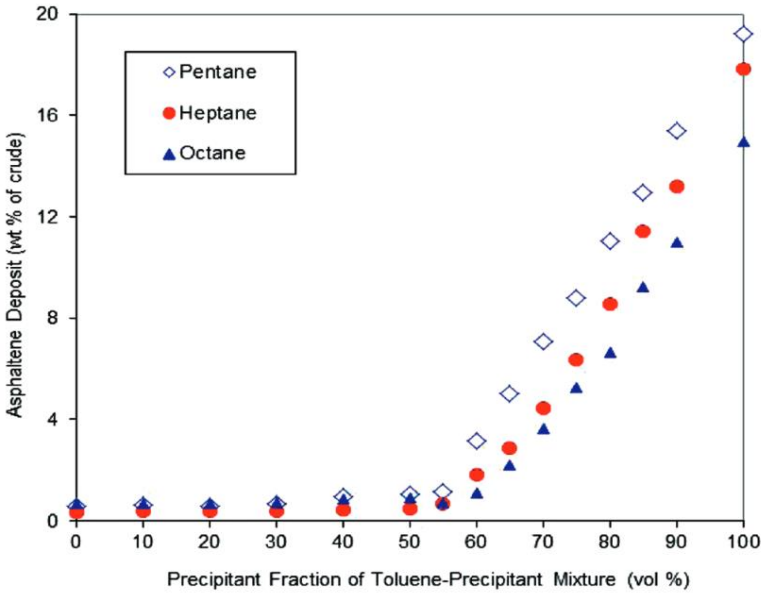

Figure 2-14. AOP as a function of precipitant/solvent ratio (Lawal et al., 2012).

2.2.4 Oil density

De Boer et al. (1995) proposed a screening technique base on thermodynamic model of asphaltene solubility to screen different crude oil samples for their tendency to precipitation. They concluded that the probability of asphaltene precipitation is greater in light crude oils (in under saturated reservoirs where $P>P_b$) with lower asphaltene content for a unit change in pressure. Depressurizing crude oils below P_b will result in a quick increase in asphalt solubility (i.e., less tendency to precipitate asphaltene) due to compositional changes in the liquid. Nevertheless, heavy crude oils despite having a significantly higher asphaltene content tend to have lower probability of asphaltene precipitation near bubble point assuming that $P = P_b$ (De Boer et al., 1995).

2.2.5 Oil viscosity

Crude oils with higher viscosities often show lower asphaltene deposition because they typically include lighter crude oils that stabilize the asphaltene molecules. Soorghali et al. (2014) conducted PVT tests to examine the impact of both P and T on deposition of asphaltene and reported how increase in the resin content causes asphaltene particles to stabilize. (Soorghali et al., 2014). The authors concluded that increase in P reduces the resin's equilibrium, especially at higher resin concentrations. Precipitation of asphaltenes can occur due to differences in composition of crude oil. The solubility of asphaltenes in crude oil minimizes as the volume of dispersed gases increases (Burke et al., 1990).

2.2.6 Gas injection

Zanganeh et al (2018) conducted visual experiment to assess the impact of injection of various gas types (i.e., CO_2, H_2, CH_4, and N_2) for EOR on asphaltene precipitation and deposition. The scientists reported that N_2 as an inert gas had no impact on stability of asphaltene particles yet CH_4 and CO_2 had a considerable impact on deposition of asphaltene during gas injection. Injection of both CO_2 and CH_4 increased the amount of asphaltene deposition with CO_2 having a greater amount of asphaltene precipitation (Zanganeh et al., 2018).

2.3 Asphaltene mitigation measures

Problems caused by asphaltene may be resolved either before or after precipitation and deposition. A concise overview of the processes involved in inhibiting, mitigating, and removing asphaltenes is presented in Figure 2-15. Early approaches for asphaltene deposition mitigation mostly focused on its removal (Jeffries-Harris & Coppel, 1969). Conventional methods such as scrapers and aromatic solvents are inefficient in terms of time, cost, and their negative impact on the environment (Albannay et al., 2010). Ultrasonication and chemical injection may reduce the occurrence of asphaltene deposition. Properties of both crude oil and asphaltene, thermodynamic conditions, hardness of deposition, and treatment parameters all impact the processes of inhibition, mitigation, and removal of asphaltene (Vargas & Tavakkoli, 2018). In this section, common methods for treating asphaltene via physical and chemical techniques, as well as the processes involved in inhibiting or removing asphaltene are briefly described (Figure 2-15).

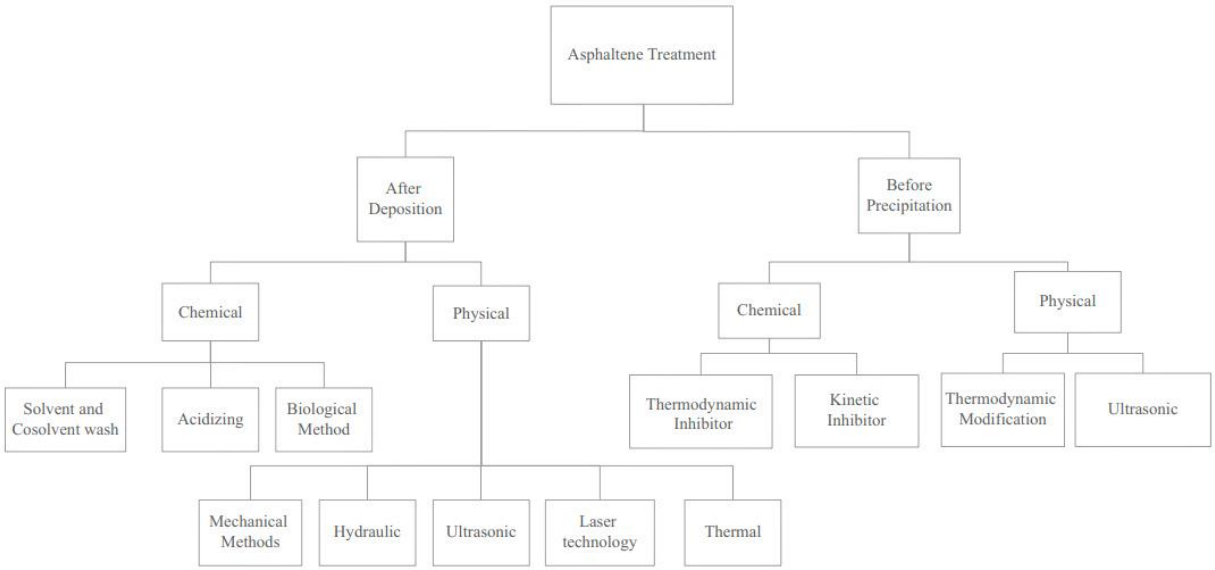

Figure 2-15. Flowchart of asphaltene treatment (Ghamartale et al., 2021).

Asphaltene may accumulate in reservoirs, wellbores, production wells, and surface treatment facilities under certain thermodynamic conditions. Severe obstructions caused by asphaltene deposition result in increased pressure drop and reduced production flow rate, leading to a complete stoppage in production. Identifying the exact place where the principal deposition (blockage) occurs poses challenges in treating asphaltene. There are chemical, thermal, physical, and biological therapies available. Chemical and physical techniques are often used. Aromatic solvents are used in chemical operations, whereas mechanical processes are used in physical approaches. While there are certain instances when heat methods have been reported to dissolve asphaltene accumulation, it is more common for wax to be the cause. Although environmentally harmless, biological methods exhibit slower treatment rates and are now under investigation in laboratories (Ghamartale et al., 2021).

2.3.1 Chemical methods

Asphaltene is a component of crude oil that dissolves in aromatic solvents like toluene and xylene (Bauget et al., 2001). Thus, aromatic solvents are often regarded as suitable solvents for dissolving asphaltene deposits. They lack environmental sustainability and have detrimental effects on both the environment and human health. Consequently, researchers are now exploring new environmentally harmless compounds such as biodegradable microbes. Acidizing and acid washing are techniques used to prevent accumulation of asphaltene around the wellbore. Acids do

not dissolve the accumulated asphaltene; instead, they breakdown the rock and provide new holes for the flow of oil. The efficacy of this approach diminishes with repetition since it does not eliminate the asphaltene (Ghamartale et al., 2021).

2.3.2 Physical methods

Researchers have investigated physical methods as an alternative to address limitations of chemical asphaltene inhibitors. For instance, electromagnetic/electrostatic, mechanical and hydraulic techniques are possible physical solutions (Mansoori, 2010). Some of physical methods have been tested under laboratory conditions.

Asphaltenes may address flow assurance in two ways. The first method lowers asphaltene precipitation and deposition by preventing agglomeration. Second method is asphaltene elimination after deposition. Preventing asphaltene deposition is usually preferable than treating it. Different chemical, physical, and biological methods may cure asphaltene deposition problem. Though promising, chemical methods harm the ecosystem. Physical techniques are not ecologically damaging but may damage industrial equipment and be less efficient than chemical operations. Slow biology is uneconomical in the field. High uncertainty in hydrocarbon resources make these techniques susceptible to reservoir conditions. For different crude oils, methods vary. Multiple techniques may be used to increase treatment efficiency. Thus, economic aspects should be addressed while determining the best therapy for each case (Ghamartale et al., 2021).

2.4 Nanotechnology

Nanotechnology and nanoscience has revolutionized many aspect of technology and human life in the 21st century from medicine to the space. Researchers have turned to nanotechnology to investigate and improve materials at atomic scale. At the scale of nano meters, the characteristics of materials ranging in size from 1 to 100 nm provide new approaches to enhance properties of the current materials and build unique ones with exceptional features. In science, “nano” signifies “billionth” or 10^{-9}. Thus, a nanometer is defined as one “billionth” of a meter. Nanotechnology involves the research, engineering, and use of nanoscale materials (Zhou et al., 2007). Nanoscale dimensions are 100 nm or less. Nanoscience has revolutionized material science by increasing the sensitivity of analytical techniques at the nanoscale level, allowing numerous applications.

Nanotechnology, is advancing various sectors in the petroleum industry with different pace. The oil refining and chemical sector are ahead of other sectors and in future nano-based materials and methods could help with drilling and production issues, as well. Nanomaterials are used as catalysts in refineries. Zeolite and alumina mesoporous catalysts loaded with various NPs are an example. Nanotechnology may remove dangerous chemicals like nitrogen oxides, sulfur oxides, and related acids and acid anhydrides from vapor using nano-filters and NPs. Another hurdle is removing mercury from oil and gas. Nanomaterials like copper oxide NPs may help solve this problem. Nanotechnology advances carbon capture and storage. Scientists and engineers are also working on oil sulfur removal. Nanomaterials for such purposes are being produced and tested (Saleh & Al-Hammadi, 2017).

Nanotechnology has various uses in life, making it the latest technique to create things with great efficiency. In processing of petroleum, effectiveness of many conversion processes increases when nanometer-scale materials are used because of superior material characteristics as particle size decreases. The main advantages of "nano-tech" catalysis are the huge surface area for reaction, which reduces undesirable and side reactions. NP catalysts are being used more to address the rising demand for chemicals and fuels due to their high activity, low deactivation, and minimal coke production (Etim et al., 2017). Use of NPs for adsorption and inhibition of asphaltene is discussed in this section.

2.4.1 Nanoparticles and nanocomposites

In theory, nanoparticles size are 1–100 nm (Rao et al., 2002). Physical and chemical qualities of NPs are somewhere between element atoms and bulk material. The advantages of these materials over bulk (microparticles > 1 μm) include size-dependent functionalities. Color change and phase shift become important when the size approaches the nanoscale (Etim et al., 2017). NP photovoltaic cells absorb more radiation than thin films of continuous sheets due to their unique physical features. Quantum confinement in semiconductor particles, surface plasmon resonance (SPR) in certain metal particles, and chemical reactivity used in photography are further examples of size-dependent feature changes (Lindsay, 2010). Materials with more surface atoms have higher surface-to-volume ratios available and chemical potentials (Zhou et al., 2009).

At least one phase of a NP/NC has 1, 2, or 3 dimensions smaller than 100 nm. Thus, a NC/NP contains a bulk matrix and at least one nano-dimensional aspect with distinct

characteristics. Due to structure and chemistry differences, the reinforcing phase's high surface-to-volume ratio, and/or aspect ratio, nanocomposite properties differ greatly from constituent and conventional composite materials (Etim et al., 2017). A reinforcement surface area shows that a tiny quantity of nanoscale reinforcement affects NP/NC macroscale characteristics. For instance, adding carbon nanotubes increases conductor bulk material thermal and electrical conductivity. Some NPs/NCs improve dielectric, optical, heat resistance, and mechanical properties. Porous media, gels, colloids, and copolymers are NCs. A NC's mechanical, thermal, electrical, optical, catalytic, and electrochemical capabilities change greatly from its component compsition. Size limits for these effects include 5 nm for catalysis, 20 nm for softening a hard-magnetic nanomaterial, 50 nm for refractive index alteration, and 100 nm for super magnetism, matrix dislocation, or restriction mechanical strengthening (Kamigaito 1991).

2.4.2 Application of NPs/NCs for asphaltene adsorption and inhibition

Asphaltene can absorbed onto a variety of surfaces including minerals and metals. NPs can be used to inhibit aggregation and precipitation of asphaltene. The effectiveness of a nano-inhibitor depends on factors including their size, surface area, surface acidity, solution pH, and asphaltene characteristics (Ghamartale et al., 2021). NPs have a high surface area (Shojaati et al., 2017). Smaller NPs with large specific surface area are more effective asphaltene precipitation inhibitors. However, they effectiveness also depends on chemistry of the NP (Madhi et al., 2017). Acidity of NPs and pH of the solution also can affect their inhibitory properties. Higher inhibitory efficacies can be achieved by modification of surface affinity of NPs using chemicals (Ghamartale et al., 2021). This is also known as functionalization.

Ansari et al. (2023) investigated asphaltene adsorption onto surfaces of magnetite, hematite, calcite, and dolomite NPs in presence and absence of water. Adsorption tests were conducted in two and three phase systems using asphaltene-solvent mixture + NPs + water. The findings indicated that the asphaltene, specifically its nitrogen and aromatic rings as a functional group significantly affect asphaltene adsorption. The significance of these factors was also validated using the relevancy factor function (RFF) as a sensitivity analysis method. Iron oxide NPs exhibited the greatest asphaltene adsorption capacity. The asphaltene adsorption reduced in absence of water. Adsorption isotherm models demonstrated how the adsorption operation was affected by adsorption of asphaltene on the exterior shell of FeO and lime NPs. Hydrogen binding

is what holds asphaltene particles together, and the addition of water may alter this bonding greatly. This indicates that adsorption of substance decreases when the outermost layers of an adsorbent is subjected to humidity because water competes for surface adsorption sites. However, water does not totally inhibit adsorption of asphaltene. The researchers concluded that, Oxygen content, H/C, and average asphaltene particle size had an inverse effect of adsorption of asphaltene onto NPs. Iron oxide NPs outperformed lime NPs in competitors for asphaltene adsorption as their adsorption capacities are determined as the following order: Magnetite > Hematite > Calcite > and Dolomite.

Setoodeh et al. (2020) investigated the effect of coating Fe_3O_4 NPs with SiO_2, graphene oxide (GO), and chitosan to create CNs for adsorption of asphaltene. Adsorption test were conducted in presence and absence of each coating in both synthetic oil and crude oil. In the synthetic oil medium, asphaltene adsorption capacity of the NCs increased with decrease in NP content and temperature and increase in initial asphaltene concentration. The best performance was demonstrated by GO-Fe_3O_4 NC. The experiments with crude oil were conducted in an additional step using the optimum NC concentration under atmospheric which yielded results similar to that of the synthetic oil (Setoodeh et al., 2020).

The volume of adsorbed asphaltene decreased with increasing temperature. This demonstrates the exothermic nature of the adsorption process. As the temperature increases more asphaltene particles collide with one another raising the likelihood of aggregation and results in increase in asphaltene precipitation and decrease in asphaltene adsorption onto NCs. Additionally, the electrostatic interaction between asphaltene molecules and NCs reduces with increase in temperature. The Q_t readings of NCs in deceasing order is as the following: GO-Fe_3O_4 > SiO_2-Fe_3O_4 > Fe_3O_4 > chitosan-Fe_3O_4 (Setoodeh et al., 2020). They concluded that SiO_2 coatings reduced adsorption while GO coating and chitosan increased the adsorption.

Alemi et al. (2021) reported applying polymer-coated single-walled carbon nanotubes (SWCNT) to examine their impact on AOP shift. The dimension of carbon particles was between 9 to 11 nm determined by TEM examination. The dynamic viscosity changes as a consequence of *n*-C_7 titration at different SWCNT dosages at 25°C are shown in Figure 2-16. As the precipitating agent concentration (*n*-C_7) rises, crude oil's viscosity decreases until the asphaltene particulates split from the solution. Here AOP is the deviation point. A comparison between the treated and untreated crude oil with varying doses of SWCNTs is presented in Figure 2-16 that indicates

presence of carbon nanotubes has caused a delay in asphaltene precipitation. The highest increase in AOP which indicates the greatest delay in asphaltene synthesis was seen at a concentration of 100 ppm of SWCNTs. The effectiveness of carbon nanotubes in preventing asphaltene precipitation has diminished at higher concentrations (200 and 400 ppm). Increasing the concentration of SWCNTs from 50 to 100 ppm leads to a greater formation of an electron cloud in the crude oil phase resulting in a stronger and more $\pi - \pi$ interactions between the electron cloud of the SWCNTs' aromatic rings and the asphaltenes. Increasing the concentration of SWCNTs to higher values (200 and 400 ppm) eventually results in self-aggregation of carbon nanotube particles. This self-aggregation leads to a decrease in performance of the SWCNTs for adsorbing asphaltenes (Alemi et al., 2021).

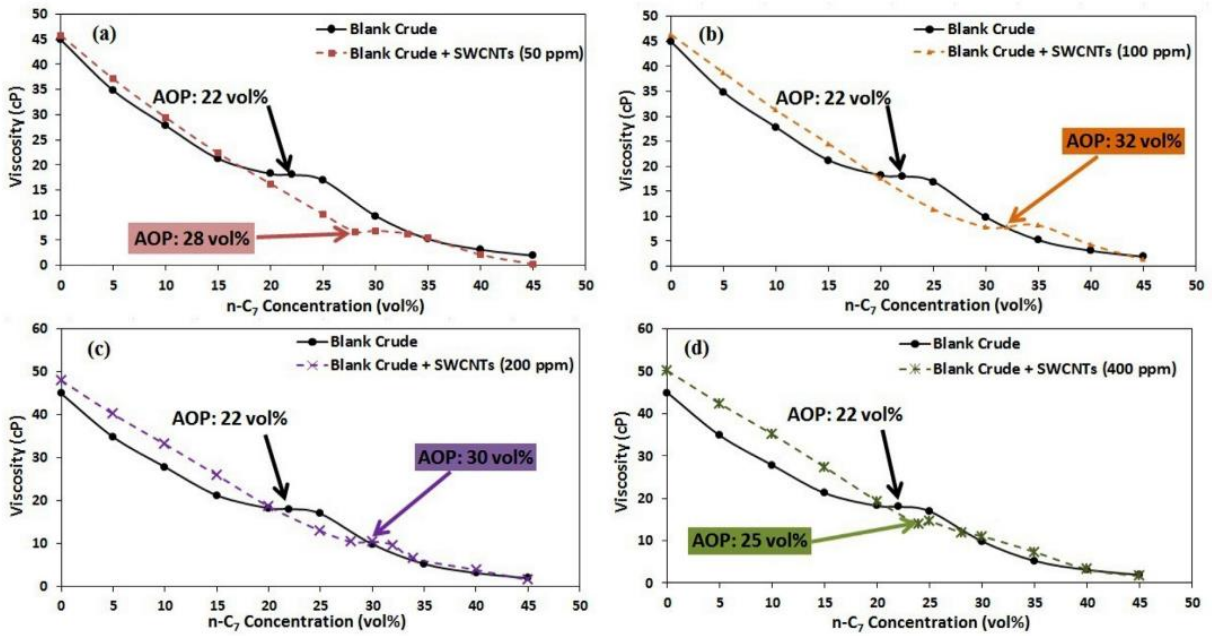

Figure 2-16. Impact of SWCNTs concentration on viscosity modification of crude oil (Alemi et al., 2021).

2.4.3 NPs/NCs characteristics' effect on asphaltene inhibition

According to Tarboush and Husein (2015), it is possible to recover NPs/NCs. The NPs/NCs jointly with the adsorbed asphaltene were retrieved using centrifugation at a speed of 5,000 rpm for 20 minutes. The top phase was poured out and the bottom phase was collected. The material that was adsorbed by UV and deposited was let to drain for 24 hours after centrifugation. It is important to mention that despite centrifugation for up to 1 hour, a tiny quantity of NPs/NCs remained at the bottom. This is due to the extremely strong permanence of the NPs/NCs in heavy oil. Still, the

gathered specimen was suitable for conducting every test and was considered to be relevant (Tarboush & Husein, 2015).

Asphaltenes' adsorption process is impacted by NP/NC size. Comparisons had been made between 48 nm alumina NPs and 200 μm particles that mainly differed in size. The findings indicate that compared to micro-alumina, nano-alumina has a greater adsorption capacity which is expected. Additionally, asphaltene oxidation on nano-alumina closely matches the Langmuir model. Together, these findings suggest that there may be various pore architectures, functional class categories, and area thicknesses in the collected elements (Nassar et al., 2011).

The NPs/NCs' surface acidity has a big impact on how well they are able to adsorb. *n*-C_7 asphaltenes were absorbed by an aromatic solvent using three various categories of NPs (metal oxides, amphoteric and basic). Asphaltenes absorb onto acidic NPs more effectively compared with other types of NPs (Hosseinpour et al., 2013). A titration method was used to assess the acidity of asphaltenes (Fan & Buckley, 2007). Comparable findings were made where Alumina NPs were evaluated for removal of *n*-C_7 (Nassar et al., 2011a). Acidic alumina has a significant ability for adsorbing asphaltenes despite having the smallest surface size.

The characteristics of NPs must match those of the asphaltenes to improve the adsorption. For instance, basic NPs must be selected if asphaltenes is basic (high pH). If the asphaltenes' contact charges are negative, then the net electrical charge of NPs' surface needd to be positive with the goal to improve the thermodynamics of adsorption (Mazloom et al., 2020).

Miadonye and Evans (2010) investigated solubility of asphaltene in various solvents. They reported a comparative analysis of the molecular connections occurring in different crude oil mixtures. They concluded that toluene decreases viscosity and increases dipole–dipole and heteromolecular relations owing to asphaltenes' polar elements. Intense hydrogen binding and low homo-molecular contacts dominate heavy naphtha, further effective viscosity reducer. Hydrogen binding reduces asphaltene precipitation and blending enthalpy similar dipole–dipole interactions. Hexane and light naphtha have increased the blending temperatures and asphaltene precipitation owing to their molecular packing and homo-molecular connections (Miadonye & Evans, 2010).

2.4.4 Nanocomposites (Polythiophene, NiO, Fe_3O_4)

In this section, asphaltene-adsorbing NPs and NCs with close relation in composition to the N used in this research work are reviewed. NPs possess a large surface area and can be surface functionalized. They work differently depending on their chemical composition, synthesis method, size, and surface features. NPs' physico-chemical attraction for some surfaces provides several uses including controlled adsorption of undesirable elements within a fluid. Attraction for asphaltenes and the capacity to place at the oil-water contact enables successful demulsification of stable crude oil emulsions. Another method is to permanently connect catalytic NPs to a matrix, termed nanocomposites or NCs. NCs usually outperform NPs in durability, processability, and inherent benefits from NP-matrix interplay. Magnetic NPs can also improve demulsification by adsorbing the emulsion droplets (Wang et al., 2015). An external magnetic field causes the droplets to cluster and separate. Functionalization processes can add certain functional groups to provide interfacial activity, one of the most notable features of NPs (Farooq et al., 2021).

Table 2-1. Overview of research on the adsorption of asphaltene by various NPs/NCs.

NP/NC	Measurement	Isotherm type	Results (capacity comparison)	References
NiO	UV	Langmuir	NiO had the greatest adsorption capability, while ZrO_2 demonstrated the fewest.	(Hosseinpour et al., 2013)
Fe_3O_4-NiO	TGA	Langmuir	Titanium dioxide and nickel oxide have a higher BET surface area when compared with different nanoparticles.	(Nassar et al., 2011)
Fe_3O_4, NiO	TGA	Langmuir	Order of catalytic activity and oxidation: NiO > Co_3O_4 > Fe_3O_4	(Nassar et al., 2011b)
In situ generated versus commercial NiO	TGA	-	In situ generated NiO has a greater adsorption capacity compared with commercial NiO. In situ NiO disperses better and ultilayer adsorption occurs.	(Tarboush & Husein, 2012)
Fe_3O_4	UV-vis	Langmuir	Adsorption affinity is directly linked to molecular weight of asphaltene. The rate of adsorption rises as the MW of asphaltene decreases.	(Nassar et al., 2012)

NiO	UV, TGA	SLE	The catalytic efficiency of the NPs decreased as the size of asphaltene aggregates grows.	(Franco et al., 2015)
Fe_3O_4	UV/TGA	Langmuir	According to the TGA data, the NPs accelerated the oxidation of asphaltene in the reverse order of their greatest adsorption capacity, measured in mg/g. (Al_2O_3 > Fe_2O_3 = Fe_3O_4)	(Ezeonyeka et al., 2018)
Fe_3O_4-Chitosan	UV	Langmuir	Fe_3O_4-Chitosan composite exhibits efficient adsorption of asphaltene and has the capacity to regulate emulsions' stability.	(Kazemzadeh et al., 2018)

NiO metal NPs have shown a great capacity for asphaltene adsorption. Franco et al. (2013) investigated the adsorption behavior of NiO mixed with nanoparticulated alumina. Authors concluded that an increase in NiO concentration leads to higher adsorption (Franco et al., 2013). In addition, it can be used in any type of crude oil, light or heavy. Researchers considered both Langmuir and Freundlich isotherm adsorption models to understand adsorption kinetics of asphaltene adsorption onto NiO NPs. NiO has a significant capacity for adsorption with catalytic function (Tarboush & Husein, 2012). Efficient synthesis and evaluation of scattered NiO NPs with characteristic diameters of 12±5 nm allowed determination of adsorption dynamics and asphaltene adsorption.

Because of its superior thermal endurance and exceptional environmental harmony, polythiophene has drawn a lot of interest. Polythiophene polymer inhibits NP aggregation and enhances its absorption capacity. Additionally, polythiophene compounds are semiconductor and have improved physical qualities and processing simplicity (Uygun et al., 2009). As shown in Figure 2-17, PT has conjugated double bonds structure that gives the polymer good intrinsic conducting ability.

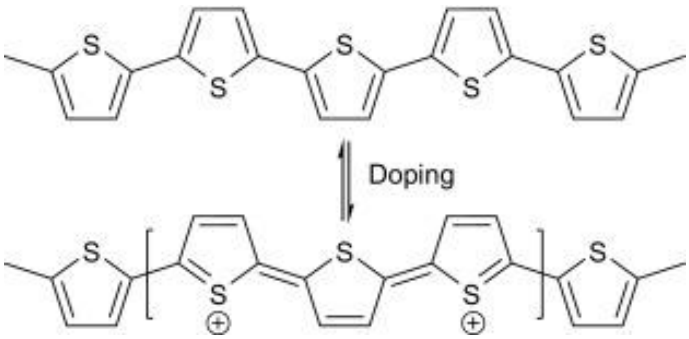

Figure 2-17. Structure of polythiophene (Ramesan & Suhailath, 2017).

Coating pure NPs with polymer can enhance adsorption of asphaltene (Talebi et al., 2023). Tazikeh et al. (2020) investigated the effect of Fe_3O_4 coated by Polythiophene coating in asphaltene precipitation inhibition. During the experiment, metastable zone width was examined. Asphaltene particles were adsorbed onto the surface of the NC. In synthetic crude oil, adsorption mechanism greatly shifted the AOP. The optimum amount of NC for shifting asphaltene precipitation was found 0.1 wt% of Fe_3O_4-PT (Tazikeh et al., 2020). Heavy oil has higher absorption compared with light crude oils as illustrated in Figure 2-18. In addition, equilibrium time in light crude oils was less than heavy oil. Fe_3O_4 has high adsorbent capacity because of its surface chemistry and solubility (Tombácz et al., 2007). In an observational investigation, Nassar et al. (2012) showed that asphaltenes' ability to bind at Fe_3O_4 to a greater degree enhanced with lowering MW of the crude oil.

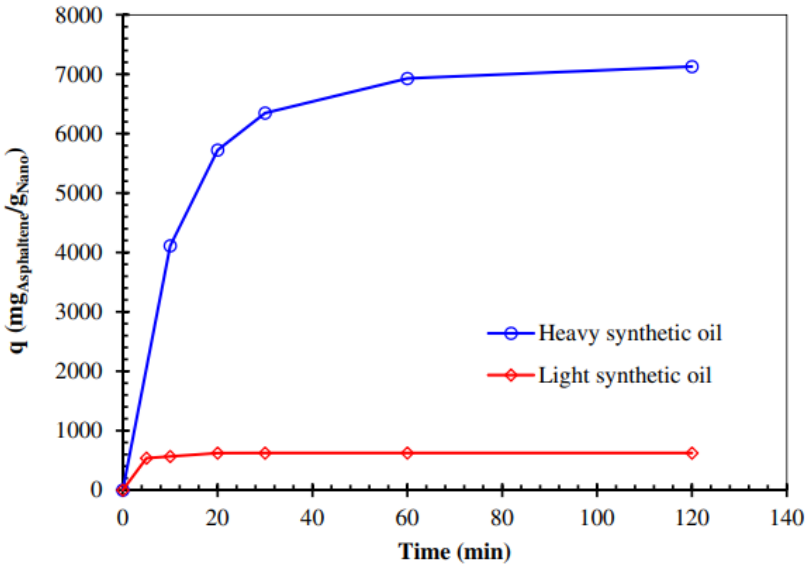

Figure 2-18. Adsorption kinetics of asphaltene adsorption (Tazikeh et al., 2020).

Fe_2O_3 coated with PT is a magnetic NC. Magnetic property of this NC potentially affects the adsorption performance of asphaltene particles. The magnetic NC attracts more asphaltene particles with strong magnetic power and enhances adsorption capacity of the Fe_2O_3-PT NC.

Setoodeh et al. (2018) investigated adsorption of asphaltene by adding PT coating on Fe_3O_4 NPs. The objective was to look into possible benefits of coating for asphaltene adsorption. Capacity of the NC for asphaltene adsorption in a synthetic crude oil, asphaltene-toluene mixture, was assessed. The measured surface area for Fe_3O_4 NP and Fe_3O_4-PT NC are reported 71.64 m^2/g and 73.63 m^2/g, respectively. The fact that these nanomaterials possess a very high surface area and are functionalized makes it a top candidate for asphaltene adsorption. The amount of asphaltene adsorption onto Fe_3O_4 NP and Fe_3O_4-PT NC in a synthetic crude oil medium is shown in Figure 2-19. Where Y-axis indicates adsorbed amount of the asphaltene and X-axis indicates mass ratio of the NP. Identical patterns were observed in the data when it came to adsorption from synthetic crude oil. Compared to Fe_3O_4 NP, Fe_3O_4-PT NC showed a greater adsorption. The q_t readings reported are higher than experiments with asphaltene-toluene, because the initial concentration of asphaltene (1.38 wt%) was greater than that of the synthetic crude oil. As the initial NP content increased, the adsorption was dropped. The tendency of the NP to aggregate rises with increasing NP dosage because their active sites shrink and the amount of asphaltene compounds that can be adsorbed on their outermost layer is reduced. The adsorption rates of asphaltene on NP and NC were reported 65.94% and 78.98%, correspondingly.

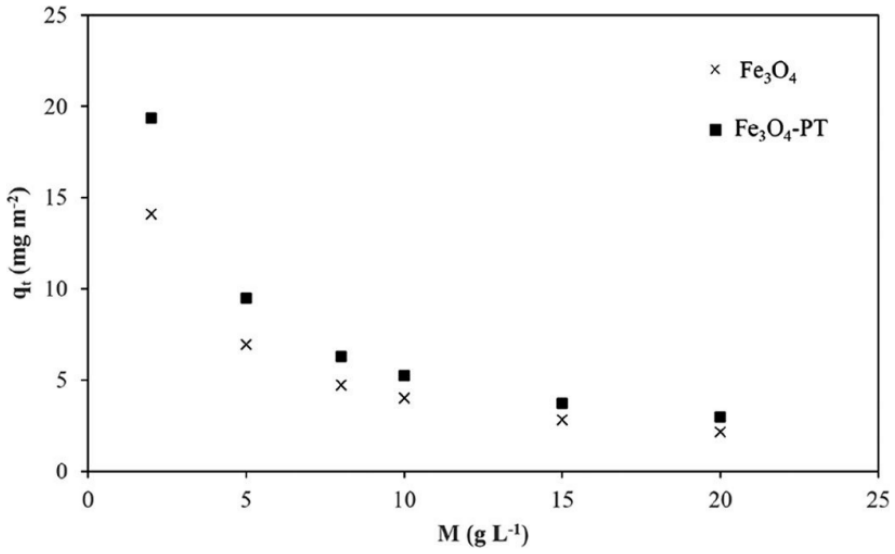

Figure 2-19. The amount of asphaltene adsorption for Fe_3O_4 NP, Fe_3O_4-PT NC (Setoodeh et al., 2018).

These research works have demonstrated the feasibility of using nanomaterials for asphaltene adsorption and inhibition from crude oil medium. The adsorption capacity of nanomaterials would increase with increase in pressure. These findings indicate that coating NPs with polythiophene can improve asphaltene adsorption and inhibition. Thus, it might be used as a unique improved agent for asphaltene precipitation prevention. Overall, the encouraging findings of these research works points to the use of various NPs functionalized with polymer coatings to enhance their asphaltene adsorption capacity.

2.5 Performance evaluation of nano-inhibitors for asphaltene

Various isotherm models were suggested in the literature to explain the process of asphaltene adsorption from fluid systems onto NPs. In this section, first these adsorption isotherms are explained and then the model fitting parameters of the adsorption isotherms are shown.

2.5.1 Classification of adsorption isotherms

Adsorption of nitrogen is a key technique for characterizing microscopic particle structure. IUPAC adsorption isotherm categorization is shown in Figure 2-20. Type I isotherm is common for adsorption on porous oxides. N_2 adsorption over macroporous or nonporous absorbents causes isotherm class II. Zero monolayer occurs for category III isotherm indicating poor absorbent contacts. Type IV isotherm describes mesoporous adsorption. Isotherm class V, like class III, is caused by poor adsorbent–adsorbate couplings in narrow relative pressure spans (P/P_o, where P is the equilibrium pressure and P_o is the saturation vapor pressure at the adsorption temperature. Type VI isotherms show incremental multilayer adsorption over homogeneous nonporous surfaces. The height about every phase in this isotherm relies on the capacity of each adsorbed layer; while, the edge varies on temperature and system form (Thommes et al., 2015). Since NPs are commonly colloidal aggregates in the continuing stage, asphaltenes may adsorb onto them using any of the following IUPAC categories. Any of the foregoing isotherms could be detected based on the pore dimension of the NP aggregates, the size and association condition of asphaltenes including related physical or chemical interacts regarding the NPs (Mazloom et al., 2020).

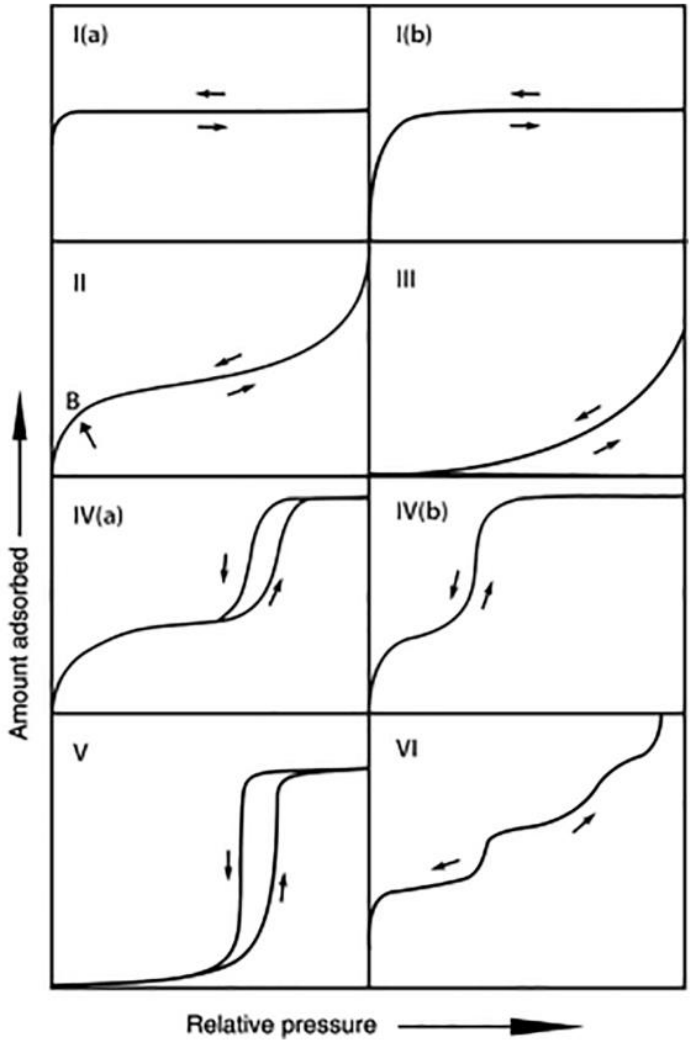

Figure 2-20. Classification of adsorption isotherms (Thommes et al., 2015).

2.5.2 Models of asphaltene adsorption isotherms

Several experimental and analytical models are proposed in the literature to explain the process of asphaltenes adsorption onto NPs. Assessing isotherms characterize the connection between asphaltene adsorption onto NPs in modeling adsorption kinetics of the process. The Freundlich and Langmuir models are accurate models that have been used modeling of asphaltene adsorption by NPs (Mazloom et al., 2020). Ezeonyeka et al. (2018) reported that asphaltenes monomers are adsorbed onto NPs rather than nanoaggregates (Ezeonyeka et al., 2018). Langmuir isotherm is used to model monolayer adsorption onto a homogenous surface (Foo & Hameed, 2010). The Freundlich model can be used for describing multilayer adsorption onto a heterogeneous surface.

Equations 2-1 and 2-2 show nonlinear and linear expression of the Langmuir isotherm model:

$$Q_e = Q_{max}(\frac{K_L C_e}{1+K_l C_e} \quad \text{Equation 2-1}$$

$$\frac{C_e}{Q_e} = \frac{1}{K_L Q_{max}} + \frac{C_e}{Q_{max}} \quad \text{Equation 2-2}$$

where, K_L is the Langmuir equilibrium adsorption constant that gives adsorption affinity. If the value of K_L is relatively larger it indicates that there is a strong interaction between adsorbate and adsorbent while smaller value implies a weak interaction.

The linear and nonlinear expressions of the Freundlich isotherm are given below (Freundlich, 1907):

$$\log Q_e = \log(K_f) + (\frac{1}{\mathrm{n}})\log(C_e) \quad \text{Equation 2-3}$$

$$Q_e = K_F C_e^{(\frac{1}{n})} \quad \text{Equation 2-4}$$

where, K_F is Freundlich adsorption constant, 1/n is adsorption intensity factor. Higher values of K_F means a larger adsorption capacity. In addition, if 1/n decreases, the adsorption affinity will increase.

Nassar et al. (2011) applied the Freundlich isotherm model to analyze adsorption kinetics of asphaltene onto various alumina surfaces. They reported a good fit between the Freundlich model and their experimental data proving existence of a multilayer adsorption mechanism. The linearity seen in the model (Figure 2-21) shows that it can be used successfully to model adsorption of asphaltenes on various alumina surfaces (Nassar et al., 2011).

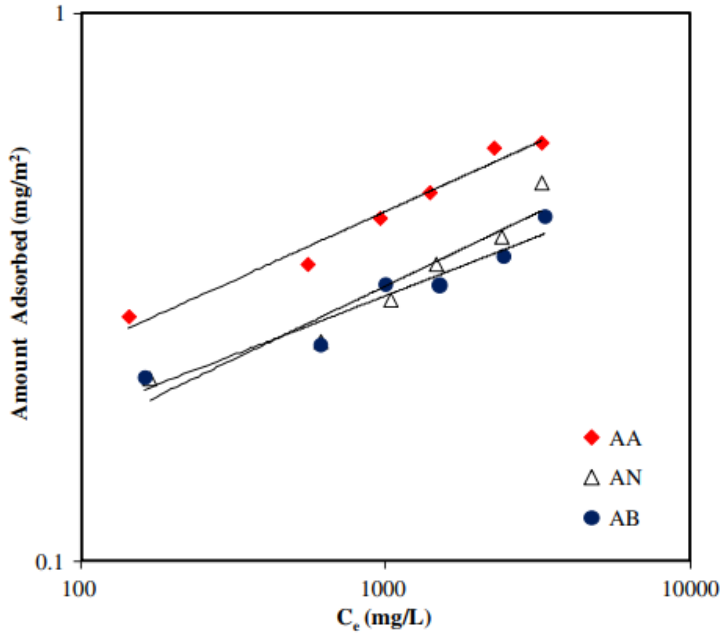

Figure 2-21. Freundlich isotherm model of asphaltene isotherms onto various alumina surfaces (Nassar et al., 2011).

2.5.3 Thermogravimetric analysis

One effective method for determining thermal stability of elements, especially polymer compounds, is thermogravimetric analysis or TGA analysis. The technique involves measuring a sample's mass loss whereas the temperature is increasing over time at a certain rate. TGA analysis is a useful tool for measuring a sample's moisture and volatile levels (Ebnesajjad & Ebnesajjad, 2013). Through TGA approach, it is possible to evaluate catalytic activity of NPs on asphaltene oxidation and behavior. Nassar et al. (2011) investigated adsorption and oxidation of asphaltenes onto two aluminas with various particle sizes (Nassar et al., 2011). Figure 2-22 illustrates the distribution for the percent conversion with the increase in the temperature for pure asphaltenes and for asphaltenes adsorbed onto micro- and nano-aluminas. Micro-alumina demonstrated higher catalytic activity on asphaltene oxidation than nano-alumina. This enhanced the catalytic effect

described by micro-alumina provided that textural properties play an important role in catalysis (Nassar et al., 2011).

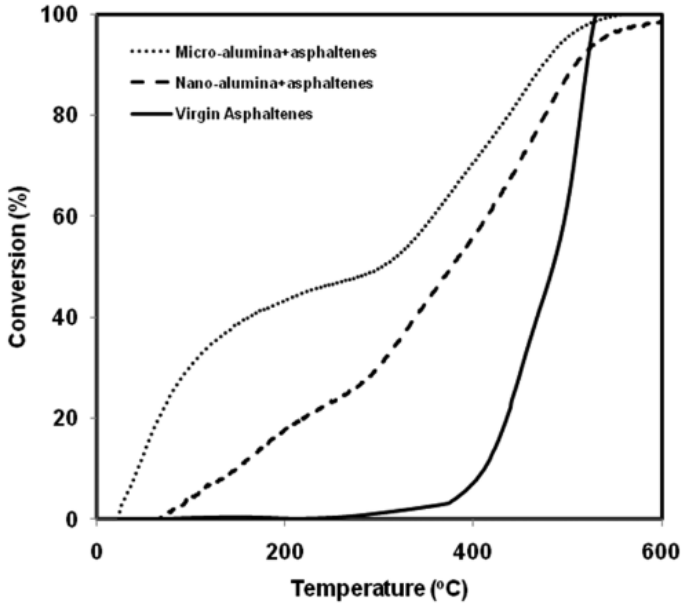

Figure 2-22. Fraction conversion of a pure/virgin asphaltene and asphaltene plus NPs obtained from TGA analysis (Nassar et al., 2011).

3 MATERIALS AND METHODS

In this chapter, first the materials used in this research work including the heavy crude oil sample, the NC, and solvents (*n*-heptane, toluene) are described. Then, the techniques used for purification of the heavy crude oil and asphaltene extraction, characterization of the NC (XRD, FTIR, DLS, SEM, TGA, and BET) and the asphaltene are described in a step by step manner. Finally, the step by step experimental procedures used for sample preparation and conduction of the tests to assess efficacy of the novel nan-inhibitor including TGA analysis and UV-vis Spectroscopy technique are presented and described.

3.1 Materials

3.1.1 Crude oil sample

A paraffinic heavy crude oil from West Kazakhstan was used to extract asphaltene. Density of the heavy crude oil is 0.946 g/cm^3 and dynamic viscosity of the heavy crude oil at 25°C was determined 153 cP. The asphaltene content was around 24.4-25.6%.

3.1.2 Nanocomposite

The NiO-Fe_3O_4-Polythiophene NC was provided by Dr. Shafiei.

3.1.3 Solvents

n-heptane was used for asphaltene extraction precipitation tests. Pure C_7H_{16} provided by Ekos-1 (TS 2631-023-444931179-98) was used in asphaltene extraction process and preparation of synthetic crude oil. The toluene was provided by Sigma-Aldrich and ACS reagent with >99.7 (GC), formula C_7H_8, MW: 92.14 g/mol, and density of 0.865 g/mol at 25°C.

3.2 Methods

3.2.1 Asphaltene Extraction

Asphaltene extraction began with purification of the heavy crude oil sample in an aging cell (OFI Testing Equipment (OFITE) High Temperature Aging Cell). The aging cell was used for filtration of 850 ml of the heavy crude oil sample. First, the sample was loaded in the accumulator and then the heavy crude oil was injected at a rate of 3.51 cc/min, under a pressure of 180 psi, and room temperature. Finally, the filtrate was collected at the outlet of the accumulator. Using a magnetic

stirrer for four hours at 600 rpm (Figure 3-1), the heavy crude oil and *n*-heptane were mixed with 1:40 ratio of oil to solvent in accordance with the IP-143 standard (Guin et al., 2022). Asphaltene was subsequently precipitated because of presence of *n*-heptane which makes the asphaltene content unstable in the crude oil and enabled its precipitation at the bottom of the beaker. Following this stage, a Whatman paper #42 was used to filter the accumulated asphaltene from the mixture (Figure 3-2). The asphaltene was then purified using a Soxhlet extraction device (Figure 3-3). *N*-heptane was added to the distillation flask and the separated asphaltene was placed inside the apparatus. The distillation flask was heated up to 100°C to reach the boiling point of the *n*-heptane. The generated vapor climbed up the siphon and once cooled down by the condenser, then the drops of *n*-heptane fell down to the chamber of the Soxhlet extraction and dissolved the impurities. This process continued until drops of the solvent turned clear. Following this procedure, the purification continued with replacing the *n*-heptane with toluene. Toluene was sued to dissolve the purified asphaltene accumulated on the filter paper and separating it from inorganic materials. The process continue until all of the asphaltene was dissolved in toluene. Then, the mixture was heated up to 100°C to evaporate the toluene (Figure 3-4). The final step was solidifying the asphaltene granules by desiccation of the residual asphaltene in oven at 80°C for 4 hours. The weight of the sample was measured three times every two hours to ensure the weight of the pure asphaltene is constant.

Figure 3-1. Mixing crude oil with *n*-heptane.

Figure 3-2. Filtration of asphaltene by filter paper.

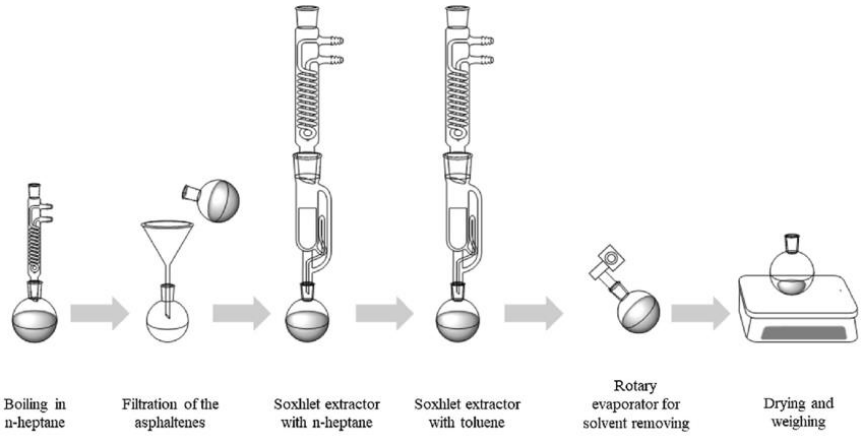

Figure 3-3. The procedure of asphaltene extraction (Schwettmann et al., 2022).

Figure 3-4. Evaporation of toluene.

3.2.2 Nanocomposite and asphaltene characterization

Characterization of the NC was a crucial step in this research work, because it helps to identify factors that influences adsorption and inhibition function of the NC. In this section, the analytical techniques used to characterize the NC are briefly described. XRD analysis was used for identification of crystalline structure and crystal size calculation, FTIR spectroscopy was used to identify the functional and chemical bonding, DLS was used for identification of hydrodynamic size of the NC and to prove that NC contains particles with nano size. In addition, BET method was sued to determine the surface area and pore size of the sample. TGA analysis was used to determined thermal stability of the NC and pure asphaltene.

3.2.2.1 Fourier-transform infrared spectroscopy

Fourier Transform Infrared spectroscopy or FTIR technique was used to determine chemical composition and functional groups of the novel NC and chemical composition of the pure asphaltene. Measurement of a specimen's mid-infrared light absorbance spectrum and intensity is known as FTIR. A sufficient amount of energy exists in mid-infrared light (4000 – 400 cm^{-1}) to stimulate atomic oscillations to greater energy levels (Swann & Patwardhan, 2011). Most infrared absorbance zones have wavelengths that correspond to certain chemical compounds. Hence, IR is most useful for qualitative investigation of organic and organometallic compounds. A recently synthesized chemical or a specific substance can be identified via FTIR (D'Amico & Gunnella, 2008).

Figure 3-5 illustrates basic mechanism of FTIR. A typical FTIR instrument consists of a source, interferometer, sample compartment, detector, amplifier, A/D convertor, and software compose (Baravkar et al.,2011). The source produces the radiation that passes through the specimen over the interferometer and reaches the detector. Then the beep is exaggerated and transferred to numeric signal by the magnifier and analog-to-digital transducer, correspondingly. At the end, the signal is conveyed to a computer in that Fourier transform occurs. FTIR spectrometer works on rule named Fourier transform (Mbonyiryivuze et al., 2015).

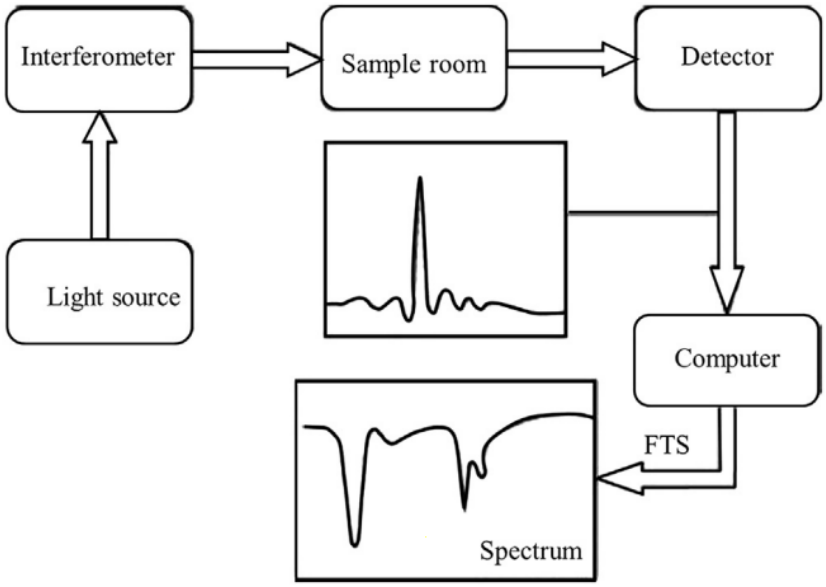

Figure 3-5. FT-IR mechanism used in this research work (Wen et al., 2021).

3.2.2.2 Scanning electron microscopy (SEM)

Scanning electron microscopy or SEM analysis is a useful tool that provides morphology and composition of the specimen by taking high resolution images in nanometers scale. Scale range is large and can provide images at different nano/micro scales. SEM is able to analyze the surface topography/morphology of the NC via identification of electrons on the surface of the NC. A targeted beam of electrons is created, accelerated, and passed over a variety of lenses and holes (Figure 3-6). This targeted beam subsequently impacts the NC's surface. The NC is put on a platform in the chamber and a couple of pumps operates to clear the entire chamber and the column. The vacuum pressure can vary depending on how the microscope is built. Check wires located atop the objective glass are in charge of adjusting the location of the beam on the NP. Wires permit the beam to run across the NCs surface. Data can be gathered about a specific location on the NC using the imaging system. Several impulses are generated as a consequence of contact between the electron and the NC. Correct sensors are subsequently used to find those signals (Zhou et al., 2007). A number of variables such as the dimensions of the electron beam site and the area of contact between the electron beam and the specimen, affect the highest precision that can be achieved in a SEM. Certain SEMs allow for precision lower than 1 nm. However, they are unable to give atomic resolution.

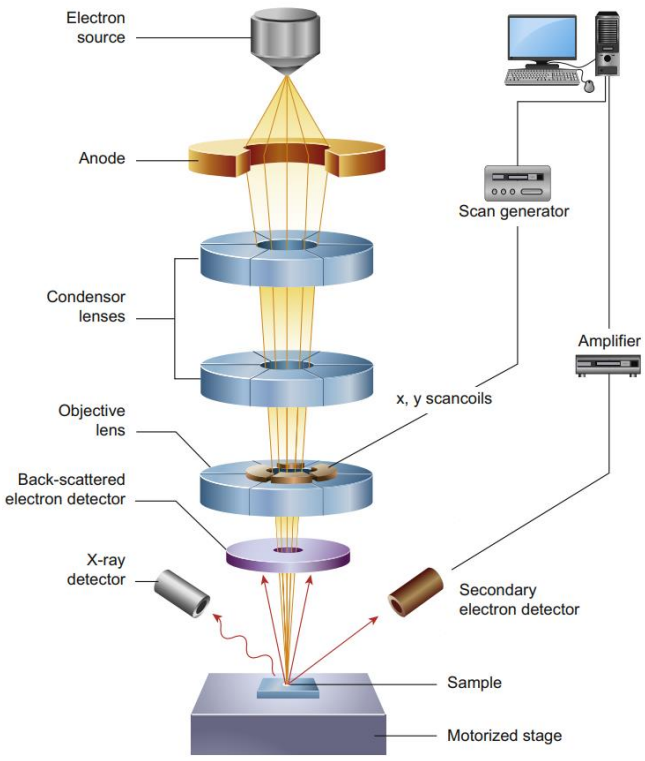

Figure 3-6. SEM microscope used in this research work (Inkson, 2016).

3.2.2.3 Brunauer-Emmett-Teller (BET)

When it comes to describing new absorbent materials, surface area is among the key crucial parameters. The BET technique determines NPs surface area by measuring the physical adsorption of gas. The assessment covers the entire microscopic area of NC because the gas particles are able to penetrate all voids and fissures in addition to passing through gaps among granules. BET analysis estimate adsorption isotherm. It uses relative pressure compare to amount adsorbed gas. Then adsorption curve obtains (Hanaor et al., 2014).

BET working mechanism illustrated in figure 3-7. Adsorbing is the term used to describe the adsorption of gaseous particles or atoms to a surface. Nitrogen is typically used in BET surface area evaluation due to their intense engagement with majority of solids as well as its accessibility. In order to produce measurable levels of adsorption, the outermost layer is refrigerated utilizing fluid N_2, as the contact amongst the vapor and solid parts is often minimal. Next, a predetermined volume of nitrogen gas is gradually delivered inside the specimen's compartment. By establishing partial vacuum circumstances, comparative pressure lower than atmospheric pressure can be reached. Nothing additional adsorption takes place after the saturated pressure, even with

additional pressure increases. Pressure converters with extreme precision and accuracy track shifts in pressure brought on by the adsorption operation. Following the formation of the adsorption layers, the specimen is taken out of the nitrogen environment and warmed up, which releases and quantifies the accumulated nitrogen from the medium. A BET equilibrium, that depicts the volume of gas adsorbed as a proportion of relative pressure, is one way the information is presented (Hwang & Barron, 2011).

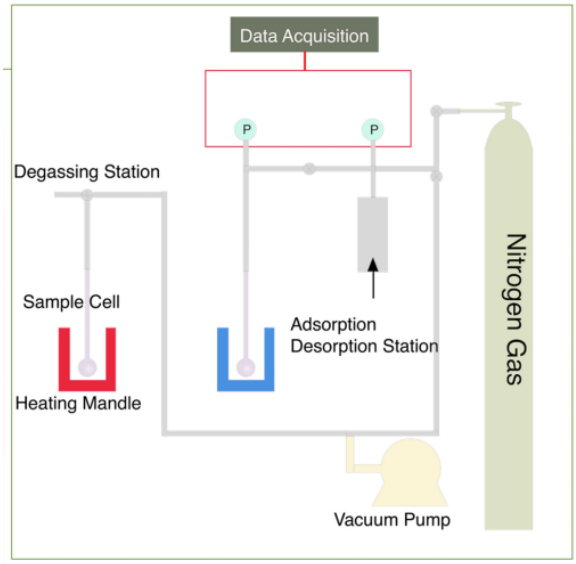

Figure 3-7. Nitrogen porosimeter schematic diagram for determination of BET surface area (Vordos et al., 2018).

3.2.2.4 BET sample preparation

Dried pure NC's mass is recorded at first process, then it has entered into tube for future analysis. Then NC specimen de-gassed by vacuum pump and heated in the tube to vaporize water remains. De-gassing process usually takes 1 hour or more to get better results.

3.2.2.5 X-ray diffraction (XRD)

XRD is a method for figuring out the crystalline and atomic structure of a chemical. It works by transmitting X-rays through sample and calculating intensity of ray. Figure 3-8 shows XRD working mechanism. The spot and angle of peaks are analyzed in order to identify the structure of sample. The intensity of the X-rays is shown as an expression of the angle. In addition to having capable to establish the median locations of atoms in crystal, it is also possible to find out how the

real structure differs from the theoretical one, due to things like inner tension or flaws (Whittig & Allardice, 1986).

Optic beams that are impinge on a crystalline grid with a low enough wavelength refract away through the grid points. The scattered parallel pulses productively interact and produce recognizable apex in intensity at specific angles of incident. Diffraction is an occurrence in which x-rays are dispersed by crystal atoms and then redirected in certain ways out toward the crystal. Bragg's law defines the empirical relationship between the reinforcement of the dispersed photons and the atomic plane spacing length.

$$\Lambda = 2dsin\theta \qquad \text{Equation 3-1}$$

where, λ is wavelength, d is distance between planes. Atoms arranged systematically and periodically in a three-dimensional matrix define crystalline formations. Every crystal has atomic flatness that are always distanced by the same amount of area as crystals are made up of consistently distributed atoms. The crystalline forms are distinguished by their plane-to-plane spacing. XRD is useful to find crystalline phase and thickness of layers, even to atomic disposition.

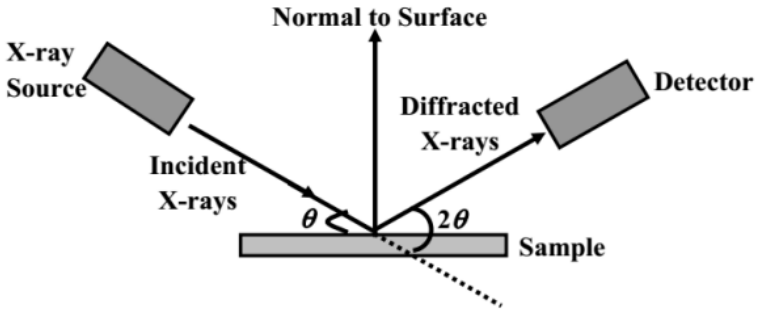

Figure 3-8. XRD working principles (Andualem, 2020).

3.2.2.6 Dynamic Light Scattering DLS

Before using any NC, it is necessary to analyze the size pattern and zeta potential using dynamic light scattering (DLS). The DLS method gives us details on the material's characteristics at "long wavelengths," which are constrained by the light's spectrum. DLS gives us insight into the dynamics of nano and micron-sized particulates in addition to stability. Zeta potential is used to calculate the electrophoretic movement, surface charge, and surface potential of colloidal particulates (Karmakar, 2019).

DLS approach was provided by Particle Metrix ZetaView with wave length of 488 nm. Brownian movement measurement is applied to estimate the size of individual particulates. A particulate size range is the result of multiple distinct particulates, ranging from 100 to 1000. It is possible to integrate the assessment of size with other attributes of the item, including area and particulate intensity, and zeta potential. The particulate's strength of dispersion, the effectiveness of the magnifying optics, and the camera's sensibility all affect the lower boundary of the operational spectrum, or the tiny discernible particulate size. Because of their relatively high refraction gauge, metallic NC are powerful scatters that may be detected at sizes as small as ~10 nm (Bohren & Huffman, 1998b).

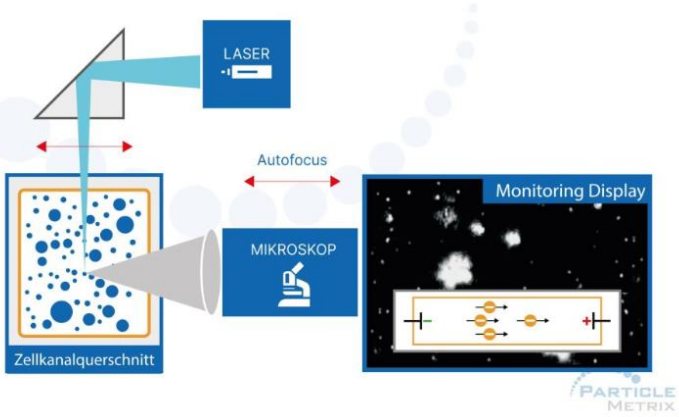

Figure 3-9. DLS working principle (Neelen, 2023).

A laser beam is used to illuminate the specimen in order to view the particulates therein. Positioned at a 90° angle to the irradiation flat, a light-sensitive CMOS footage sensor records the dispersed light emitted by particulates (Figure 3-9). Ultra-microscopy, as the system is often called, permits the observation and capturing of particular elements that are smaller than what is typically seen using a microscope. Brownian motion evaluation of the distinct monitors is used to determine the size of apiece particulate, providing size and concentration to be determined simultaneously (Zsigmondy, 1909).

3.2.2.7 TGA analysis

In order to evaluate thermal stability and detect volatility of NC, TGA approach applied using Simultaneous Thermal Analyzer (STA) 6000. This process considers heating NC between 30-

800°C with rate if 10°C/min. Results will be considered in mass loss change to temperature increasing in the system.

3.2.3 Assessment of the performance of nanocomposite

To acquire information about the properties and activity of nanocomposites beneath various concentration, this laboratory works incorporates UV-spectroscopy and Thermogravimetric Analysis (TGA).

3.2.3.1 TGA-thermogravimetric analysis

It can be possible to test the thermal endurance of sample using the advanced tool known as thermogravimetric analysis (TGA). This technique involves monitoring variations in a sample's mass as its temperature rises. TGA is often used to detect a specimen's volatility. The equipment comprises of a configurable heater and an extraordinarily accurate magnitude for monitoring mass fluctuations in the specimen. Overlooking the oven, the equilibrium is thermally insulated against the warmth. The specimen, whose location needs to be repeatable, is at the tip of the wire. To increase the sensibility, efficiency, and clarity of measuring, the scale has to be shielded from heat impacts (for example, by using an isothermal tank). Infrared spectrum attachment to TGA enables investigation and detection of vapors produced by specimen deterioration. There is a micro-oven built into TGA equipment which is able to quickly cool. Platinum is used in the warming component, which is stable even at 1000°C. The heat limit may be increased to 1500°C using an outside oven with a warming source consisting of a combination of platinum and rhodium (Ebnesajjad & Ebnesajjad, 2013). By detecting mass change, we can determine amount of asphaltene adsorbed. It works by calculating mass of pure nanocomposite and nanoparticles with asphaltene adsorbed, and at the end, we calculate their difference. This difference gives weight of asphaltene adsorbent. Preparation of synthetic oil for TGA is crucial stage in experiment. Six samples of synthetic oil with 6 different asphaltene concentrations is shown in the Table 3-1.

Table 3-1. Concentration and volume of synthetic oil samples.

C solution, ppm	C solution, wt.%	V solution, ml	V of toluene, ml
100	0.01	0.6	29.4
200	0.02	1.2	28.8
400	0.04	2.4	27.6
1000	0.1	6.0	24.0

2000	0.2	12.0	18.0
5000	0.5	30.0	0.0

Data in the table calculated using the dilution method. Then mass of NC calculated 0.15 g to produce 5 g/l mixture. After preparation of synthetic oil, mixtures were mingled in ultrasonic bath for 25 min to dissipate NC in oil. Then samples were mixed for 24 hours at 250 rpm shaker to attain asphaltene adsorption. After this, centrifuge used for 15 minutes at 10000 rpm to split precipitation from supernatant (Figure 3-10). These steps of the experiment were done at room temperature. Then precipitation was inserted in vacuum oven for 24 hours at 50°C. Finally, 6 precipitant samples were sent to TGA for measure amount of asphaltene adsorbed.

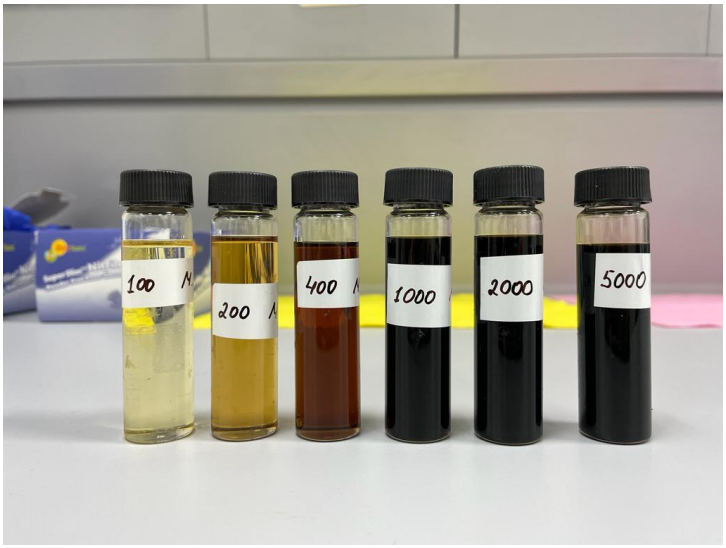

Figure 3-10. Supernatant liquid with NC.

Conditions for TGA experiment are:

- Heating rate: 10°C/min
- Airflow rate: 30 ml/min
- Heating range: 30 to 800°C

In this analysis mass loss calculated by Equation 3-2:

$$mass\ loss = \frac{Mf}{Mi} \times 100 \qquad \text{Equation 3-2}$$

Where, M_i is initial mass of sample, and M_f is final mass of NC with adsorbed asphaltene.

3.2.3.2 Asphaltene Onset Point (AOP)

Indirect method of AOP determination do not require high pressure apparatus and the heavy crude oil specimens used are relatively straightforward to obtain compared to bottom-hole specimens. This is considered as an appealing and practical method of investigation of the likelihood of asphaltenes precipitation in a particular crude oil. Furthermore, compared to earlier direct approaches, the indirect method, which has been invented and advocated in the last ten years, offers some benefits including straightforward detection of deposition of small size particulates (Padró et al., 2023). The proposed method uses the indirect approach that Tavakkoli modified and suggested because it can identify asphaltene precipitation (Tavakkoli et al., 2015). According to Beer-Lambert rule, which establishes that absorbance is a linear proportion of the fluid dosage, this linear trend is valid. The absorbance suddenly drops under the range predicted by specimen diluting between 50 and 90 et% due to asphaltene precipitation. As a result, the linear tendency is no longer relevant. The aforementioned reasoning leads to the conclusion that at about 40 and 55 wt% of additional *n*-heptane is necessary to identify asphaltene precipitation (Padró et al., 2023).

In this method, first of all, it is needed to prepare synthetic oil samples with adding n-heptane for observing precipitation of asphaltene. It will be done in both presence and absence of NC for better understanding influence of NC for AOP shifting. Synthetic oil was prepared at 0.5 wt% concentration of asphaltene. To properly calculate needed mass of asphaltene at certain concentration:

$$wt\%\ of\ asph = 100 \times \frac{m\ asph}{V\ sol \times 0.865 + masph} \qquad \text{Equation 3-3}$$

Equation 3-3 can be used to prepare synthetic crude oil with different concentration of asphaltene and NC. The mix of NC, toluene, and asphaltene must be put in ultrasonic bath for 25 minutes to dissipate the NC in the mix. After preparation of the synthetic oil, *n*-heptane is added at concentrations of 10 to 90% to prepare 40 ml samples. Then the specimens were placed for aging approximately for 2-3 hours. After this, centrifuge used for 15 minutes at 10,000 rpm to split the precipitate from supernatant. Absorption of every specimen was assessed at 700 nm and range of wavelengths of spectrometer was between 200 to 900 nm. Toluene was used in the UV spectroscopy as baseline. The volume of each sample, *n*-heptane, and mass of NC are presented in Table 3-2.

Table 3-2. Sample data for UV-spectroscopy.

***n*-heptane, %**	**volume of synthetic oil, ml**	**volume of *n*-heptane, ml**	**mass of NC at 0.1% wt.**	**mass of the NC at 0.2 wt%**	**mass of NC at 0.3 wt%**	**mass of NC at 0.4 wt%**
10	36	4	0.031	0.062	0.094	0.125
20	32	8	0.027	0.055	0.083	0.11
30	28	12	0.024	0.048	0.072	0.097
40	24	16	0.021	0.041	0.062	0.08
43	22.8	17.2	0.019	0.039	0.059	0.079
45	22	18	0.019	0.038	0.057	0.076
48	20.8	19.2	0.018	0.036	0.054	0.072
50	20	20	0.017	0.034	0.052	0.069
60	16	24	0.014	0.028	0.041	0.055
70	12	28	0.01	0.02	0.031	0.041
80	8	32	0.007	0.013	0.02	0.028
90	4	36	0.003	0.007	0.01	0.013

3.2.3.3 UV-vis spectroscopy calibration curve

Calibration curve was fixed at 700 nm UV-spectroscopy wavelength. This wavelength considered sufficient for recording values for asphaltene absorbance. The calibration curve for pure synthetic oil considering different concentration of asphaltene in ppm is presented in Figure 3-11.

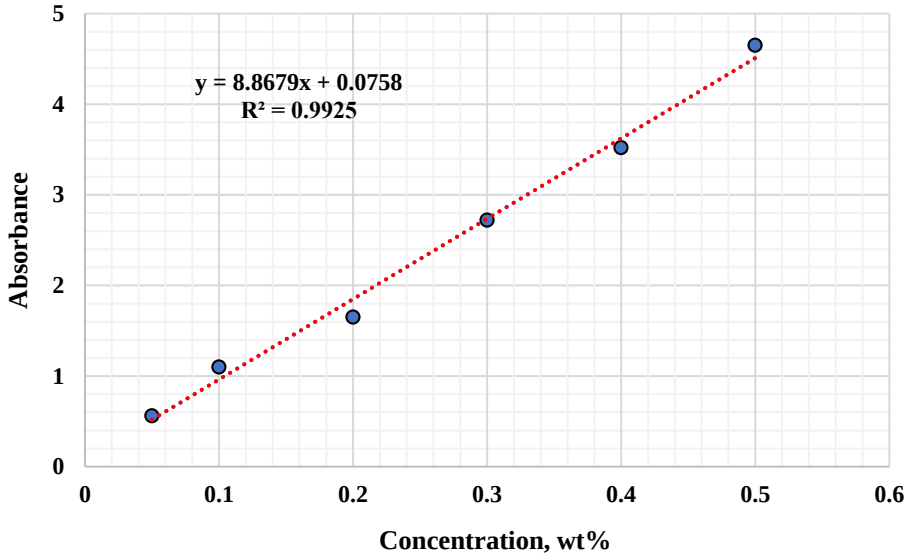

Figure 3-11. Calibration curve for asphaltene in toluene.

From the Figure 3-11 it can be seen that the Beer-Lambert relationship rule, which establishes that absorbance is a linear proportion of the asphaltene concentration, is valid. To change concentration of synthetic oil, dilution methods applied to initial concertation 5000 ppm of asphaltene:

$$C_1V_1 = C_2V_2 \qquad \text{Equation 3-4}$$

By using Equation 3-4, dilution of synthetic oil can be calculated where C is concentration of asphaltene and V is volume of oil.

4 RESULTS AND DISCUSSION

In this chapter, the results obtained from the conducted experiments are presented and discussed. In the first part, results of NC characterizations by using XRD, SEM, FTIR, TGA, and BET are presented and discussed. Different properties of the NC such as surface area, functional groups, surface morphology, particle size, crystallite size, thermal stability are determined. In the second part, to assess efficacy of the novel NC in adsorption and removal of asphaltene from synthetic crude oil, the results obtained from TGA analysis and UV-spectroscopy conducted in absence and presence of the NC are used for AOP determination and investigation of adsorption kinetics of the asphaltene plus construction of adsorption isotherm models. A discussion of possible mechanisms of asphaltene precipitation inhibition by the novel nano-inhibitor is also presented. In addition, a comparison is made with the literature to compare the performance of the novel asphaltene nano-inhibitor developed and tested in this research work with other NC-based nano-inhibitors.

4.1 Characterization of the NiO-Fe_3O_4-Polythiophene NC

4.1.1 X-ray diffraction

X-ray diffraction analysis conducted by using SmartLab Rigaku was used to determine the structure and patterns of the lattice of crystallites that make up the NiO-Fe_3O_4-Polythiophene NC. The XRD patterns of the peaks of the NC are presented in Figure 4-1 where the x-axis shows the 2Θ angle and the y-axis reads the intensity. Higher diffraction intensity peaks mean bigger size of the particulates. In the ICDD 19-629 reference, typical peaks of Fe_3O_4 are 311, 440, 511, 220, 400 and 422 *hkl* plane (Yamaura & Fungaro, 2013). The following peaks shown in the Figure 4-1 matched the reference peaks 30.26, 35.65, 43.34, 57.35, 53.8 and 62.97 2Θ degrees, respectively. Peaks of NiO are 111, 200, 220, 311, and 222 hkl plane which corresponded to the card ICDD 4-0835 (Richardson et al., 2003). From the XRD analysis this is indicated by peaks 30.26, 35.65, 43.34, 57.35 and 62.97 2Θ degrees. Each of those diffraction spikes are properly referenced to the NC's face-centered cubic (FCC) crystallographic structure.

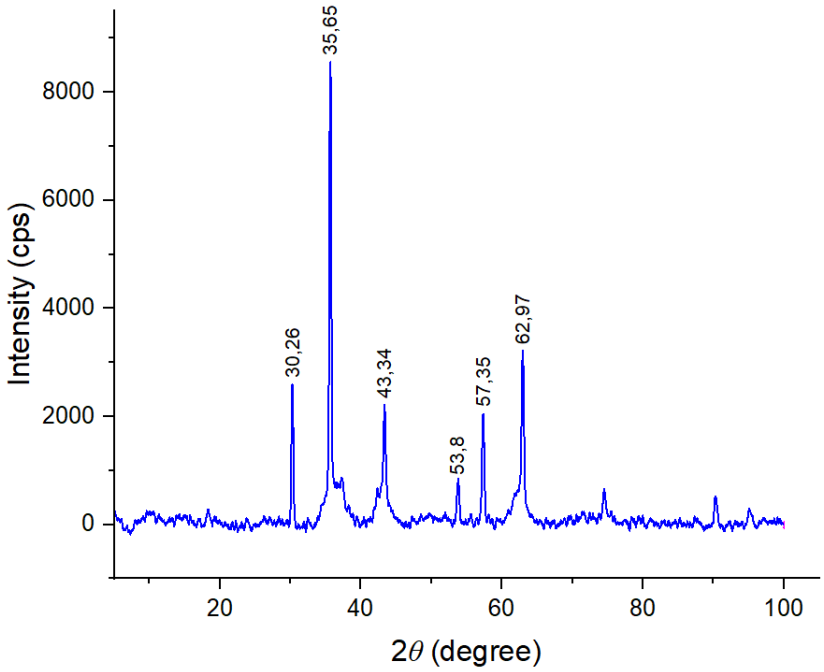

Figure 4-1. XRD analysis of the NiO-Fe_3O_4-Polythiophene NC.

The crystallite size of the NC was also calculated using the XRD analysis data. For estimation of crystallite size, the relationship proposed by Scherrer was used as it follows:

$$D = \frac{(0.9\times\lambda)}{\beta_{1/2}\times\cos\theta} \qquad \text{Eq. 4-1}$$

where 0.9 is the Scherrer constant, λ is wavelength of the X-ray 0.15406, β is the angular width at half maximum intensity of the peak in rad and θ is the diffraction angle in radian (Yamaura & Fungaro, 2013). Average crystallite size of the NiO-Fe_3O_4-Polythiophene NC is 33.2 nm.

4.1.2 Scanning Electron Microscopy

Scanning Electron Microscopy images of the NiO-Fe_3O_4-Polythiophene NC captured by using the Scanning Electron Microscope ZEISS Crossbeam 540 are illustrated in Figure 4-2. The SEM was used to explore surface morphology of the NC and also determine its particle size in a qualitative manner. The NC is made of cluster with a low aspect ratio with high sphericity. The size of the clusters varies from a few 64 to 400 nm. The range in size is high and it shows that the thickness of the polythiophene coating is high. The NC has a polycrystalline morphology. The crystallite or particle size determined using the XRD data is smaller than the minimum size determined by using

the SEM. This is because the SEM analysis is qualitative and its resolution does not allow identifying the crystallite size, clearly.

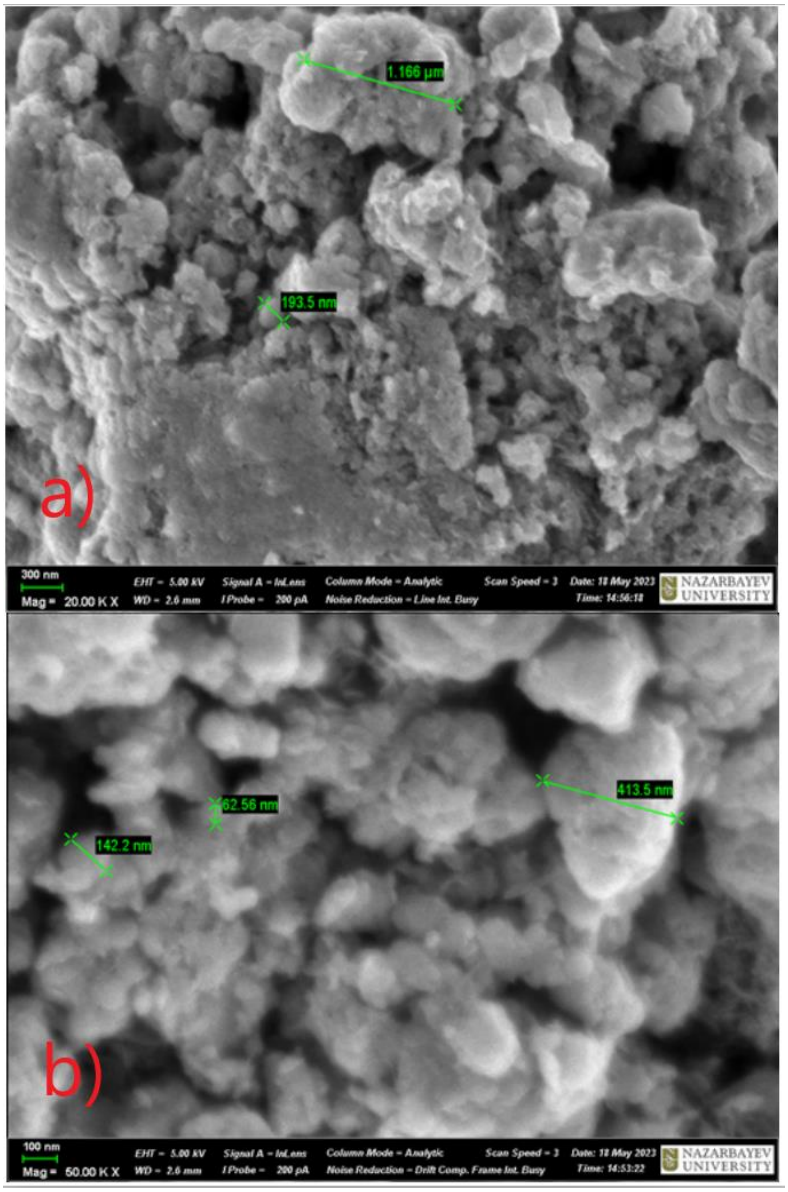

Figure 4-2. SEM analysis of the NiO-Fe_3O_4-Polythiophene NC.

4.1.3 Fourier-Transform infrared spectroscopy

FTIR spectra of the NC taken by using the Nicolet iS10 FTIR apparatus is illustrated in Figure 4-3. The FTIR analysis revealed several peaks in range of 400 to 4,000 cm^{-1} that indicate elemental bonding and functional groups of the NC. The peak 3337 cm^{-1} corresponds to OH hydroxyl function groups, which results from NC's adsorption of water (Bautista et al., 2005). The strong

peak at 1551 cm^{-1} is attributed to the symmetrical and asymmetrical stretching vibration of the thiophene ring at C=C (Li et al., 2009). The distortion of the CH in-plane oscillations and C-H bending is responsible for the peak 1416 cm^{-1} (Acharya et al., 2010). The point 785 cm^{-1}, which is attributed to the polythiophene C-S bend vibrations and C-S-C ring deform stretching show that the thiophene monomers successfully completed the polymerization and formed polythiophene (Senthilkumar et al., 2011). The final peaks 532 and 409 cm^{-1} corresponds to stretching vibration of Fe-O and Ni-O metal oxides in the NC.

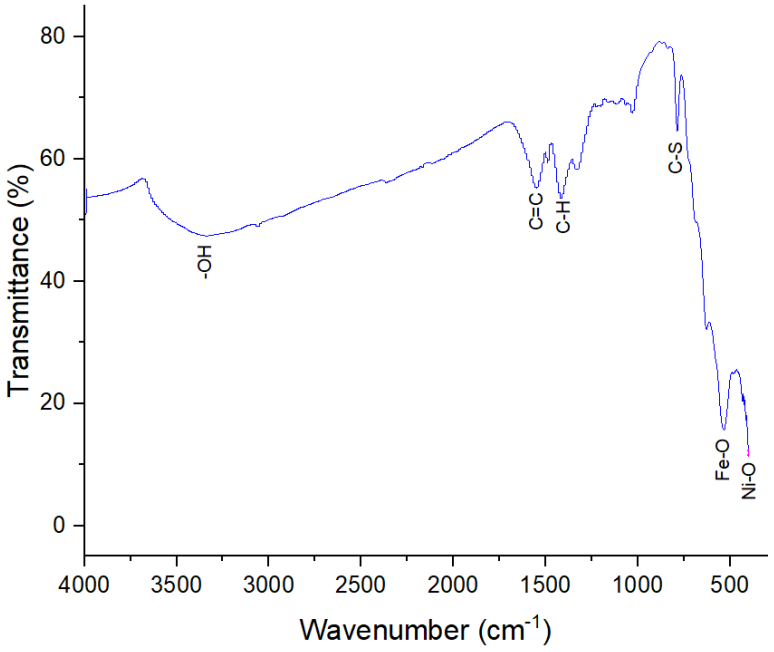

Figure 4-3. FTIR spectra of the NiO-Fe_3O_4-Polythiophene NC.

4.1.4 Dynamic light scattering (DLS)

In this research work, mean hydrodynamic size of the NC was determined by DLS technique. The DLS measurement was done using a Nanoparticle Tracking Analysis Instrument (PMX-230 ZetaView TWIN Laser) system operating at a temperature of 25°C with disposable microcuvettes and with a wavelength of 488 nm. The particle size ranges from 50 to 300 nm. The mean particle size is around 155 nm. Due to high surface area of the NC 55.83 m^2/g and small particle size, the Polythiophene-NiO-Fe_3O_4 NC provides additional loading sites for adsorption of asphaltene particulates. When integrated with additional SEM approaches, the DLS analysis provided a quantitative information on hydrodynamic dimensions of the NC. In addition, surface charge of

the NC was measured by using the zeta potential method. The NC's surface charge was positive 0.032 mV in the first stationary layer, and shifted to negative -0.938 mV in the second layer.

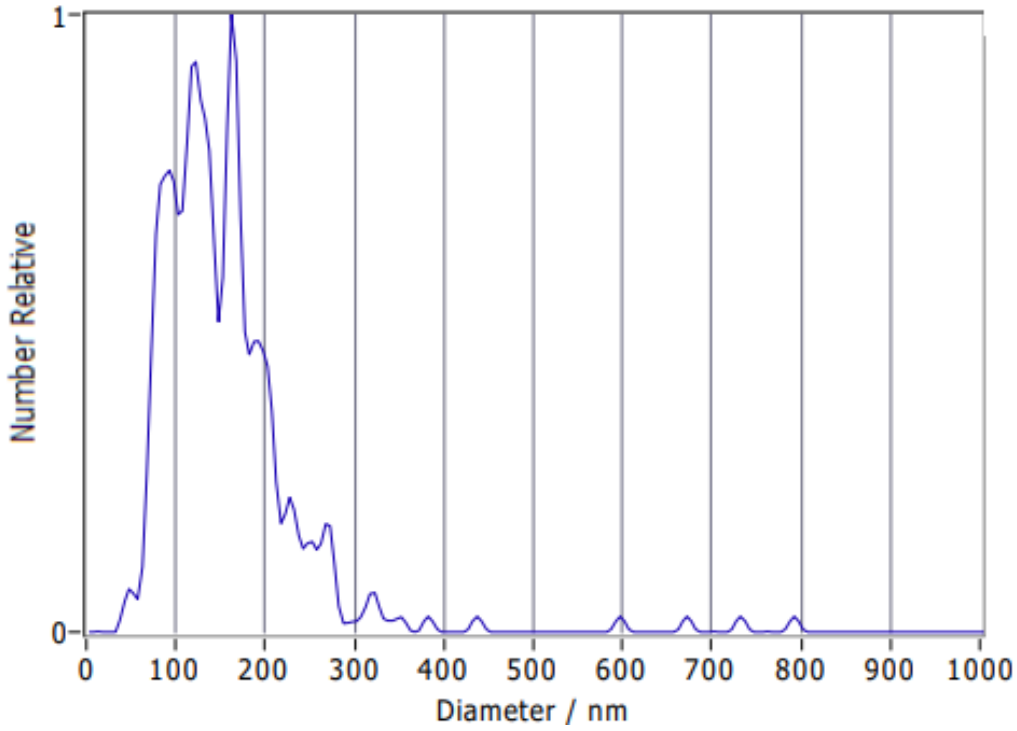

Figure 4-4. DLS measurement of the NiO-Fe_3O_4-Polythiophene NC.

4.1.5 BET

The total area of the accessible regions of the particulates multiplied by their weight per unit is their particular surface area. The relationship between surface area and particulate dimension is reverse. One method for determining a powder's particular surface area is N_2 gas adsorption. To calculate the overall surface area, the Brunauer-Emmett-Teller (BET) technique is frequently used (Akbari et al., 2011). In this research work, the surface area of the NC powder was determined as 55.83 m^2/g using the BET method. The adsorption isotherm plot for the NC is presented in Figure 4-6 that indicates a type IV isotherm. This suggests development of a monolayer accompanied by multilayers in the NC. The BET analysis suggests that the NC is a mesoporous particulate with an average pore size of 11.8 nm.

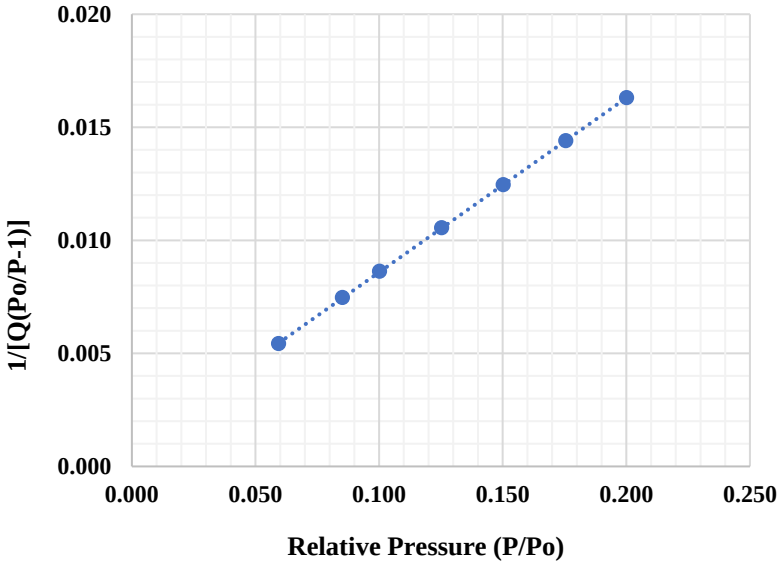

Figure 4-5. BET analysis of the NiO-Fe_3O_4-Polythiophene NC.

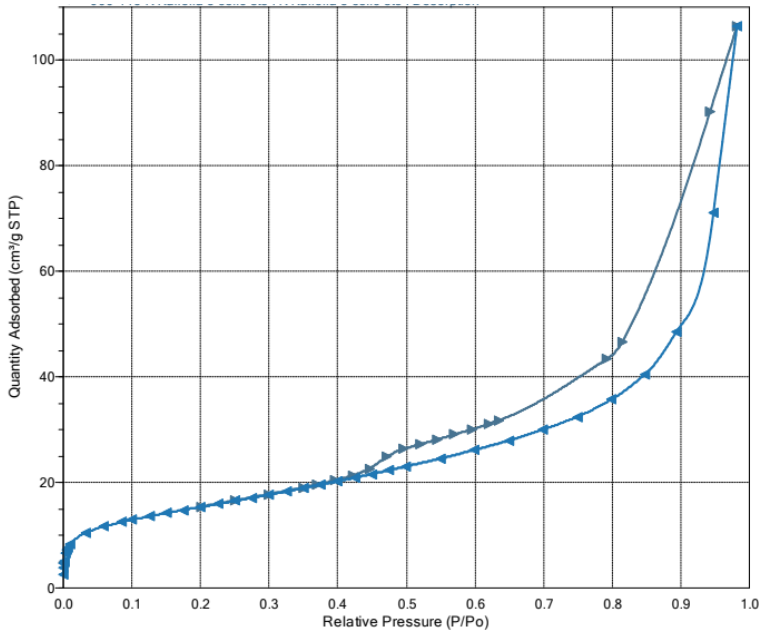

Figure 4-6. Isotherm plot from BET analysis of the NC showing a type IV isotherm.

4.1.6 Thermogravimetric analysis

The weight loss of the NC consists of three different stages, based on the TGA study shown in Figure 4-7. Because of NC's thermal dehydration, the initial step happened between 30 and 340 ℃. The mass loss at this stage was approximately 4.19%. The second stage takes place between 340℃ and 570℃ because of degradation of molecules and organic compounds. The mass loss reduction was approximately 9% during the second stage. Third final stage occurred between 570℃ and 800℃ due to combustion of the organic compounds. The mass loss decrease is approximately 8.02%. Total mass loss is 21.21%, which indicates high thermal stability of the novel NC. At the start, mass of pure NC was 24.15 mg and after heating the mass was decreased to 19 mg. It should be noted here that for the oilfield temperature of 80℃ the amount of mass of the NC is negligible, below 3%, demonstrating a very high thermal stability for oilfield applications.

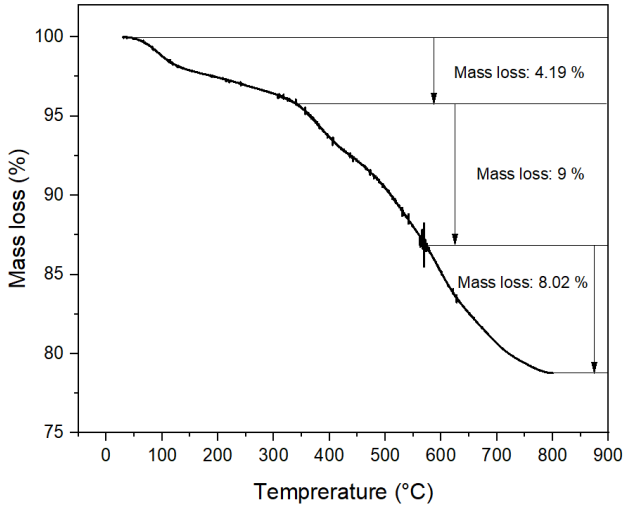

Figure 4-7. TGA analysis of the NiO-Fe_3O_4-Polythiophene NC.

4.2 Performance evaluation of the novel NC for asphaltene adsorption and inhibition

4.2.1 Thermogravimetric analysis (TGA)

The mass loss data for pure asphaltene, pure NC, and NC + asphaltene with different NC concentrations were determined using the TGA analysis as shown in Figure 4-8. Asphaltene is generally a heavy hydrocarbon faction, therefore until 340°C, there is no discernible weight decrease. The asphaltene begins to break down around 340°C and there is the greatest mass drop around 460°C (~35%). This is due to the fact that, an oxidation-related burning process leads to breakage of carbon-carbon links at this temperature. Above 460°C and higher, the second stage of oxidation of asphaltene occurred. This is because of molecular reconfiguration and polycyclic aromatic hydrocarbons breakdown (Hosseinpour et al., 2014). Overall mass loss of the pure or virgin asphaltene was determined 53.5%. In presence of the NC, the oxidation temperature of the asphaltene shifted up implying catalytic impact of the NC on asphaltene oxidation. The fraction conversion ratio of the asphaltene adsorbed onto the NC is shown in Figure 4-9. The fraction conversion ratio of the asphaltene adsorbed onto the NC is defined as:

$$\alpha = \frac{Wo - Wt}{Wo - Wf} \qquad \text{Eq. 4-2}$$

where, W_O is initial weight of the specimen, W_t is weight of the specimen during every given temperature point, W_f the final weight of the specimen. As can be seen in Figure 4-8, presence of the NC significantly improved the oxidation of the asphaltene. It seems that thermal breakdown, or decomposition, began above 340°C and attained its highest value approximately 800°C in absence of the NC indicating presence of a burning process throughout oxidation. Introduction of the NC significantly accelerated the oxidative process starting at 150°C as can be seen in Figure 4-9. The reduction in oxidation temperatures demonstrates the catalytic effect of the NC on asphaltene oxidation.

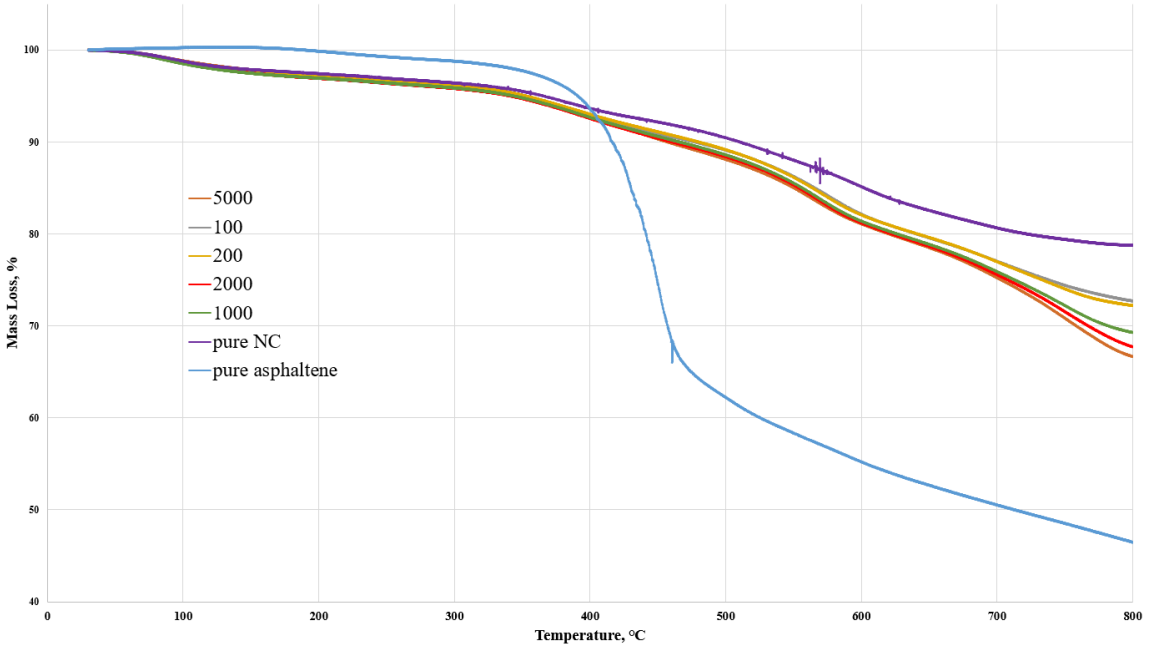

Figure 4-8. The mass loss of the adsorbed asphaltene onto the NC.

Mass loss rate profile of 5,000 ppm concentration of asphaltene with NC, pure NC, and virgin asphaltene are presented in Figure 4-10. It can be concluded that, the novel Polythiophene-NiO-Fe_3O_4 NC has decreased the oxidation point and combustion of the adsorbed asphaltene onto NC happens at lower temperatures.

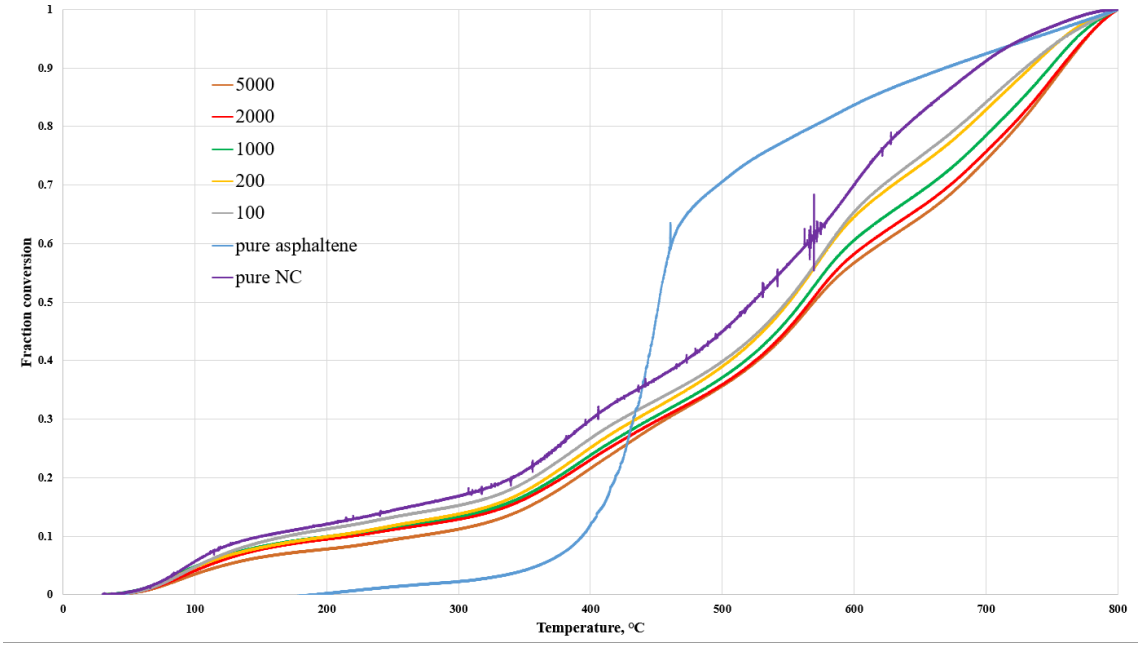

Figure 4-9. Fraction conversion of the adsorbed asphaltene onto the NC.

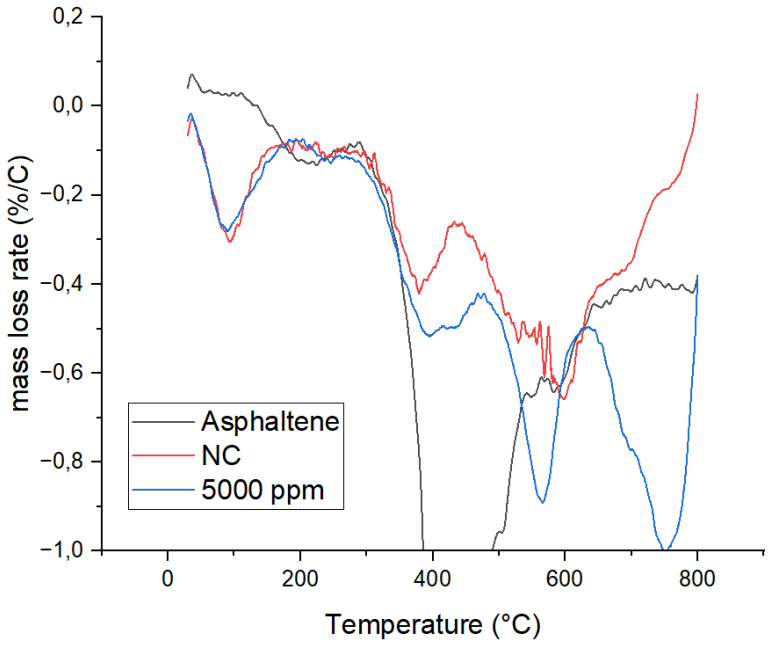

Figure 4-10. Derivative of mass loss rate as a function of temperature.

Mass loss of minimum concentrated 100 ppm asphaltene + NC is approximately equal to 27.3 %. Where maximum 5000 ppm asphaltene + NC indicates 33.3 %. Which means that, by increasing concentration of asphaltene mass loss of sample increases. It can be explained by catalytic effect of NC, however by increasing concentration of asphaltene, it will accumulate onto NC surface and reduce active sites of NC (Nassar et al., 2011b). The figure 4-11 illustrates mass loss profile of the adsorbed 5000 ppm asphaltene onto NC. As mentioned before, mass loss was equal to 33.3%. Between 30°C to 330°C, mass loss was 4.5% and this is associated with low temperature oxidation. Above 330°C to 800°C mass loss was equal to 28.8% and this referred to total oxidation of asphaltene.

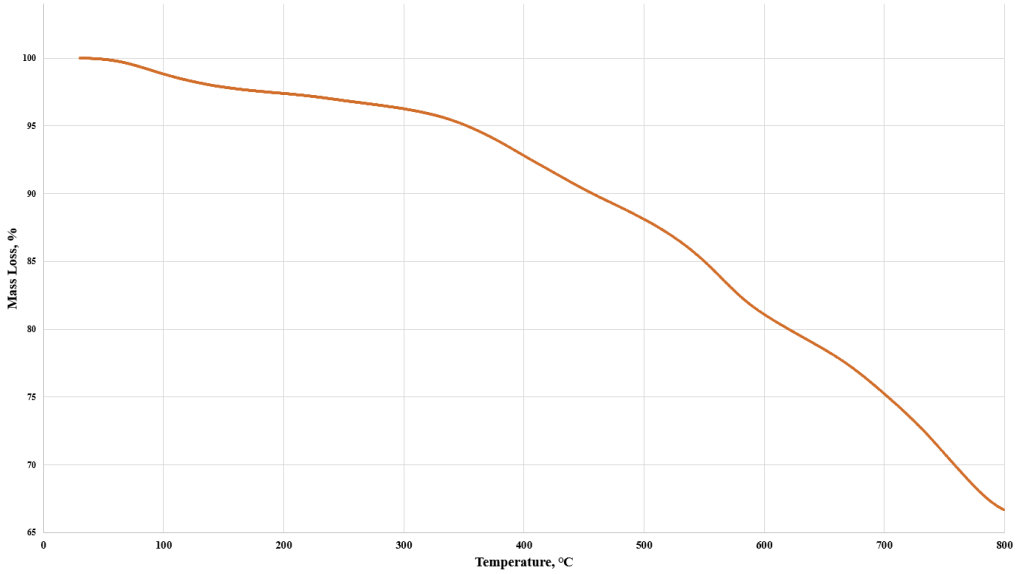

Figure 4-11. The mass loss of the adsorbed 5000 ppm asphaltene onto NC.

4.2.2 Asphaltene Onset Point (AOP) determination

AOP determination technique was used to evaluate the efficiency of the novel NC in this research work. There is no NC present in the first test. This can be used to understand the AOP for the synthetic oil with asphaltene concentration 0.5 wt% in absence of the NC. To investigate how the NC affects the AOP, several tests were conducted in presence of the NC with different concentrations (0.1, 0.2, 0.3, and 0.4 wt%) to find the optimum concentration. The absorbency versus *n*-heptane concentration from 10 to 90 vol% for the synthetic crude oil containing 0.1, 0.2, 0.3, and 0.4 wt% NC is shown in Figure 4-12. As one can see from Figure 4-12, there exists a direct association between concentration points and adsorption to Beer-Lambert's rule (absorbance value proportional to concentration of sample) up to 40 vol% (Shojaati et al., 2017). Nonetheless, a shift from the linear is observed at 40 vol% *n*-heptane content. Because of this abrupt decrease in adsorption, the linear pattern is invalid across this dosage range. In conclusion, asphaltene accumulates at 40 vol%, which causes the absorbance to decrease. The AOP points determined for 0.1, 0.2, 0.3, and 0.4 wt% concentration of the NC are presented in Table 4-1 and also shown in Figure 4-12.

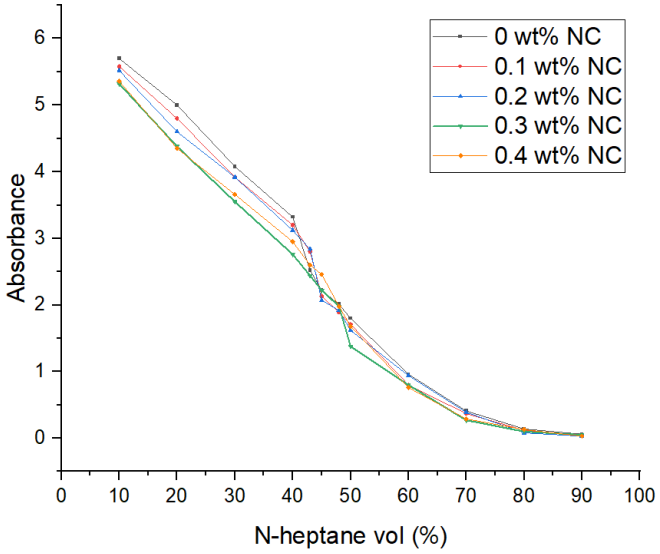

Figure 4-12. AOP determination with different concentration of NC.

Table 4-1. AOP determination results.

NC concentration, wt% NC	**AOP (*n*-heptane), %**
0	40
0.1	43
0.2	43
0.3	48
0.4	45

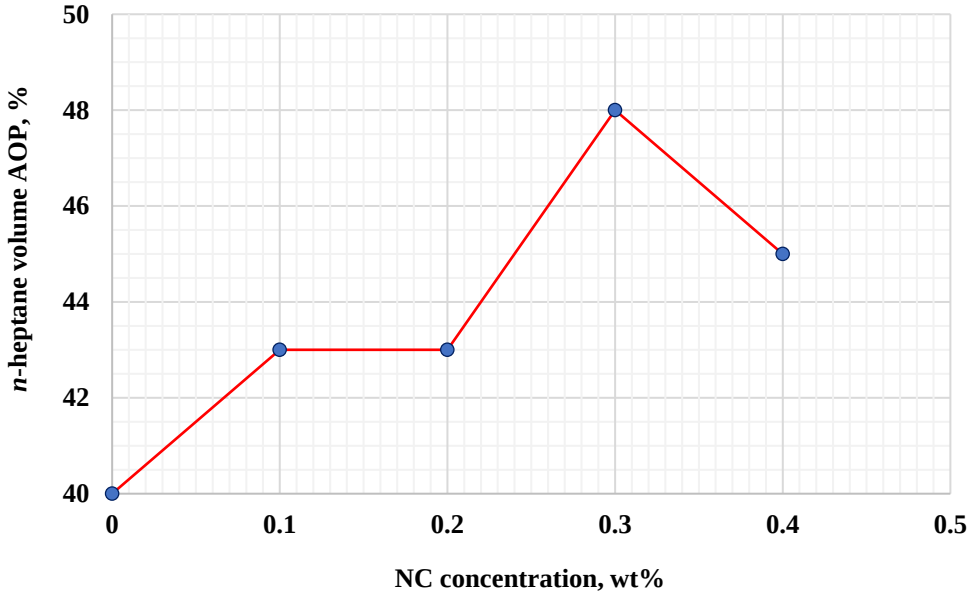

Figure 4-13. AOP determination by various concentration of NC.

The precise starting point of asphaltene precipitation is determined by selecting three points (43, 45, and 48 vol% *n*-heptane) within the range of 40 and 50 vol% of *n*-heptane. Centrifugation was then used to remove the asphaltenes adsorbed onto the nanoparticulate (Tazikeh et al., 2020). Removing the asphaltene decreased the AOP and consequently the quantity of asphaltene in the synthetic crude oil. As can be seen clearly in Figure 4-12, the AOP shifted from 40% of *n*-heptane to 43% in NC concentrations of 0.1 and 0.2 wt%. However, compared to concentrations of 0.3 and 0.4 wt%, the amount of shift was not considerable. The most effective concentration of NC to absorb asphaltene particles in synthetic oil, were determined in 0.3 wt%. The AOP points shifted from 40 to 48% *n*-heptane, shown in table 4-1. However, AOP with NC concentration 0.4 wt% shows 45% of *n*-heptane. Figure 4-13 demonstrates all results of UV-spectroscopy testing. Nevertheless, the optimum concentration of NC was observed by 0.3 wt%, due to the high shifting and minimal dose of NC is needed for this concentration. Whenever the concentration of NC increases, they actually agglomerate. As a result, there are reduced of their active sites and fewer asphaltene gets absorbed on the NC (Setoodeh et al., 2018).

4.2.3 Asphaltene adsorption isotherms

Supernatant obtained from the TGA tests was used to construct adsorption isotherm models. Adsorption was measured using UV-vis spectroscopy method with samples prepared with initial asphaltene content of 100 ppm to 5000 ppm. It was established that 5 g/L is the appropriate proportion for the NC to synthetic crude oil solution. The equilibrium concentration of asphaltene was determined 5000 ppm.

The calibration curve created using UV-spectroscopy analysis without NC is presented in Figure 4-14. By using this curve, the equilibrium concentrations were calculated to construct the adsorption kinetics isotherm models. For modelling adsorption isotherm of asphaltene Freundlich and Langmuir isotherm models were applied.

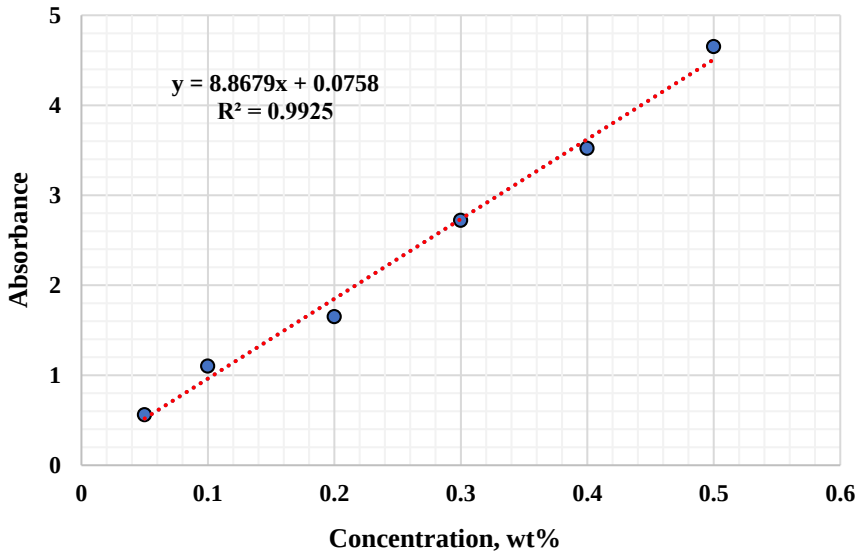

Figure 4-14. Calibration curve for pure asphaltene without NC.

Langmuir model equation:

$$\frac{C_e}{q_e} = \frac{1}{K_l \times q_{max}} + \frac{C_e}{q_{max}} \qquad \text{Eq. 4-3}$$

Freundlich model equation:

$$\log(q_e) = \log(K_f) + \left(\frac{1}{n}\right) log C_e \qquad \text{Eq. 4-4}$$

where Q_e is equilibrium adsorbed amount of asphaltene, K_l and K_f are Langmuir and Freundlich constants, n is intensity factor, and Ce is equilibrium concentration of asphaltene.

Table 4-2 demonstrates key values of Langmuir and Freundlich models. K_l is equal to 0.0047 and K_f constant is higher, which means that there is strong binding between nanocomposite and adsorbed asphaltene particles. Maximum adsorption capacity was equal to 1.116 (mg/m^2), which manifest that synthesized NC has high adsorption capacity. Figure 4-15 illustrates adsorption isotherm model, where x-axis shows Ce and y-axis provides values of Q_e. Figures 4-16 and 4-17 illustrates both Langmuir and Freundlich model with experimental data. Obtained R^2 values in both models was closely equal to 0.98 and 0.95. This means that adsorption of absorbent happens in both mono and multilayers or in monolayer followed by multilayer formation (Hwang & Barron, 2011). This adsorption type also provided and proved by BET approach analysis. In addition, obtained value of 1/n = 0.14 confirms that, adsorption process is enough vigorous. In conclusion, both models show good fit with experimental results.

Table 4-2. Langmuir and Freundlich isotherm model parameters.

Langmuir			**Freundlich**		
Q max (mg/m^2)	K_l (kg/mg)	R^2	K_f ($mg^{1-(1/n)}kg^{1/n}g^{-1}$)	1/n	R^2
1.116	0.0047	0.98	17	0.14	0.95

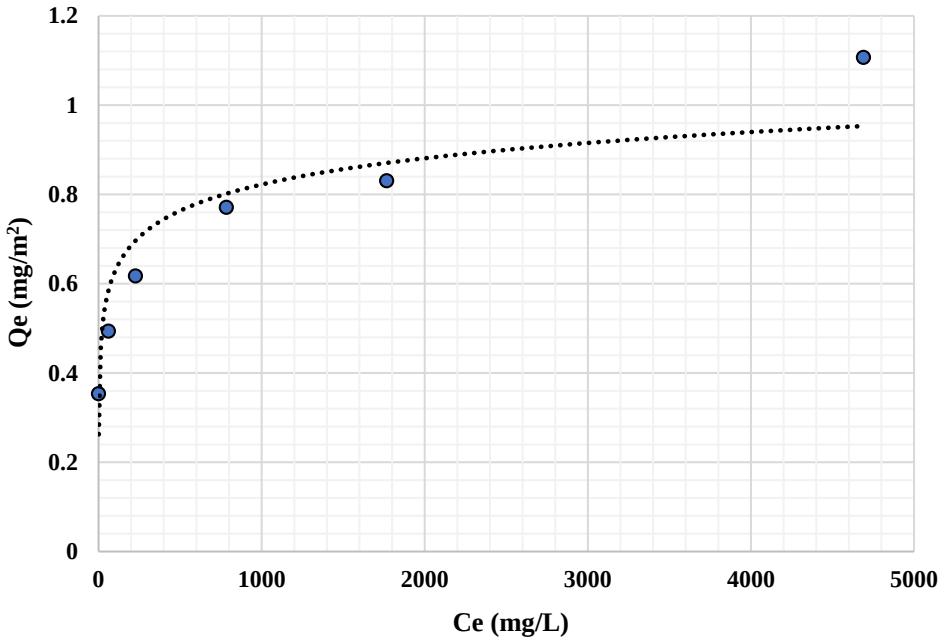

Figure 4-15. Adsorption isotherms of asphaltene adsorption onto the novel NC. The data points are the experimental data.

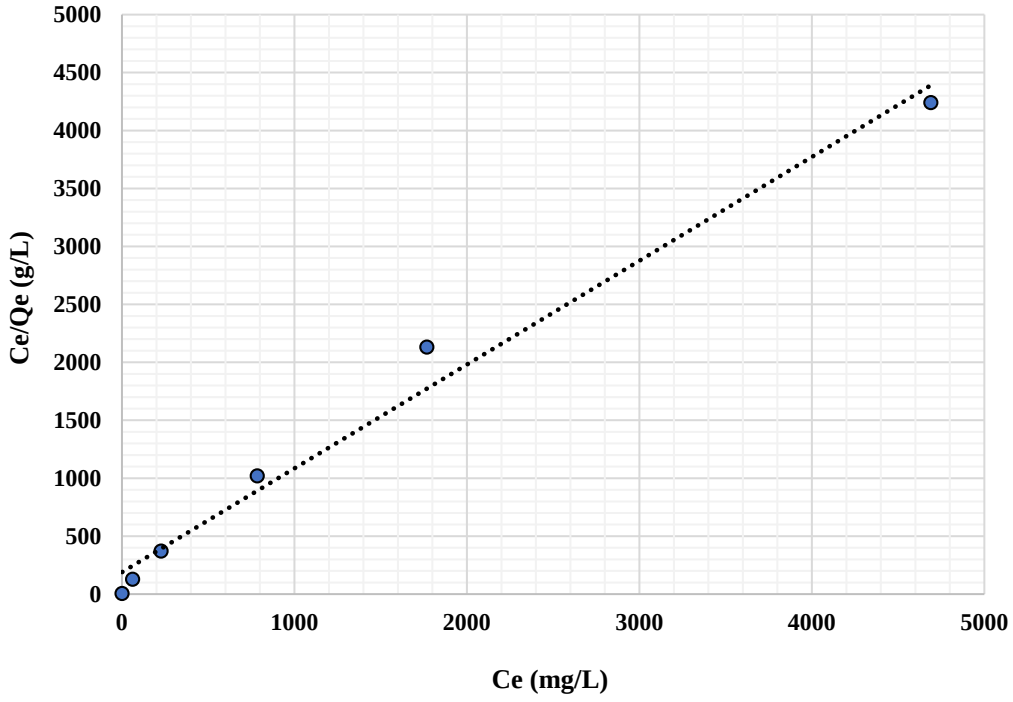

Figure 4-16. Langmuir model isotherm of the adsorbed asphaltene onto the novel NiO-Fe_3O_4-Polythiophene NC. The data points are the experimental data.

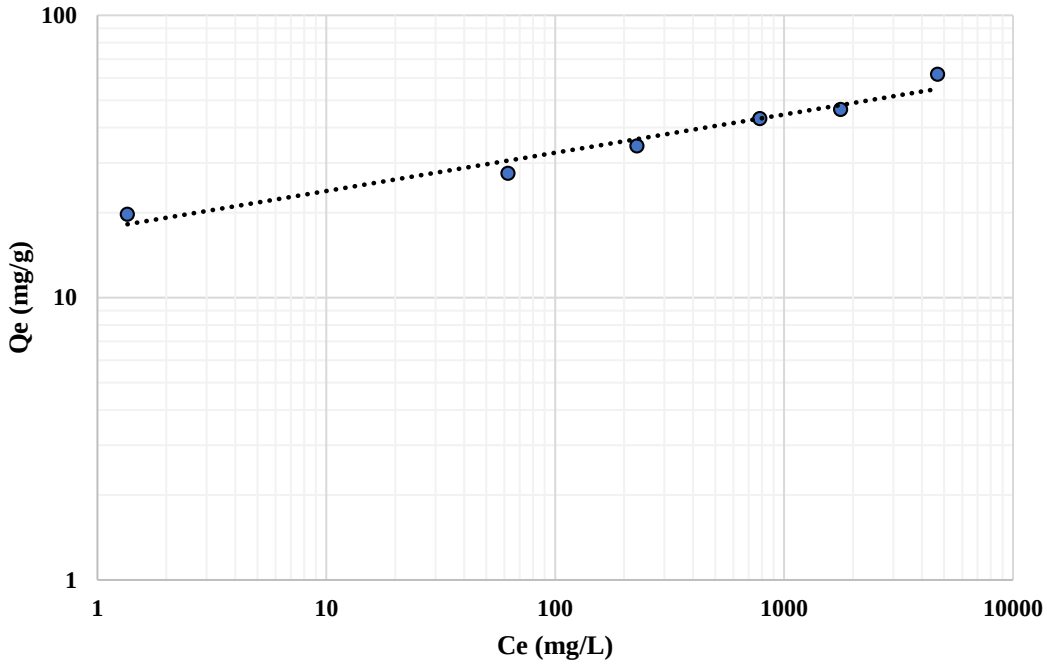

Figure 4-17. Freundlich isotherm model of adsorbed asphaltene onto the novel NiO-Fe_3O_4-Polythiophene NC. The data points are the experimental data.

4.2.4 Comparison with other nano-inhibitors

To have a clear picture of efficacy of the developed nano-inhibitor it is important to compare its performance with other nano-inhibitors. This is despite the fact that a direct comparison is nearly impossible as even if the same asphaltene was used to test the both inhibitors there are still differences between both NCs such as particle size and surface area which affects their adsorption capacity. Nevertheless, in this section an attempt is made to compare performance of the novel NiO-Fe_3O_4-Polythiophene NC for asphaltene inhibition with three other NCs. Arstanova (2023) developed and tested a novel CuO-SiO_2-Montmorillonite-K+-Thiazine inhibitor. Ten (2023) developed and tested a novel Thiazine-Fe_3O4-TiO_2-SiO_2-Bentonite inhibitor. Both performed well under laboratory conditions. Kaliolla (2024) also developed and tested a SiO_2-KCl-Xanthan inhibitor with promising results. Overall, the developed novel nano-inhibitor showed promising inhibitory efficiency for asphaltene adsorption and precipitation prevention at laboratory conditions.

Table 4-3. Comparison characteristics and efficiency of different NCs.

NC	Average crystallite size XRD (nm)	Average cluster diameter (nm) SEM	BET Surface area (m^2/g)	Optimum NC concentration by AOP determination, wt%	AOP shift (*n*-heptane ratio, %)	NC thermal stability by mass loss, %	Q max (mg/m^2)
Present work: Polythiophene-NiO-Fe_3O_4	33.2	60-400	55.8	0.3	8	21.3	1.116
Thiazine-Fe_3O_4-TiO_2-SiO_2-Bentonite (Ten, 2023)	46	60-240	43.84	0.3	7	10	0.75
CuO-SiO_2-Montmorillionite-K^+-Thiazine (Arstanova, 2023)	70.7	83-257	46.4	0.3	7	12.3	0.626
SiO_2-KCl-Xanthan (Kaliolla, 2024)	41	30-300	31.95	0.3	8	50	1.34

The average crystallite size of NiO-Fe_3O_4-Polythiophene is 33.2 nm, where in Thiazine-Fe_3O_4-TiO_2-SiO_2-Bentonite is calculated 46 nm. CuO-SiO_2-Montmorillionite-K^+-Thiazine has the largest crystallite size 70.7 nm provided through XRD analysis. In terms of particle clusters size determined by SEM images, Polythiophene-NiO-Fe_3O_4 NC has the highest range in size. It means that thickness of coating layer is thick. The average diameter of the NC in SEM is larger compared to those in XRD, as seen by the XRD and SEM graphs, suggesting that the NC possess a polycrystalline morphology. Surface area of all NC are similarly high, which enhances the adsorption capacity. Maximum AOP shift determined is 48% of *n*-heptane. In terms of mass loss of NC during heating, Thiazine-Fe_3O_4-TiO_2-SiO_2-Bentonite NC shows the lowest mass loss with only 10%, which indicates highest thermal stability compare to another NC. In addition, all four

novel NC shows high adsorption capacity, which can be potentially effective nano-inhibitor for asphaltene inhibition and adsorption.

SiO_2-KCl-Xanthan and NiO-Fe_3O_4-Polythiophene NCs' performance evaluation on asphaltene adsorption were done under the same conditions and with same asphaltene. The asphaltene used by Kaliolla (2024) is similar to the asphaltene used in this present study which enables a better comparison between the two nano-inhibitors. A summary of properties of the NCs and their inhibitory efficiency is presented in Table 4-3. The NiO-Fe_3O_4-Polythiophene inhibitor is superior to the SiO_2-KCl-Xanthan inhibitor despite the fact that the crystallite size is twice bigger. The inhibitor is also more thermally stable and supports both mono and multilayer deposition. TGA analysis of the both NCs is shown in Figure 4-18. SiO_2-KCl-Xanthan NC's mass loss is approximately 50%, where the NiO-Fe_3O_4-Polythiophene has around 21% mass loss. It can be concluded that, NiO-Fe_3O_4-Polythiophene is more thermally stable.

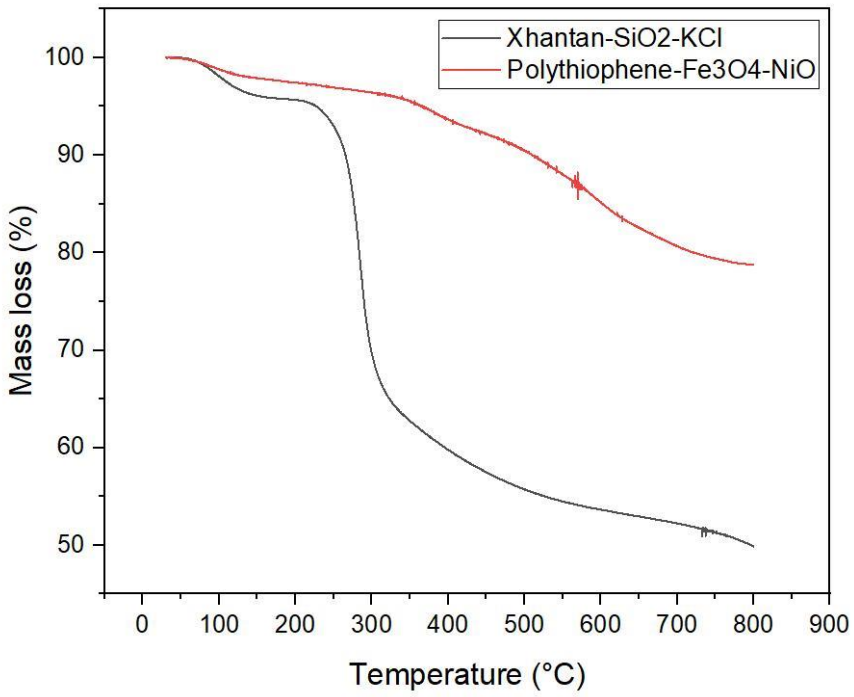

Figure 4-18. TGA analysis of two pure NCs. NiO-Fe_3O_4-Polythiophene is more thermally stable.

5 CONCLUSIONS AND RECOMMENDATIONS

The primary aim of this work was evaluation of performance of a novel Polythiophene-NiO-Fe_3O_4 NC for asphaltene adsorption and inhibition from a synthetic crude oil medium based on UV-vis spectroscopy and supernatant obtained from TGA analysis. The NC was characterized using different approach like XRD, FTIR, SEM, BET and DLS. X-ray diffraction revealed the crystallite structure and size of the NC. SEM was applied to explore surface morphology and particle size of NC. FTIR spectra provided elemental bonding and functional groups of the NC. The NC's specific surface area was calculated from BET results. The mean hydrodynamic particle size was defined by DLS technique. UV-vis spectroscopy provided defining asphaltene onset point in both presence and absence of the NC. TGA analysis enabled exploring thermal stability of the NC and modeling asphaltene adsorption kinetics isotherms. The important outcomes of this research work are as the following:

- Crystallite size was calculated 33.2 nm from XRD analysis. The average size of the NC's particles estimated 60-400 nm from SEM image. The average diameter of the NC in SEM is larger compared to those in the XRD, suggesting that NC possess a polycrystalline morphology. NC has face-centered cubic (FCC) crystallographic structure. NC surface area was received 55.83 m^2/g from BET result.
- Optimum concentration of NC was observed by 0.3 wt%, due to the high shifting of AOP from 40% to 48% volume of *n*-heptane, provided by UV-vis spectroscopy method. This proved that the novel NC provides high asphaltene inhibitory effect.
- Total mass loss of the NC determined by TGA was 21.21%, which indicates high thermal stability of the novel NC. The NC significantly accelerates the oxidation procedure of asphaltene exhibiting catalytic effect. The outcomes prove that, the novel NC is effective in asphaltene adsorption and inhibition under laboratory conditions.
- Asphaltene adsorption kinetics isotherms modeling results showed that both Langmuir (R^2 = 0.98) and Freundlich (R^2 = 0.95) isotherm models match well with the experimental data suggesting that adsorption of absorbent happens in both mono and multilayer forms.

Overall, in this research work, a novel NiO-Fe_3O_4-Polythiophene NC-based nano-inhibitor was developed and tested for adsorption and inhibition of asphaltene from a synthetic crude oil medium with satisfactory results. However, all experiments were carried under laboratory

conditions and it is recommended to assess the novel inhibitor's efficiency under reservoir conditions. In addition, exploration of role of individual NP components and their properties in asphaltene adsorption under laboratory conditions is recommended.

REFERENCES

Abdallah, W. A., & Yang, Y. (2012). Raman spectrum of asphaltene. *Energy & fuels*, *26*(11), 6888-6896.

Acharya, A., Mishra, R., & Roy, G. S. (2010). Characterization of CDSE/polythiophene nanocomposite by TGA/DTA, XRD, UV-vis spectroscopy, SEM-EDXA and FTIR. *Armenian journal of physics*, *3*(3), 195-202.

Akbar, S., & Saleh, A. A. (1989). A comprehensive approach to solve asphaltene deposition problem in some deep wells. *All Days*. https://doi.org/10.2118/17965-ms

Akbari, B., Tavandashti, M. P., & Zandrahimi, M. (2011). Particle size characterization of nanoparticles–a practical approach. *Iranian Journal of Materials Science and Engineering*, *8*(2), 48-56.

Albannay, A., Masuzawa, T., & Dabbouk, C. (2010). Alternative methods in preventing asphaltene deposition. *All Days*. https://doi.org/10.2118/137556-ms

Alemi, F. M., Dehghani, S. A. M., Rashidi, A., Hosseinpour, N., & Mohammadi, S. (2021). A mechanistic study toward the effect of single-walled carbon nanotubes on asphaltene precipitation and aggregation in unstable crude oil. *Journal of Molecular Liquids*, *330*, 115594.

Alimohammadi, S., Zendehboudi, S., & James, L. (2019). A comprehensive review of asphaltene deposition in petroleum reservoirs: Theory, challenges, and tips. *Fuel*, *252*, 753-791.

Alomair, O., Matar, K., & Alsaeed, Y. H. (2015). Experimental study of Enhanced-Heavy-Oil recovery in Berea sandstone cores by use of Nanofluids applications. *SPE Reservoir Evaluation & Engineering*, *18*(03), 387–399. https://doi.org/10.2118/171539-pa

Alshareef, A. H. (2019). Asphaltenes: definition, properties, and reactions of model compounds. *Energy & Fuels*, *34*(1), 16-30.

Amanullah, M., & Al-Tahini, A. M. (2009). Nano-Technology - its significance in smart fluid development for oil and gas field application. *All Days*. https://doi.org/10.2118/126102-ms

Anand, N. 2018. Review of Asphaltene Properties and Precipitation Modeling. PhD dissertation, The University of Texas, Austin, Texas, USA. http://hdl. handle.net/2152/72835.

Andualem, W. W. (2020). Green Synthesis of Cuo Nanoparticles for the Application of Dye Sensitized Solar Cell.

Anjos, M. M. D., Oliveira, G. E., Lucas, E. F., & González, G. (2004a). The onset of precipitation of asphaltenes in solvents of different solubility parameters. In *Springer eBooks* (pp. 283–287). https://doi.org/10.1007/b97114

Ansari, S., Mohammadi, M. R., Bahmaninia, H., Hemmati-Sarapardeh, A., Schaffie, M., Norouzi-Apourvari, S., & Ranjbar, M. (2023). Experimental measurement and modeling of asphaltene adsorption onto iron oxide and lime nanoparticles in the presence and absence of water. *Scientific Reports*, *13*(1), 122.

Arenas-Alatorre, J., Schabes-Retchkiman, P., & Rodríguez-Lugo, V. (2016). Electron microscopy characterization of crystalline nanostructures present in asphaltene. *Energy & Fuels*, *30*(5), 3752–3757. https://doi.org/10.1021/acs.energyfuels.5b02407

Arsatanova K. (2023). Synthesis, characterization, and performance assessment of a novel CuO-SiO2-Monmorillonite-K+-Thiazine nanocomposite for asphaltene precipitation inhibition.

Bai, Y., Bai, Q., Bai, Y., & Bai, Q. (2019). Subsea risk and reliability. *Subsea Engineering Handbook (Second Edition), Yong Bai and Qiang Bai (Eds.). Gulf Professional Publishing, Boston*, 239-261.

Baravkar, A. A., Kale, R. N., & Sawant, S. D. (2011). FTIR Spectroscopy: principle, technique and mathematics. *International Journal of Pharma and Bio Sciences*, *2*(1), 513-9.

Bauget, F., Langévin, D., & Lenormand, R. (2001). Dynamic surface properties of asphaltenes and resins at the Oil–Air interface. *Journal of Colloid and Interface Science*, *239*(2), 501–508. https://doi.org/10.1006/jcis.2001.7566

Bautista, M. C., Bomati-Miguel, O., del Puerto Morales, M., Serna, C. J., & Veintemillas-Verdaguer, S. (2005). Surface characterisation of dextran-coated iron oxide nanoparticles prepared by laser pyrolysis and coprecipitation. *Journal of Magnetism and Magnetic Materials*, *293*(1), 20-27.

Bin-Shan, J., Luan, Z., Wu, Z., & Lu, G. (2001). A study of removal of organic formation damage by experiments and modeling approaches. *All Days*. https://doi.org/10.2118/68752-ms

Boduszynski, M. M. (1982). Asphaltenes in petroleum asphalts. In *Advances in chemistry series* (pp. 119–135). https://doi.org/10.1021/ba-1981-0195.ch007

Bohren, C. F., & Huffman, D. R. (1998b). Absorption and scattering of light by small particles. https://doi.org/10.1002/9783527618156

Bojkovic, A., Vermeire, F. H., Kuzmanovic, M., Dao Thi, H., & Van Geem, K. M. (2021). Analytics driving kinetics: advanced mass spectrometric characterization of petroleum products. *Energy & Fuels*, *36*(1), 6-59.

Bondon, A., Autret, M., & Simonneaux, G. (1994). Identification of modified natural porphyrin isomers: 1H and 13C NMR assignments by NOESY and reverse heteronuclear shift correlation. *Magnetic Resonance in Chemistry*, *32*(2), 78–82. https://doi.org/10.1002/mrc.1260320203

Broseta, D., Robin, M., Savvidis, T., Féjean, C., Durandeau, M., & Zhou, H. (2000, April). Detection of asphaltene deposition by capillary flow measurements. In *SPE/DOE Improved Oil Recovery Symposium*. OnePetro.

Buckley, J. S., & Liu, Y. (1998). Some mechanisms of crude oil/brine/solid interactions. *Journal of Petroleum Science and Engineering*, *20*(3–4), 155–160. https://doi.org/10.1016/s0920-4105(98)00015-1

Burke, N. E., Hobbs, R. E., & Kashou, S. F. (1990). Measurement and Modeling of Asphaltene Precipitation (includes associated paper 23831). *Journal of Petroleum Technology*, *42*(11), 1440-1446.

D'Amico, F., & Gunnella, R. (2008). *Control of structural conformation and electronic properties of organicsemiconductors thin films* (Doctoral dissertation, PhD Thesis, Department of Physics, Camerino University).

De Boer, R. B., Leerlooyer, K., Eigner, M. R. P., & Van Bergen, A. R. D. (1995). Screening of crude oils for asphalt precipitation: theory, practice, and the selection of inhibitors. *SPE Production & Facilities*, *10*(01), 55-61.

Demirbas, A. (2016). Deposition and flocculation of asphaltenes from crude oils. *Petroleum Science and Technology*, *34*(1), 6-11.

Dubey, R. S., Rajesh, Y. B. R. D., & More, M. A. (2015). Synthesis and characterization of SiO2 nanoparticles via sol-gel method for industrial applications. Materials Today: Proceedings, 2(4-5), 3575-3579.

Ebnesajjad, S., & Ebnesajjad, C. (2013). *Surface treatment of materials for adhesive bonding*. William Andrew.

Eskin, D., Ratulowski, J., Akbarzadeh, K., & Pan, S. (2011). Modelling asphaltene deposition in turbulent pipeline flows. *The Canadian Journal of Chemical Engineering*, *89*(3), 421-441.

Etim, U., Peng, P., & Zhang, Y. (2017a). Nanotechnology applications in petroleum refining. In *Topics in mining, metallurgy and materials engineering* (pp. 37–65). https://doi.org/10.1007/978-3-319-60630-9_2

Ezeonyeka, N. L., Hemmati-Sarapardeh, A., & Husein, M. M. (2018). Asphaltenes Adsorption onto Metal Oxide Nanoparticles: A Critical Evaluation of Measurement Techniques. *Energy & Fuels*, *32*(2), 2213–2223. https://doi.org/10.1021/acs.energyfuels.7b03693

Fakher, S., Ahdaya, M., Elturki, M., & Imqam, A. (2019). Critical review of asphaltene properties and factors impacting its stability in crude oil. *Journal of Petroleum Exploration and Production Technology*, *10*(3), 1183–1200. https://doi.org/10.1007/s13202-019-00811-5

Fan, T., & Buckley, J. S. (2007). Acid number measurements revisited. SPE Journal, 12(04), 496-500.

Farooq, U., Patil, A., Panjwani, B., & Simonsen, G. (2021). Review on application of nanotechnology for asphaltene adsorption, crude oil demulsification, and produced water treatment. *Energy & Fuels (Print)*, *35*(23), 19191–19210. https://doi.org/10.1021/acs.energyfuels.1c01990

Fleming, N. (2013). Technology Focus: Nanotechnology (February 2013). *Journal of Petroleum Technology*, *65*(02), 140. https://doi.org/10.2118/0213-0140-jpt

Foo, K., & Hameed, B. (2010). Insights into the modeling of adsorption isotherm systems. *Chemical Engineering Journal*, *156*(1), 2–10. https://doi.org/10.1016/j.cej.2009.09.013

Fossen, M., Kallevik, H., Knudsen, K. D., & Sjöblom, J. (2011). Asphaltenes precipitated by a Two-Step Precipitation Procedure. 2. Physical and chemical characteristics. *Energy & Fuels*, *25*(8), 3552–3567. https://doi.org/10.1021/ef200373v

Franco, C. A., Franco, C., Zabala, R. D., Bahamón, Í., Forero, A. M., & Cortés, F. B. (2021). Field applications of nanotechnology in the oil and gas industry: Recent advances and perspectives. *Energy & Fuels*, *35*(23), 19266–19287. https://doi.org/10.1021/acs.energyfuels.1c02614

Franco, C. A., Nassar, N. N., Montoya, T., Ruíz, M. A., & Cortés, F. B. (2015). Influence of asphaltene aggregation on the adsorption and catalytic behavior of nanoparticles. *Energy & Fuels*, *29*(3), 1610–1621. https://doi.org/10.1021/ef502786e

Franco, C. A., Zabala, R., & Cortés, F. B. (2017). Nanotechnology applied to the enhancement of oil and gas productivity and recovery of Colombian fields. *Journal of Petroleum Science and Engineering*, *157*, 39-55.

Franco, C., Patiño, E., Benjumea, P., Ruiz, M. A., & Cortés, F. B. (2013). Kinetic and thermodynamic equilibrium of asphaltenes sorption onto nanoparticles of nickel oxide supported on nanoparticulated alumina. Fuel, 105, 408-414.

Freundlich, H. (1907). Über die Adsorption in Lösungen. *Zeitschrift Für Physikalische Chemie (München. 1991)*, *57U*(1), 385–470. https://doi.org/10.1515/zpch-1907-5723

Galoppini, M. (1994). Asphaltene Deposition Monitoring and Removal Treatments: an experience in ultra deep wells. *All Days*. https://doi.org/10.2118/27622-ms

Gaweł, B., Eftekhardadkhah, M., & Øye, G. (2014). Elemental Composition and fourier Transform infrared spectroscopy analysis of crude oils and their fractions. *Energy & Fuels*, *28*(2), 997–1003. https://doi.org/10.1021/ef402286y

Ghamartale, A., Afzali, S., Rezaei, N., & Zendehboudi, S. (2021). *Asphaltene Deposition Control by Chemical Inhibitors: Theoretical and Practical Prospects*. Gulf Professional Publishing.

Groenzin, H., & Mullins, O. C. (2000). Molecular Size and Structure of Asphaltenes from Various Sources. *Energy & Fuels*, *14*(3), 677–684. https://doi.org/10.1021/ef990225z

Guerrero-Martin, C. A., Montes, D., Da Silva, M. M. M., Páez, E. G. M., Guerrero-Martin, L. E., Salinas-Silva, R., Camacho-Galindo, S., Lucas, E. F., & Szklo, A. (2023). Asphaltene Precipitation/Deposition Estimation and Inhibition through Nanotechnology: A Comprehensive Review. *Energies*, *16*(13), 4859. https://doi.org/10.3390/en16134859

Guin, S., Vanamamalai, M., Saraswat, M., Bansal, V., Mandal, T., Arora, A., & Saxena, D. (2022). Correlation of methodologies for predicting asphaltene content of low sulfur heavy stock fuel oil from CCR content. *Petroleum Science and Technology*, 1–11. https://doi.org/10.1080/10916466.2022.2143811

Hanaor, D. A., Ghadiri, M., Chrzanowski, W., & Gan, Y. (2014). Scalable surface area characterization by electrokinetic analysis of complex anion adsorption. *Langmuir*, *30*(50), 15143-15152.

Hassanzadeh, M., & Abdouss, M. (2022). A comprehensive review on the significant tools of asphaltene investigation. Analysis and characterization techniques and computational methods. *Journal of Petroleum Science and Engineering*, *208*, 109611. https://doi.org/10.1016/j.petrol.2021.109611

Hassanzadeh, M., & Abdouss, M. (2023). Molecular structure: the first and most significant factor in the precipitation of asphaltenes. *SPE Journal*, *28*(02), 894-907.

Hosseinpour, N., Khodadadi, A. A., Bahramian, A., & Mortazavi, Y. (2013). Asphaltene adsorption onto acidic/basic metal oxide nanoparticles toward in situ upgrading of reservoir oils by nanotechnology. *Langmuir*, *29*(46), 14135-14146.

Hosseinpour, N., Mortazavi, Y., Bahramian, A., Khodatars, L., & Khodadadi, A. A. (2014). Enhanced pyrolysis and oxidation of asphaltenes adsorbed onto transition metal oxides nanoparticles towards advanced in-situ combustion EOR processes by nanotechnology. *Applied Catalysis A: General*, *477*, 159–171. https://doi.org/10.1016/j.apcata.2014.03.017

Husein, M. M., & Alkhaldi, S. J. (2014). In situ preparation of alumina nanoparticles in heavy oil and their thermal cracking performance. Energy & fuels, 28(10), 6563-6569.

Hussein, A. (2023). Asphaltene deposition. In *Elsevier eBooks* (pp. 377–427). https://doi.org/10.1016/b978-0-323-99118-6.00020-4

Hwang, N., & Barron, A. R. (2011). BET surface area analysis of nanoparticles. *The connexions project*, 1-11.

Inkson, B. J. (2016). Scanning electron microscopy (SEM) and transmission electron microscopy (TEM) for materials characterization. In *Elsevier eBooks* (pp. 17–43). https://doi.org/10.1016/b978-0-08-100040-3.00002-x

Jamialahmadi, M., Soltani, B., Müller-Steinhagen, H., & Rashtchian, D. (2009). Measurement and prediction of the rate of deposition of flocculated asphaltene particles from oil. *International Journal of Heat and Mass Transfer*, *52*(19–20), 4624–4634. https://doi.org/10.1016/j.ijheatmasstransfer.2009.01.049

Jeffries-Harris, M., & Coppel, C. P. (1969). Solvent stimulation in low gravity oil reservoirs. *Journal of Petroleum Technology*, *21*(02), 167–175. https://doi.org/10.2118/2158-pa

Karmakar, S. A. N. A. T. (2019). Particle size distribution and zeta potential based on dynamic light scattering: Techniques to characterize stability and surface charge distribution of charged colloids. *Recent Trends Mater. Phys. Chem*, *28*, 117-159.

Kazemzadeh, Y., Sharifi, M., & Riazi, M. (2018). Optimization of Fe3O4/Chitosan nanocomposite concentration on the formation and stability of W/O emulsion. *Materials Research Express*, *6*(3), 035031. https://doi.org/10.1088/2053-1591/aaf7d9

Khanifar, A., Alian, S. S., Demiral, B., & Darman, N. B. (2011). Study of Asphaltene Precipitation and Deposition Phenomenon during WAG Application. *All Days*. https://doi.org/10.2118/143488-ms

King, S., & Cotney, C. (1996). Development and application of unique natural solvents for treating paraffin and asphaltene related problems. *All Days*. https://doi.org/10.2118/35265-ms

Koolen, H. H. F., Gomes, A. F., De Moura, L. G. M., Marcano, F., Cardoso, F. M., Klitzke, C. F., Wojcik, R., Binkley, J., Patrick, J. S., Swarthout, R. F., De Tarso Vieira E Rosa, P., & Gozzo, F. C. (2018). Integrative mass spectrometry strategy for fingerprinting and tentative structural characterization of asphaltenes. *Fuel*, *220*, 717–724. https://doi.org/10.1016/j.fuel.2017.12.078

Kord, S., Mohammadzadeh, O., Miri, R., & Soulgani, B. S. (2014). Further investigation into the mechanisms of asphaltene deposition and permeability impairment in porous media using a modified analytical model. *Fuel*, *117*, 259–268. https://doi.org/10.1016/j.fuel.2013.09.038

Krishnamoorti, R. (2006). Technology Tomorrow: Extracting the benefits of Nanotechnology for the oil industry. *Journal of Petroleum Technology*, *58*(11), 24–26. https://doi.org/10.2118/1106-0024-jpt

Langmuir, I. (1918). THE ADSORPTION OF GASES ON PLANE SURFACES OF GLASS, MICA AND PLATINUM. *Journal of the American Chemical Society*, *40*(9), 1361–1403. https://doi.org/10.1021/ja02242a004

Lawal, K. A., Crawshaw, J. P., Boek, E. S., & Vesovic, V. (2012). Experimental investigation of asphaltene deposition in capillary flow. *Energy & fuels*, *26*(4), 2145-2153.

Lei, W., Portehault, D., Liu, D., Qin, S., & Chen, Y. (2013). Porous boron nitride nanosheets for effective water cleaning. Nature communications, 4(1), 1777.

Leon, O., Rogel, E., Espidel, J., & Torres, G. (2000). Asphaltenes: structural characterization, self-association, and stability behavior. *Energy & Fuels*, *14*(1), 6-10.

Leontaritis, K. J. (1996). The asphaltene and wax deposition envelopes. *Fuel Science & Technology International*, *14*(1–2), 13–39. https://doi.org/10.1080/08843759608947560

Leontaritis, K. J., Amaefule, J., & Charles, R. (1994). A systematic approach for the prevention and treatment of formation damage caused by asphaltene deposition. *SPE Production & Facilities*, *9*(03), 157–164. https://doi.org/10.2118/23810-pa

Li, L., Yuan, X., Sun, J., Xu, X., Li, S., & Wang, L. (2013). Vital role of nanotechnology and nanomaterials in the field of oilfield chemistry. *International Petroleum Technology Conference*. https://doi.org/10.2523/16401-ms

Li, X. G., Li, J., Meng, Q. K., & Huang, M. R. (2009). Interfacial synthesis and widely controllable conductivity of polythiophene microparticles. *The Journal of Physical Chemistry B*, *113*(29), 9718-9727.

Lindsay, S. (2010). *Introduction to nanoscience*. American Chemical Society.

Luo, P., Wang, X., & Gu, Y. (2010). Characterization of asphaltenes precipitated with three light alkanes under different experimental conditions. *Fluid Phase Equilibria*, *291*(2), 103–110. https://doi.org/10.1016/j.fluid.2009.12.010

Madhi, M., Bemani, A., Daryasafar, A., & Khosravi Nikou, M. R. (2017). Experimental and modeling studies of the effects of different nanoparticles on asphaltene adsorption. *Petroleum Science and Technology*, *35*(3), 242-248.

Majumdar, R. D., Gerken, M., Mikula, R., & Hazendonk, P. (2013). Validation of the Yen–Mullins Model of Athabasca Oil-Sands Asphaltenes using Solution-State 1H NMR Relaxation and 2D HSQC Spectroscopy. *Energy & Fuels*, *27*(11), 6528–6537. https://doi.org/10.1021/ef401412w

Mansoori, G.A. (2010). Remediation of asphaltene and other heavy organic deposits in oil wells and in pipelines.

Marei, N. N., Nassar, N. N., & Vitale, G. (2016). The effect of the nanosize on surface properties of NiO nanoparticles for the adsorption of Quinolin-65. Physical Chemistry Chemical Physics, 18(9), 6839-6849.

Mazloom, M. S., Hemmati-Sarapardeh, A., Husein, M. M., Behbahani, H. S., & Zendehboudi, S. (2020). Application of nanoparticles for asphaltenes adsorption and oxidation: A critical review of challenges and recent progress. *Fuel*, *279*, 117763.

Mbonyiryivuze, A., Mwakikunga, B., Dhlamini, S. M., & Maaza, M. (2015). Fourier Transform Infrared Spectroscopy for Sepia Melanin. *Physics and Materials Chemistry*, *3*(2), 25-29.

Medina, M., Willis, T., Onukwu, A., & Schon, S. (2011). Technology Challenges, Opportunities of Next 25 years. *The Way Ahead*, *07*(03), 15–17. https://doi.org/10.2118/0311-015-twa

Medina, O. E., Olmos, C. M., Lopera, S. H., Cortés, F. B., & Franco, C. A. (2019). Nanotechnology Applied to thermal Enhanced oil recovery Processes: A review. *Energies (Basel)*, *12*(24), 4671. https://doi.org/10.3390/en12244671

Merdrignac, I., Desmazieres, B., Terrier, P., Delobel, A., & Laprevote, O. (2004). Analysis of raw and hydrotreated asphaltenes using off-line and on-line SEC/MS coupling. *Proceedings of the Heavy Organic Deposition, Los Cabos, Baja California, Mexico*.

Miadonye, A., & Evans, L. (2010). The solubility of asphaltenes in different hydrocarbon liquids. Petroleum Science and Technology, 28(14), 1407-1414.

Mohammadi, M., Akbari, M., Fakhroueian, Z., Bahramian, A., Azin, R., & Arya, S. (2011). Inhibition of asphaltene precipitation by TIO2, SIO2, and ZRO2 nanofluids. *Energy & Fuels*, *25*(7), 3150–3156. https://doi.org/10.1021/ef2001635

Mohammadi, S., Rashidi, F., Mousavi-Dehghani, S. A., & Ghazanfari, M. H. (2016). On the effect of temperature on precipitation and aggregation of asphaltenes in light live oils. *The Canadian Journal of Chemical Engineering*, *94*(9), 1820-1829.

Monshi, A., Foroughi, M. R., & Monshi, M. R. (2012). Modified Scherrer equation to estimate more accurately Nano-Crystallite size using XRD. *World Journal of Nano Science and Engineering*, *02*(03), 154–160. https://doi.org/10.4236/wjnse.2012.23020

Montoya, T., Coral, D. F., Franco, C. A., Nassar, N. N., & Cortés, F. B. (2014). A Novel Solid–Liquid Equilibrium Model for Describing the Adsorption of Associating Asphaltene Molecules onto Solid Surfaces Based on the "Chemical Theory." *Energy & Fuels*, *28*(8), 4963–4975. https://doi.org/10.1021/ef501020d

Mullins, O. C. (2011). The asphaltenes. *Annual review of analytical chemistry*, *4*, 393-418.

Murgich, J., Rodríguez, & Aray, Y. (1996). Molecular recognition and molecular mechanics of micelles of some model asphaltenes and resins. *Energy & fuels*, *10*(1), 68-76.

Nassar, N. N., Hassan, A., & Pereira-Almao, P. (2011). Effect of the particle size on asphaltene adsorption and catalytic oxidation onto alumina particles. Energy & Fuels, 25(9), 3961-3965.

Nassar, N. N., Hassan, A., & Pereira-Almao, P. (2011). Effect of surface acidity and basicity of aluminas on asphaltene adsorption and oxidation. Journal of colloid and interface science, 360(1), 233-238.

Nassar, N. N., Hassan, A., & Pereira-Almao, P. (2011). Metal oxide nanoparticles for asphaltene adsorption and oxidation. *Energy & Fuels*, *25*(3), 1017–1023. https://doi.org/10.1021/ef101230g

Nassar, N. N., Hassan, A., & Pereira-Almao, P. (2011b). Comparative oxidation of adsorbed asphaltenes onto transition metal oxide nanoparticles. *Colloids and Surfaces A: Physicochemical and Engineering Aspects*, *384*(1–3), 145–149. https://doi.org/10.1016/j.colsurfa.2011.03.049

Nassar, N. N., Hassan, A., Carbognani, L., Lopez-Linares, F., & Pereira-Almao, P. (2012). Iron oxide nanoparticles for rapid adsorption and enhanced catalytic oxidation of thermally cracked asphaltenes. Fuel, 95, 257-262.

Neelen, M. (2023). Technology. Particle Metrix. https://particle-metrix.com/technology/#measurements

Ngata, M. R., Yang, B., Aminu, M. D., Iddphonce, R., Omari, A., Shaame, M., ... & Yanyi-Akofur, D. (2021). Review of Developments in Nanotechnology Application for Formation Damage Control. *Energy & Fuels*, *36*(1), 80-97.

Nghiem, L. X., Hassam, Nutakki, R., & George, A. E. (1993). Efficient modelling of asphaltene precipitation. *All Days*. https://doi.org/10.2118/26642-ms

Ok, S., & Mal, T. K. (2019). NMR spectroscopy analysis of asphaltenes. *Energy & Fuels*, *33*(11), 10391-10414.

Padró, J. M., Novotny, A., Smal, C., & Cismondi, M. (2023). Application and revision of the indirect method for determination of asphaltene precipitation onsets for light and medium oils in Argentina. *Upstream Oil and Gas Technology*, *10*, 100087.

Paul, D. R., & Robeson, L. M. (2008). Polymer nanotechnology: Nanocomposites. *Polymer*, *49*(15), 3187–3204. https://doi.org/10.1016/j.polymer.2008.04.017

Powers, D., Sadeghi, H., Yarranton, H. W., & Van Den Berg, F. G. A. (2016). Regular solution based approach to modeling asphaltene precipitation from native and reacted oils: Part 1, molecular weight, density, and solubility parameter distributions of asphaltenes. *Fuel*, *178*, 218–233. https://doi.org/10.1016/j.fuel.2016.03.027

Ramesan, M. T., & Suhailath, K. (2017). Role of nanoparticles on polymer composites. In *Micro and Nano Fibrillar Composites (MFCs and NFCs) from Polymer Blends* (pp. 301-326). Woodhead Publishing.

Rao, C. N. R., Kulkarni, G. U., Thomas, P. J., & Edwards, P. P. (2002). Size-dependent chemistry: properties of nanocrystals. *Chemistry–A European Journal*, *8*(1), 28-35.

Richardson, J. T., Scates, R., & Twigg, M. V. (2003). X-ray diffraction study of nickel oxide reduction by hydrogen. *Applied Catalysis A: General*, *246*(1), 137-150.

Sagala, F., Hethnawi, A., & Nassar, N. N. (2022). Challenges and Uncertainties of Using Nanoparticles in Oil and Gas Applications. In Nanoparticles: An Emerging Technology for Oil Production and Processing Applications (pp. 497-506). Cham: Springer International Publishing.

Saleh, T. A., & Al-Hammadi, S. A. (2017). Insights into the Fundamentals and Principles of the Oil and Gas Industry: The Impact of Nanotechnology. In *Topics in mining, metallurgy and materials engineering* (pp. 1–35). https://doi.org/10.1007/978-3-319-60630-9_1

Sanchez, N. (2007). A general approach for asphaltene modeling. *All Days*. https://doi.org/10.2118/107191-ms

Schwettmann, K., Höhne, P., & Stephan, D. (2022). Comparison of column chromatography and solid-phase extraction on virgin and aged bituminous maltene phases. *Materials and Structures*, *55*(10), 242.

Seifried, C. M., Crawshaw, J., & Boek, E. S. (2013). Kinetics of asphaltene aggregation in crude oil studied by Confocal Laser-Scanning Microscopy. *Energy & Fuels*, *27*(4), 1865–1872. https://doi.org/10.1021/ef301594j

Senthilkumar, B., Thenamirtham, P., & Selvan, R. K. (2011). Structural and electrochemical properties of polythiophene. *Applied Surface Science*, *257*(21), 9063-9067.

Setoodeh, N., Darvishi, P., & Esmaeilzadeh, F. (2018). Adsorption of asphaltene from crude oil by applying polythiophene coating on Fe3O4 nanoparticles. *Journal of Dispersion Science and Technology*, *39*(4), 578-588.

Setoodeh, N., Darvishi, P., Lashanizadegan, A., & Esmaeilzadeh, F. (2020). A comparative study for evaluating the performance of five coatings applied on Fe3O4 nanoparticles for inhibition of asphaltene precipitation from crude oil. *Journal of Dispersion Science and Technology*, *41*(11), 1616-1632.

Sheu, E. Y. (2001). Petroleum AsphalteneProperties, Characterization, and Issues. *Energy & Fuels*, *16*(1), 74–82. https://doi.org/10.1021/ef010160b

Shirdel, M. (2012). Development of a coupled Wellbore/Reservoir simulator for damage prediction and remediation. *All Days*. https://doi.org/10.2118/160914-stu

Shojaati, F., Riazi, M., Mousavi, S. H., & Derikvand, Z. (2017). Experimental investigation of the inhibitory behavior of metal oxides nanoparticles on asphaltene precipitation. *Colloids and Surfaces A: Physicochemical and Engineering Aspects*, *531*, 99-110.

Silva, S. L., Silva, A. M. S., Ribeiro, J. C., Martins, F., Da Silva, F. A., & Silva, C. M. (2011). Chromatographic and spectroscopic analysis of heavy crude oil mixtures with emphasis in nuclear magnetic resonance spectroscopy: A review. *Analytica Chimica Acta*, *707*(1–2), 18–37. https://doi.org/10.1016/j.aca.2011.09.010

Soorghali, F., Zolghadr, A., & Ayatollahi, S. (2014). Effect of resins on asphaltene deposition and the changes of surface properties at different pressures: a microstructure study. *Energy & fuels*, *28*(4), 2415-2421.

Soulgani, B. S., Tohidi, B., Jamialahmadi, M., & Rashtchian, D. (2011). Modeling Formation Damage due to Asphaltene Deposition in the Porous Media. *Energy & Fuels*, *25*(2), 753–761. https://doi.org/10.1021/ef101195a

Speight, J. G. (2014). *The chemistry and technology of petroleum*. CRC press.

Sullivan, M., Smythe, E. J., Fukagawa, S., Harrison, C., Dumont, H., & Borman, C. (2020). A fast measurement of asphaltene onset pressure. *SPE Reservoir Evaluation & Engineering*, *23*(03), 0962-0978.

Swann, G. E., & Patwardhan, S. V. (2011). Application of Fourier Transform Infrared Spectroscopy (FTIR) for assessing biogenic silica sample purity in geochemical analyses and palaeoenvironmental research. *Climate of the Past*, *7*(1), 65-74.

Talebi, A., Shafiei, M., Kazemzadeh, Y., Escrochi, M., & Riazi, M. (2023). Asphaltene prevention and treatment by using nanomaterial: A comprehensive review. *Journal of Molecular Liquids (Print)*, *382*, 121891. https://doi.org/10.1016/j.molliq.2023.121891

Tarboush, B. J. A., & Husein, M. M. (2012). Adsorption of asphaltenes from heavy oil onto in situ prepared NiO nanoparticles. Journal of colloid and interface science, 378(1), 64-69.

Tarboush, B. J. A., & Husein, M. M. (2015). Inferring the role of NiO nanoparticles from the thermal behavior of virgin and adsorbed hydrocarbons. Fuel, 147, 53-61.

Tavakkoli, M., Grimes, M. R., Liu, X., Garcia, C. K., Correa, S. C., Cox, Q. J., & Vargas, F. M. (2015). Indirect method: a novel technique for experimental determination of asphaltene precipitation. *Energy & Fuels*, *29*(5), 2890-2900.

Tazikeh, S., Amin, J. S., & Zendehboudi, S. (2020). Experimental study of asphaltene precipitation and metastable zone in the presence of polythiophene-coated Fe3O4 nanoparticles. *Journal of Molecular Liquids*, *301*, 112254.

Ten Y. (2023). Synthesis, characterization, and performance assessment of a novel Thiazine-Fe3O4-TiO2-SiO2-Bentonite nanocomposite for asphaltene precipitation inhibition.

Tombácz, E., Illés, E., Majzik, A., Hajdú, A., Rideg, N., & Szekeres, M. (2007). Ageing in the inorganic nanoworld: Example of magnetite nanoparticles in aqueous medium. Croatica Chemica Acta, 80(3-4), 503-515.

Trbovich, M., & King, G. E. (1991). Asphaltene deposit removal: Long-Lasting treatment with a Co-Solvent. *All Days*. https://doi.org/10.2118/21038-ms

Uygun, A., Turkoglu, O., Sen, S., Ersoy, E., Yavuz, A. G., & Batir, G. G. (2009). The electrical conductivity properties of polythiophene/TiO2 nanocomposites prepared in the presence of surfactants. *Current Applied Physics*, *9*(4), 866-871.\

Vargas, F. M., & Tavakkoli, M. (2018). Asphaltene deposition. In *CRC Press eBooks*. https://doi.org/10.1201/9781315268866

Voloshin, A. I., Ragulin, V. V., & Telin, A. G. (2005, February). Development and introduction of heavy organic compound deposition diagnostics, prevention and removing. In *SPE International Conference on Oilfield Chemistry?* (pp. SPE-93128). SPE.

Vordos, N., Giannakopoulos, S., Vansant, E. F., Kalaitzis, C., Nolan, J. W., Bandekas, D. V., Karavasilis, I., Mitropoulos, A. C., & Touloupidis, S. (2018). Small-angle X-ray scattering (SAXS) and nitrogen porosimetry (NP): two novel techniques for the evaluation of urinary stone hardness. *International Urology and Nephrology*, *50*(10), 1779–1785. https://doi.org/10.1007/s11255-018-1961-3

Vuković, J. P., Novak, P., Plavec, J., Friedrich, M., Pajc, L. M., & Hrenar, T. (2015). NMR and Chemometric Characterization of Vacuum Residues and Vacuum Gas Oils from Crude Oils of Different Origin. *Croatica Chemica Acta*, *88*(1), 89–95. https://doi.org/10.5562/cca2612

Wang, J., Buckley, J. S., & Creek, J. L. (2004). Asphaltene deposition on metallic surfaces. *Journal of dispersion science and technology*, *25*(3), 287-298.

Wang, X., Shi, Y., Graff, R. W., Lee, D., & Gao, H. (2015). Developing recyclable pH-responsive magnetic nanoparticles for oil–water separation. *Polymer*, *72*, 361–367. https://doi.org/10.1016/j.polymer.2014.12.056

Wen, S., Liu, J., & Deng, J. (2021). Methods for the detection and composition study of fluid inclusions. In *Elsevier eBooks* (pp. 27–68). https://doi.org/10.1016/b978-0-12-819845-2.00003-x

Whittig, L. D., & Allardice, W. R. (1986). X-ray diffraction techniques. *Methods of Soil Analysis: Part 1 Physical and Mineralogical Methods*, *5*, 331-362.

Wu, H., & Kessler, M. R. (2015). Asphaltene: structural characterization, molecular functionalization, and application as a low-cost filler in epoxy composites. *RSC Advances*, *5*(31), 24264–24273. https://doi.org/10.1039/c5ra00509d

Xiong, R., Guo, J., Kiyingi, W., Xu, H., & Wu, X. (2023). The deposition of asphaltenes under high-temperature and high-pressure (HTHP) conditions. *Petroleum Science*, *20*(1), 611–618. https://doi.org/10.1016/j.petsci.2022.08.026

Xu, Q., Zhang, Z., Zhang, S., Wang, F., & Yan, Y. (2014). Molecular structure models of asphaltene in crude and upgraded Bio-Oil. *Chemical Engineering & Technology*, *37*(7), 1198–1204. https://doi.org/10.1002/ceat.201300158

Yamaura, M., & Fungaro, D. A. (2013). Synthesis and characterization of magnetic adsorbent prepared by magnetite nanoparticles and zeolite from coal fly ash. *Journal of materials science, 48*, 5093-5101.

Yi, T., Fadili, A., Ibrahim, M., & Al-Matar, B. S. (2009). Modeling the effect of asphaltene on the development of the Marrat field. *All Days*. https://doi.org/10.2118/120988-ms

Yousef, K., Ehsan, E. S., Keyvan, K., Saeed, S., Mehran, M., & Yaser, A. (2015). Behavior of Asphaltene Adsorption onto the Metal Oxide Nanoparticle Surface and Its Effect on Heavy Oil Recovery.

Zabala, R. D., Franco, C. A., & Cortés, F. B. (2016). Application of nanofluids for improving oil mobility in Heavy Oil and Extra-Heavy Oil: a field test. *All Days*. https://doi.org/10.2118/179677-ms

Zabala, R. D., Mora, E., Botero, O. ., Cespedes, C., Guarín, L., Franco, C. A., Cortés, F. B., Patino, J. E., & Ospina, N. (2014). Nano-Technology for asphaltenes inhibition in Cupiagua South Wells. *IPTC 2014: International Petroleum Technology Conference*. https://doi.org/10.3997/2214-4609-pdb.395.iptc-17344-ms

Zanganeh, P., Dashti, H., & Ayatollahi, S. (2018). Comparing the effects of CH4, CO2, and N2 injection on asphaltene precipitation and deposition at reservoir condition: A visual and modeling study. *Fuel*, *217*, 633-641.

Zhang, Y., Siskin, M., Gray, M. R., Walters, C. C., & Rodgers, R. P. (2020). Mechanisms of asphaltene aggregation: puzzles and a new hypothesis. *Energy & Fuels*, *34*(8), 9094-9107.

Zhou, B., Hermans, S., Somorjai, G. A., Han, S., & Raja, R. (2007). Nanotechnology in catalysis. In *Springer eBooks*. https://doi.org/10.1007/978-0-387-34688-5

Zhou, W., Apkarian, R., Wang, Z. L., & Joy, D. (2007). Fundamentals of scanning electron microscopy (SEM). *Scanning microscopy for nanotechnology: techniques and applications*, 1-40.

Zhou, X., Xu, W., Liu, G., Panda, D., & Peng, C. (2009). Size-Dependent catalytic activity and dynamics of gold nanoparticles at the Single-Molecule level. *Journal of the American Chemical Society*, *132*(1), 138–146. https://doi.org/10.1021/ja904307n

Zsigmondy, R. (1909). Colloids and the ultra microscope. Journal of the American Chemical Society, 31(8), 951–952. https://doi.org/10.1021/ja01938a017